Novel Robust Controller Design to Enhance Transient Stability of Power Systems

by

Md Rasel Mahmud

B.Sc. (Hons) in Electrical & Electronic Engineering

A thesis submitted in fulfilment of the requirements for the degree of

Master of Engineering

School of Software and Electrical Engineering

Faculty of Science, Engineering and Technology

Swinburne University of Technology

Hawthorn, VIC 3122, Australia

August 2017

Declaration

I am declaring that the works presented in this thesis is my own work and to best my knowledge, this work does not contain any materials which have not previously published by any other person or submitted for the requirement of any other degree, except where due acknowledgement and reference are provided within the thesis. An explicit acknowledgement has been for the contribution from any other colleagues within and outside the university.

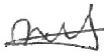

Md. Rasel Mahmud

The 29th August 2017

Abstract

This thesis aims to design a robust nonlinear controller for power systems to enhance the transient stability. The robust controller is designed based on the H_∞ mixed-sensitivity loop shaping control scheme for feedback linearized models of power systems. The partial feedback linearization scheme is used to linearize the power system model where the linearized system is independent of the operating points. The proposed H_∞ mixed-sensitivity loop shaping control scheme provides the robustness against parametric uncertainties, external disturbances, and measurement noises. The proposed robust H_∞ controller for the feedback linearized system is incorporated with the feedback linearizing control input to ensure the transient stability of power systems under different operating conditions. The proposed robust controller is designed for both single machine and multi machine power systems. The robustness of the designed controller is evaluated through the simulation results on both single machine and multimachine power systems and compared with an existing power system stabilizer (PSS) and a state feedback linearizing excitation controller under different operating conditions. Simulation results clearly demonstrate the superiority of the proposed scheme as compared to the existing controllers.

Acknowledgements

I would like to thank my principal coordinating supervisor, Associate Professor Jingxin Zhang, who helped me from the beginning of my candidature. His continuous supports and encouragements help me to complete this thesis. His efforts to revise the thesis is unforgettable and I would not be able to finish writing without his help. I always think him as my local guardian for his continuous support.

My first meeting with my associate supervisor was really helpful. At the beginning, he helped me a lot when I was planning to do some experiments though I was unable to do the experiments. He referred me to his other students to get supports.

I would like to thank Mr. Tushar Kanti Roy, from Deakin University, for helping during the simulations in MATLAB. He was always willing to help during his busy schedules. His help to develop the simulation models are also unforgettable.

I would like to thank my fellows at Swinburne and Melbourne who made my journey enjoyable during and outside my study.

I would also like to help my family members who always supported me throughout my life. I would not be able to come in Australia without their continuous support.

At the end, I am grateful to Swinburne University of Technology for providing me the resources to conduct the research and waving my tuition fees for the whole course.

Dedicated to my parents and my nephew, Faiyaz Mahmud

Contents

List of Figures

List of Tables

List of Symbols

δ	Rotor angle of the synchronous generator
ω	Running speed of the synchronous generator
ω_0	Synchronous speed of the synchronous generator
D	Damping constant of the synchronous generator
H	Inertia constant of the synchronous generator
P_m	Mechanical input power to the synchronous generator
P_e	Active electrical power output of the synchronous generator
E'_q	Quadrature-axis transient voltage of the synchronous generator
T_{do}	Direct-axis open-circuit transient time constant of the synchronous generator
E_f	Equivalent voltage in the excitation coil of the synchronous generator
E_q	Quadrature-axis voltage of the synchronous generator
x_d	Direct-axis synchronous reactance of the synchronous generator
x'_d	Direct-axis transient reactance of the synchronous generator
x_T	Reactance of the transformer
x_L	Reactance of the transmission line
I_d	Direct-axis currents of the synchronous generator
I_q	Quadrature- axis currents of the synchronous generator
V_s	Infinite bus voltage
Q_e	Reactive power output of the synchronous generator
V_t	Terminal voltage of the synchronous generator
$T'_d = \frac{x'_{d\Sigma}}{x_{d\Sigma}} T_{do}$	Direct-axis transient time constant of the field winding
δ_i	Rotor angle of the ith synchronous generator

ω_i	Rotor speed of the ith synchronous generator
ω_{0i}	Synchronous speed of the ith synchronous generator
H_i	Inertia constant of the ith synchronous generator
P_{mi}	Mechanical power input to the ith synchronous generator
D_i	Damping constant of the ith synchronous generator
P_{ei}	Active power delivered by the ith synchronous generator
E'_{qi}	Quadrature-axis transient voltage of the ith synchronous generator
E_{qi}	Quadrature-axis voltage of the ith synchronous generator
T_{doi}	Direct-axis open-circuit time constant of the ith synchronous generator
E_{fi}	Equivalent voltage in the excitation coil of the ith synchronous generator
x_{di}	Direct-axis synchronous reactance of the ith synchronous generator
x'_{di}	Direct-axis transient reactance of the ith synchronous generator
G_{ii}	Self-conductance of the ith bus
B_{ii}	Self-susceptance of the ith bus
G_{ii}	Conductance between the ith and jth buses
B_{ij}	Susceptance between the ith and jth buses
δ_{ij}	Power angle deviation between the ith and jth buses
I_{di}	Direct-axis currents of the ith synchronous generator
I_{qi}	Quadrature- currents of the ith synchronous generator
Q_{ei}	Reactive power generated by the ith synchronous generator
V_{ti}	Terminal voltage of the ith synchronous generator
x	State vector
u	Control input vector
y	Output vector

$f(x)$	Vector field representing the state relationship to characterize the system
$g(x)$	Vector field represent the state and or parametric relationship with the input
$h(x)$	Scalar function of x
$L_f h(x)$	Lie derivative of $h(x)$ along the vector field $f(x)$
$L_g h(x)$	Lie derivative of $h(x)$ along the vector field $g(x)$
v	Linear control input
A	System matrix for the feedback linearized system
B	Input matrix for the feedback linearized system
n	Order of the system
r	Relative degree of the system
β	Nonlinear coordinate transformation for the hidden states
g_i	Vector field for the ith subsystem associated with the control input
u_i	Control input of the ith subsystem with a dimension m
y_i	Output function of the ith subsystem
$h_i(x)$	Scalar function of x representing the output of the ith subsystem
N	Numbers of subsystem
v_i	Linear control input of the ith subsystem
A_i	System matrix for the ith feedback linearized subsystem
B_i	Input matrix for the ith feedback linearized subsystem
u_i	Original control input of the ith subsystem
G	Plant
C	Controller
d	Disturbance
n	External noise
$S(s)$	Sensitivity function

$T(s)$	Complementary sensitivity function
Δ	Model uncertainty

List of Abbreviations

PSS	Power system stabilizer
LQR	Linear quadratic regulator
SMIB	Single machine infinite bus
SG	Synchronous generator
AVR	Automatic voltage regulator
SISO	Single input single output
MIMO	Multi input multi output
PFBL	Partial feedback linearization

Chapter 1
Introduction

1.1 Background

Power systems are large, complex, and interconnected nonlinear dynamical systems. The continuity of power supply in power systems depends on the stable operation where the stable operations of power systems are usually characterized by different factors. These factors include matching the continuously changing load demands with the generation and maintaining the desired characteristics of major components (e.g., generators) which are connected to power systems. Recently, the modernization of existing power grids plan to operate power systems close to their stability limits which stresses the system as well. The stressed power systems are prone to any disturbance and reduce the overall stability margin.

When the changes in the steady-state conditions are slightly affected, i.e., the deviations of different physical properties are not far away from their stead-state values, these changes can be confined to the equilibrium or steady-state operating points of different physical quantities. In this case, the dynamical models, which are used to characterize the changes, can be represented to their corresponding linearized models. The stability or tendency to restrict the system to similar steady-state values are also called small-signal stability analysis [1]. The small-signal stability problem can be easily tackled by the linear controllers, which are usually designed based on the linearized models of power systems.

When the disturbances or the impact of disturbances are massive, the steady-state values of different physical quantities deviate far away which cannot be captured by the linearized

models of power systems. In most of cases, the physical quantities are settled down to new steady-state values when power systems experience such massive and aggressive disturbances. The disturbances in power networks happen due to short-circuit faults at the terminals of generators, faults in the transmission systems, sudden changes of loads along with sudden losses of power generation units. The stability of power systems associated with large disturbance is called transient stability.

During the large disturbances on any part of power systems, the operational characteristics of power systems are influenced by different devices with different responses [2]. During a large fault, for example, when a fault at the terminal of a generator happens, the reactance of the transmission lines in power system changes significantly. Therefore, the characteristics of power systems cannot be modeled by linear approximations in the case of large disturbances and the linear controllers are not capable to maintain the transient stability as the nonlinearities within the model cannot be tackled [3]. Apart from the nonlinearities within the synchronous generators in power systems, there are more nonlinearities due to interconnections which cannot be properly captured with the linearized models in their simplest forms.

The implementation of nonlinear controllers requires some physical properties or states as feedback. However, all these states are not always measurable and the measurements of these states require some additional efforts, e.g., observer design [4], which is not a cost-effective solution. Moreover, there exist plant uncertainties, external disturbances, and measurement noises which need to be incorporated into the controller design process to ensure the robustness. This thesis aims to design a novel robust feedback linearizing H_∞ controller for both single machine and multimachine power system to enhance the transient stability.

1.2 Motivations for the Proposed Research

The motivations for the proposed research are summarized in the following

- The huge amount of power transfer through existing transmission resources stresses the system and therefore, the system requires extra damping especially under large disturbances.
- The parameters of the power systems are not exactly known and some parameters vary with changes in operational characteristics.
- Linear controllers which are currently being used, cannot capture all nonlinearities within the power system model and the robust linear controllers require interconnection information. Moreover, the external disturbances and measurement noises cannot be modeled accurately during the linearization.
- The nonlinearities within the power system model need to be considered in order to enhance the transient stability under large disturbances as well as changes in operating points.

1.3 Problem Statement for the Proposed Thesis

Based on the above motivations, this thesis aims to solve the following problems to enhance the transient stability of power systems

- It is essential to design robust controller which is independent of operating points and provides robustness against parametric uncertainties along with external disturbances and measurement noises.
- The controller needs to be designed in such a way that it outperforms the existing controllers.

- The controller needs to be designed in a generalized way so that it has the ability to enhance the transient stability of power systems with both single machine and multi machines.

1.4 Contributions of this Thesis

The main contribution of this research is summarized in the following

- Design of a robust nonlinear feedback linearizing H_∞ mixed-sensitivity loop shaping controller for a single machine infinite bus (SMIB) system.
- Performance evaluation of a robust nonlinear feedback linearizing H_∞ mixed-sensitivity loop shaping controller on a SMIB system.
- Design of a robust nonlinear feedback linearizing H_∞ mixed-sensitivity loop shaping controller for a multimachine power system.
- Performance evaluation of a robust nonlinear feedback linearizing H_∞ mixed-sensitivity loop shaping controller on a multimachine power system.

The performance of the proposed controller is evaluated through simulation results where all simulations are conducted in MATLAB/SimPowerSystems by considering different operating conditions.

1.5 Thesis Outline

This section provides an outline of the overall content of the thesis as pointed in the following **Chapter 1** is used to provide a general background about the subject area. This chapter also includes the main motivations of the proposed research, problem statement, and the main contribution of this thesis.

Chapter 2 includes the dynamical modeling of key power system components which are used to design the controller. This chapter also provides an overview of the transient stability and excitation control. Finally, this chapter provides an extensive literature survey on the excitation control of both single machine and multimachine power system identify the open problem.

Chapter 3 presents a brief overview of the feedback linearization scheme for both single input single output (SISO) and multi-input multi-output (MIMO) systems as these are equivalent to the single machine infinite bus (SMIB) and multimachine power systems, respectively. This chapter also discusses about the H_∞ mixed-sensitivity loop shaping controller design for a linear system by considering the effects of parameter variations, external disturbances, and measurement noises.

Chapter 4 presents the design of a robust nonlinear feedback linearizing H_∞ mixed-sensitivity loop shaping controller for SMIB system. The performance of the designed robust nonlinear feedback linearizing H_∞ mixed-sensitivity loop shaping controller is evaluated on a SMIB system and compared with the existing power system stabilizer (PSS) and LQR-based feedback linearizing controller under different operating conditions.

Chapter 5 presents the design of a robust nonlinear feedback linearizing H_∞ mixed-sensitivity loop shaping controller for a multimachine power system. In this chapter, the performance of the designed robust nonlinear feedback linearizing H_∞ mixed-sensitivity loop shaping controller is evaluated on a multimachine power system and compared with the existing PSS and LQR-based feedback linearizing controller under different operating conditions.

Chapter 6 highlights the conclusions from the research along with some further directions for future research.

Chapter 2

Transient Stability Enhancement by Excitation Control of Synchronous Generator

2.1 Introduction

The aim of this thesis is to design a robust feedback linearizing H_∞ controller to enhance the transient stability of the power system under different operating conditions. The controller design requires mathematical models which represent the dynamic characteristics of the power systems in practical operation. Therefore, this chapter starts with the modeling of single machine and multimachine power systems for transient stability analysis and enhancement of the systems. It then introduces the basic concepts of power system transient stability and its enhancement by excitation control, followed by an extensive literature review on the state-of-the-arts controller designs for enhancing the transient stability of both single and multimachine power systems. By analysing the literature, the limitations of the existing results are identified and the solutions are proposed to overcome these limitations.

The remainder of this chapter is as follows. Section 2.2 introduces the dynamical model of a single machine power system, known as the single machine infinite bus (SMIB) system, while Section 2.3 presents the dynamical model for a multimachine power system. Based on the dynamical models in Section 2.2 and Section 2.3, Section 2.4 introduces the concept of power

system transient stability and excitation control for transient stability enhancement. Section 2.5 discusses the performance and difficulties of excitation control. Section 2.6 provides an extensive literature survey of the existing results on the design of excitation controllers for transient stability enhancement. Section 2.7 identifies the open problems in the existing results surveyed in Section 2.6 and presents a proposal for solving the open problems. Section 2.8 concludes the chapter by a brief summary.

2.2 Modeling of Single Machine Infinite Bus System

The simplest model of the power system is the connection of a synchronous generator to an infinite bus through transmission lines and transformers. In power engineering, this simple model is known as the single machine infinite bus (SMIB) system shown in Fig. 2.1.

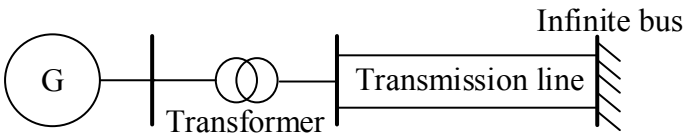

Fig. 2.1. A SMIB system

The synchronous generator (SG) in this model is a rotating electrical machine with its rotor driven by prime mover and magnetized by the field excitation. It converts the mechanical input power P_m from the prime mover to the electrical output power P_e from its stator. The rotor speed ω determines the electrical output frequency. When ω equals the synchronous speed ω_0,

the frequency is 50 Hz (60 Hz in America), therefore ω_0 is the desired rotor speed. The dynamics of SG speed ω can be represent by [1]

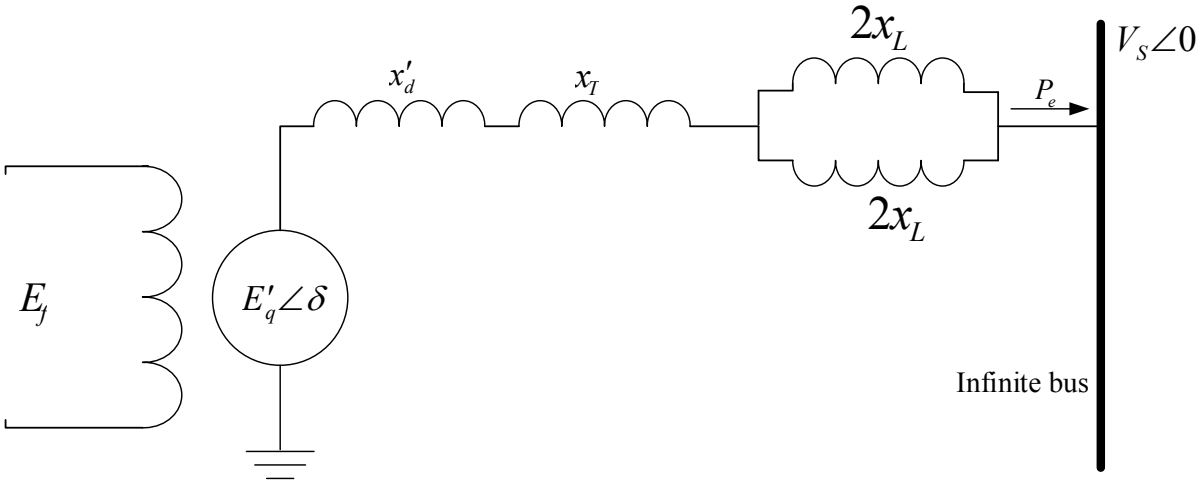

Fig. 2.2. An equivalent circuit diagram of the SMIB system with an excitation coil

$$\dot{\delta} = \omega - \omega_0 \tag{2.1}$$

$$\dot{\omega} = -\frac{D}{2H}(\omega - \omega_0) + \frac{\omega_0}{2H}(P_m - P_e) \tag{2.2}$$

where δ is the rotor rotation angle of the SG, ω is the running speed of the generator, ω_0 is the synchronous speed of the SG, H is the inertia constant, D is the damping constant, P_m is the mechanical input power to the SG, and P_e is the active electrical power output of the SG.

The SG internal voltage E'_q and the rest of the SMIB system in Fig 2.1 form an equivalent electrical circuit shown in Fig 2.2, where x'_d is the transient reactance of SG, x_T and x_L are respectively the reactances of the transformer and transmission line, E_f is the voltage of the field excitation applied to the rotor winding, and V_s is the infinite bus voltage.

The dynamics of E'_q can be described as

$$\dot{E}'_q = \frac{1}{T_{do}}\left(E_f - E_q\right) \tag{2.3}$$

where E_q is the quadrature-axis voltage and T_{do} is the direct-axis open-circuit transient time constant of SG.

As seen from equation (2.3), the excitation voltage E_f is related to the transient voltage E'_q which is in turn related to the steady-state voltage E_q and E_q is related to the output power P_e of SG. In steady state operation, the voltage, current and power variables in the equivalent circuit of Fig. 2.2 are related by the following (phasor domain) algebraic equations [1]

$$E_q = \frac{x_{d\Sigma}}{x'_{d\Sigma}} E'_q - (x_d - x'_d) I_d \tag{2.4}$$

$$I_d = \frac{E'_q}{x'_{d\Sigma}} - \frac{V_s}{x'_{d\Sigma}} \cos\delta \tag{2.5}$$

$$I_q = \frac{V_s}{x'_{d\Sigma}} \sin\delta \tag{2.6}$$

$$P_e = \frac{V_s E'_q}{x'_{d\Sigma}} \sin\delta \tag{2.7}$$

$$Q_e = \frac{V_s E'_q}{x'_{d\Sigma}} \cos\delta - \frac{V_s^2}{x_{d\Sigma}} \tag{2.8}$$

where $x_{d\Sigma} = x_d + x_T + x_L$, $x'_{d\Sigma} = x'_d + x_T + x_L$, x_d is the direct-axis synchronous reactance of SG, I_d and I_q are the direct- and quadrature-axis currents of SG respectively, P_e and Q_e are the active and reactive power of SG, respectively.

Using the above algebraic equations in (2.1)-(2.3) gives

$$\dot{\delta} = \omega - \omega_0 \tag{2.9}$$

$$\dot{\omega} = -\frac{D}{2H}(\omega - \omega_0) - \frac{\omega_0}{2H}P_m - \frac{\omega_0}{2H}\frac{V_s E'_q}{x'_{d\Sigma}}\sin\delta \tag{2.10}$$

$$\dot{E'_q} = \frac{1}{T'_d}E'_q + \frac{1}{T_{do}}\frac{(x_d - x'_d)V_s}{x'_{d\Sigma}}\cos\delta + \frac{1}{T_{do}}E_f \tag{2.11}$$

where $T'_d = \frac{x'_{d\Sigma}}{x_{d\Sigma}}T_{do}$ is the time constant of the field winding. Equations (2.9)-(2.11) give a complete dynamical model of a SMIB system, which is commonly used in the literature for the analysis and control of transient stability of SMIB system.

2.3 Modeling of Multimachine Power System

A multimachine power system consists of a number of SMIB systems which are interconnected to form a complex power system. For a system with N machines, the dynamics of the ith machine can be represented exactly the same as that of an SMIB system [1].

The dynamics of the ith SG is given by [1]

$$\dot{\delta}_i = \omega_i - \omega_{0i} \tag{2.12}$$

$$\dot{\omega}_i = \frac{D_i}{2H_i}(\omega_i - \omega_{0i}) + \frac{\omega_{0i}}{2H_i}(P_{mi} - P_{ei}) \tag{2.13}$$

where $i = 1, 2, 3, \cdots, N$, δ_i is the rotor angle of the ith SG, ω_i is the rotor speed of the ith SG, ω_{0i} is the synchronous speed of the ith SG, H_i is the inertia constant of the ith SG, , D_i is the

damping constant of the ith SG, P_{mi} is the mechanical power input to the ith SG, and P_{ei} is the active power delivered by the ith SG.

The electrical dynamics of the ith SG is given by [1]

$$\dot{E'_{qi}} = \frac{1}{T_{doi}}\left(E_{fi} - E_{qi}\right) \tag{2.14}$$

where E'_{qi} is the quadrature-axis transient voltage of the ith SG, E_{qi} is the quadrature-axis voltage of i^{th} SG, T_{doi} is the direct-axis open-circuit time constant of the ith SG, and E_{fi} is the equivalent voltage in the excitation coil of the ith SG.

Similar to SMIB system, the electrical variables of the ith SG are related by the following set of algebraic equations

$$E_{qi} = E'_{qi} - (x_{di} - x'_{di})I_{di} \tag{2.15}$$

$$I_{di} = -E'_{qi}G_{ii} - \sum_{\substack{j=1 \\ j\neq i}}^{n} E'_{qj}B_{ij}\cos\delta_{ij} \tag{2.16}$$

$$I_{qi} = E'_{qi}G_{ii} + \sum_{\substack{j=1 \\ j\neq i}}^{n} E'_{qj}B_{ij}\sin\delta_{ij} \tag{2.17}$$

$$P_{ei} = E'^{2}_{qi}G_{ii} + E'_{qi}\sum_{\substack{j=1 \\ j\neq i}}^{n} E'_{qj}B_{ij}\sin\delta_{ij} \tag{2.18}$$

$$Q_{ei} = -E'^{2}_{qi}G_{ii} + E'_{qi}\sum_{\substack{j=1 \\ j\neq i}}^{n} E'_{qj}B_{ij}\cos\delta_{ij} \tag{2.19}$$

where x_{di} is the direct-axis synchronous reactance of the ith SG, x'_{di} is the direct-axis transient reactance of the ith SG, G_{ii} and B_{ii} are the self-conductance and self-susceptance of the ith

bus, respectively, G_{ij} and B_{ij} are the conductance and susceptance between the ith and the jth buses respectively, $\delta_{ij} = \delta_i - \delta_j$ is the power angle deviation between the ith and the jth buses, I_{di} and I_{qi} are direct- and quadrature-axis currents of the ith SG respectively, P_{ei} and Q_{ei} are the active and reactive powers generated by the ith SG.

Using these algebraic equations in (2.12)-(2.14) gives

$$\dot{\delta}_i = \omega_i - \omega_{0i} \tag{2.20}$$

$$\dot{\omega}_i = \frac{D_i}{2H_i}(\omega_i - \omega_{0i}) + \frac{\omega_{0i}}{2H_i}P_{mi} - \frac{\omega_{0i}}{2H_i}\left(E_{qi}'^2 G_{ii} + E_{qi}' \sum_{\substack{j=1 \\ j\neq i}}^{n} E_{qj}' B_{ij} \sin\delta_{ij}\right) \tag{2.21}$$

$$\dot{E_{qi}'} = -\frac{1+(x_{di}-x_{di}')B_{ii}}{T_{doi}}E_{qi}' + \frac{x_{di}-x_{di}'}{T_{doi}}\sum_{\substack{j=1 \\ j\neq i}}^{n} E_{qj}' B_{ij}\cos\delta_{ij} + \frac{1}{T_{doi}}E_{fi} \tag{2.22}$$

Equations (2.20)-(2.22) give a complete dynamical model for the ith SG in a multimachine power system commonly used in the literature for the analysis and control of multimachine power systems.

2.4 Power System Transient Stability and Excitation Control

In steady state operation, the SG runs at the synchronous speed, its mechanical power input is equal to its electrical active power output and the rotor acceleration is zero, namely, $\omega = \omega_0$, $P_m = P_e$ and $\dot{\omega}(= d\omega/dt) = 0$. Due to the faults and load changes in the power system, the system equivalent reactance $x_{d\Sigma}'$ in (2.10) may vary significantly. The variations of $x_{d\Sigma}'$ cause significant changes in the electrical output power P_e, which in turn make $P_m \neq P_e$, $\dot{\omega} \neq 0$ and ω runs away from ω_0. As load changes all the time and faults occur every now and then, the

changes of P_e is an inevitable perturbation to the power system. The transient stability of power system is concerned with the behaviour of the rotor speed ω in a few seconds after a major perturbation to P_e. If the ω can return to the synchronous speed ω_0, then the system is said to be transiently stable, otherwise it is transiently unstable.

Transient stability is essentially a power balance problem. To attain transient stability, one must try to make $P_m = P_e$ again as soon as possible after each perturbation to P_e. In power system, the mechanical power input P_m is controlled by the prime mover controller, e.g., turbine governor. Because it is a mechanical process, the closed-loop response of P_m is much slower (often in the order of minutes) than the change of rotor speed ω, which is in the order of seconds. Therefore, P_m is generally not used in transient stability analysis and control of power system and is often assumed to be a constant. This applies to both SMIB systems and multimachine systems.

To maintain transient stability, different methods have been applied to the power systems, often jointly together. For example, changing transmission system configuration, adding additional loads to the bus, and excitation control. Essentially, all these methods try to manipulate the P_e in (2.2) to make ω close to and settle down at ω_0. Most of these methods are not dynamical control except excitation control.

Excitation control is based on the fact that P_e, as shown in (2.10), is a function of SG internal voltage E_q, and E_q, as shown in (2.3), is a function of field excitation voltage E_f. Hence, by properly controlling E_f, the P_e in (2.2) can be controlled to stabilize the rotor speed ω and force it to settle down at the synchronous speed ω_0 after a perturbation to P_e. The plant dynamics for such a control approach is described by (2.9)-(2.11) for SMIB systems. The plant is a third-order nonlinear system with δ, ω and E_q as internal states. The mechanical power input P_m in (2.10), as explained before, is assumed to be a constant. The control variable of the plant is the excitation voltage E_f and the output variable to be stabilized and controlled is the rotor speed ω. Similarly, the plant dynamics of the ith machine in a multimachine system is described by (2.20)-(2.22), with δ_i, ω_i and E_{qi} as the states, E_{fi} as the control variable, ω_i as the plant output to be controller and P_{mi} assumed to be a constant.

It should be pointed out that the excitation control discussed above is used after a major disturbance, such as a fault, in the system to enhance the transient stability. In normal operation, the field excitation is usually controlled by a voltage regulator to keep the output voltage of SG at a desired level, which is a very mature technique and is not the subject of this thesis.

2.5 Performance and Difficulties of Excitation Control

As described in 2.4, the excitation control is to use the field excitation voltage E_f to stabilize the rotor speed ω and to force it to settle down at the synchronous speed ω_0 in a few seconds

after a disturbance to P_e. This is essentially a standard regulation problem and the control performance is typically measured by the time response of ω after a perturbation to the system [5]. The performance measures include: the peak of oscillation, the duration of the oscillation, and the steady-state error (deviation). Designs of the excitation controller should aim to reduce/minimize these. Apart from the time response of ω, the SG's active output power P_e are also used to evaluate the performance [6].

There are a number of difficulties in the design of excitation controller to enhance the transient stability.

1) Nonlinearity: As shown in (2.9)-(2.11) and (2.20)-(2.22), the system dynamic equations are highly nonlinear and hence highly dependent on the operating conditions determined by the initial values of δ and δ_{ij}, and the mechanical input power P_m and P_{mi}.
2) Uncertainty: The parameters of (2.9)-(2.11) and (2.20)-(2.22) may change significantly, especially $x'_{d\Sigma}$ and T'_d which depend on the transmission line reactance x_L. x_L can be quite different before, during and after a fault, which may change $x'_{d\Sigma}$ and T'_d significantly.

To overcome these difficulties, various excitation controllers have been developed in the literature, which are reviewed in the next section.

2.6 Existing Results on Excitation Control

2.6.1 Existing results for SMIB system

The concept of using excitation control to enhance the transient stability of SMIB system was introduced in [7] and then generalized in [8]. It uses the linearized model of power system to design the linear controller that damps the low-frequency oscillations in power system. The main idea of [7, 8] is to provide additional damping torque into the system through the exciter of SG. This approach has been expanded and refined over the years, and is now a well-established approach for designing the linear excitation controllers in power system [9], [10]. Power system stabilizer (PSS) is one of the linear controllers based on this approach, which has been widely adopted by power industries [11]-[14]. There are also other linear excitation controllers developed based on the concept similar to that of PSS. Their main purpose is still to add extra damping into the system [15]. The main limitation of these linear controllers is that their operating regions cannot be expanded far away from the equilibrium point for which they are designed.

There are a lot of ongoing and successful developments for the expansion of operating regions of the excitation controllers. These developments are mainly based on the design of nonlinear excitation controllers for power system [16], [17]. For the excitation control of the SMIB system, several nonlinear control schemes have been proposed. For example, nonlinear backstepping, adaptive backstepping and robust adaptive control [18]-[22], sliding mode

control [23]-[25], passivity-based approach [26], [27], model predictive control [28], [29], and feedback linearization approach [30]-[38].

A nonlinear backstepping approach is proposed in [18] to design the excitation controller for SMIB system. This approach works well when nonlinear model (2.9)-(2.11) is precise, but it cannot deal with the parametric uncertainties in the model. To overcome this difficulty, an adaptive backstepping approach is proposed in [19]-[21] to further improve the performance of the backstepping approach against parametric uncertainties. However, the effect of external disturbances is not considered. A robust adaptive backstepping scheme is proposed in [22] to design an excitation controller for the SMIB system, which considers both parametric uncertainties and external disturbances along with measurement noises. The main problems with the adaptive backstepping as well as robust adaptive backstepping excitation controllers are the selection of adaptation gains. The performance of the controller degrades if these gains are not selected properly.

Sliding mode control schemes have been extensively used to design excitation controllers for the SMIB system. In [23]-[25], sliding mode excitation controllers are used to provide robustness against parametric uncertainties and external disturbances. However, the main limitation of the sliding mode excitation controller is the selection of the sliding surface during the fast transients which are very common in power system operations. Moreover, another well-

known disadvantage of such a sliding mode excitation controller is that it may excite the unmodeled dynamics of the SMIB system due to the chattering phenomenon.

There are also some works on the passivity-based approach to the design of nonlinear excitation controller for the SMIB system, e.g. [26] and [27] have used the total energy of the system to design the excitation controller for the SMIB system. However, it is practically hard and sometime, quite infeasible to calculate the accurate energy of the SMIB system, which makes this approach not so popular in power system applications.

Nonlinear model predictive control scheme allows direct design of excitation control for the SMIB system while optimizing a nonlinear objective function [28], [29]. This approach is useful for the SMIB application as the objective function is quite simple and straightforward. However, the implementation of the model predictive control scheme requires the exact parametric information of the system in order to achieve the desired control objective and the control performance may degrade if the parameters are uncertain.

Feedback linearization scheme has been widely used in power system applications. An exact feedback linearization scheme is used in [30]-[32] to design excitation controllers for the SMIB system. In [30]-[32], the linear controller for the feedback linearized system designed is a linear quadratic regulator (LQR). It uses the rotor angle of SG as a state for its state feedback, which

is generally not directly measurable. Thus, its implementation requires an additional observer or angle measurement device, which is not cost-effective. Moreover, the effect of parametric uncertainties and other disturbances are neglected in [30]-[32]. The direct feedback linearization scheme is used in [33] to design excitation controller for the SMIB system without considering uncertainties within the system. An improved version of direct feedback linearization is proposed in [34, 35] which considers only the parametric uncertainties of the SMIB system rather than the state dependent uncertainties. The direct feedback linearization scheme also suffers from the similar limitation to that of the exact feedback linearization, i.e., the measurement of the rotor angle for the state feedback. A partial feedback linearizing scheme is used in [36, 37] for the SMIB system which uses the speed deviation signal as the output function and hence eliminates the measurement of the rotor angle in the state feedback. However, the partial feedback linearizing scheme in [36, 37] does not consider any uncertainty within the system. An improved robust partial feedback linearizing controller is proposed in [38] where both state dependent and parametric uncertainties are modeled as a structured uncertainty that is explicitly used in LQR design. As the designed LQR controller depends on the pre-estimated structured uncertainty, its performance may degrade if the parameter changes are large. Therefore, the existing feedback linearization plus LQR approach does not have the capability to ensure the robustness of the closed-loop system against the variations in the system parameters, external disturbances, and measurement noises.

2.6.2. Existing results for multimachine power systems

Power systems are large complex system with grid-connected generators. Therefore, it is necessary and important to consider the multimachine power system. The controller design and stability analysis of multimachine power systems are more dependent on the practical operations of power system.

Linear controllers have been extensively used to design excitation controllers for multimachine power systems [39], [40]. Power system stabilizers (PSSs) have been used to stabilize multimachine power systems since the early days of power system operations [41], [42]. As mentioned before, the main problem with the linear excitation controller is the operating region. Apart from this, the linearization of multimachine power systems requires the information for the power system interconnections, and in reality, it is extremely hard to know the exact interconnections of different components of a power system. Moreover, the excitation controllers which are designed for specific interconnections will not work properly for other interconnections [43]. Therefore, the linear excitation controllers do not provide effective damping in multimachine power systems. As discussed before, it is very important to design the excitation controllers in such a way that these controllers are independent of the interconnections along with the operating points. But this cannot be solved using linear controllers.

The limitation of linear excitation controllers in multimachine power systems can be overcome by using nonlinear excitation controllers [44]-[46]. The nonlinear excitation controllers for multimachine power systems are designed using quite similar methods to those of the SMIB system.

In [47], a nonlinear backstepping control scheme is used to design the excitation controller for multimachine power systems, where the backstepping approach allows to use the useful nonlinearities within the system. But the backstepping approach as presented in [47] does not consider the parametric uncertainties and external disturbances and thus, this excitation controller is unable to provide robustness against these factors. In [48]-[50], adaptive backstepping is used to deal with the parametric uncertainty problems in the excitation control of multimachine power systems. But these works have not considered the external disturbances though these disturbances significantly affect the performance of the system. A robust adaptive backstepping approach is used in [51] to design the excitation controller for the multimachine power system. It considers the effects of both parametric uncertainties and external disturbances, including the measurement noises. However, all these backstepping controllers contain a lot of gain parameters which directly affect the overall performance and are difficult to choose in practice. Improper selection of these gains slows down the parameter estimation of these excitation controllers, which significantly increase the response time of these controllers to large external disturbances.

Sliding mode excitation controllers avoid the calculation of lots of gain parameters while providing robustness against parametric uncertainties and excitation disturbances in multimachine power systems [52]-[54]. But their performance strictly depends on the sliding surface. Though the selection of sliding surface is quite simple and straightforward for the SMIB system, it is extremely difficult for large-scale complex power systems due to the huge interconnections and more complicated changing characteristics of transient responses. Moreover, the inherent chattering phenomenon of sliding mode techniques may excite the unmodeled dynamics of the system, which is undesirable.

Though the passivity-based approach is mainly used for SMIB system, there are some literature on the excitation control of multimachine power systems [55], [56]. The main concept of the passivity-based approach is to utilize the total energy of the power system and provide damping in the system through excitation controller so that the energy remains finite in the steady-state [55], [56]. The accuracy of this excitation control scheme heavily relies on the calculation of the total energy for power systems. This total energy is easier to calculate for the SMIB system but quite impossible for the large-scale multimachine power systems. Therefore, the applicability of this method in real-world power system applications is questionable.

Nonlinear model-based predictive control schemes are very useful to design excitation controllers for multimachine power systems as these techniques directly allow to design

controllers by optimizing a nonlinear cost function [57], [58]. The cost function is often quite complicated for multimachine power systems, and sometimes, it takes too long to converge to its optimal solution. However, the power system stability needs to be ensured within a specific timeframe. Moreover, these model predictive approaches do not guarantee the robustness against parametric uncertainties.

Feedback linearization schemes have been extensively used to design excitation controllers for multimachine power systems [59]. There are three different types of feedback linearization which have been primarily used to design excitation controllers. These feedback linearization approaches are exact, direct, and partial feedback linearization. There are several advantages of using feedback linearization for multimachine power systems. The main advantage is that these approaches decouple the multimachine power system based on the number of machines within the system [60]. Another main advantage is the transformation of the nonlinear model into linear model which is independent of operating points and allows to use linear approaches to design the linear control input [60]. Most of the existing feedback linearization techniques for multimachine power systems use LQR-based approach to design the linear control inputs. The LQR controller uses the states of the feedback linearized system for feedback. However, all the states of feedback linearized systems (especially for the exact and direct feedback linearization) are not measurable and require state observers [61], [62]. The design and implementation of the state observers for nonlinear excitation controllers are not a cost-

effective way though these can be eliminated by using partial feedback linearization [6], [63]. Most of these feedback linearization schemes are not robust against parametric uncertainties as these approaches are highly dependent on the precision of the system parameters. Though some efforts have been made recently to ensure the robustness of these feedback linearizing controllers, these controllers still use the states as feedback, which introduces more noises into the system [92], [93]. The effects of noises can be reduced by using an output feedback controller in conjunction with partial feedback linearizing controller.

2.7. The Open Problem in the Existing Results and Proposed Solutions

2.7.1 The open problem

The previous section has provided an extensive literature review of the existing results on the excitation control of SMIB and multimachine power systems for transient stability enhancement. The review has shown that despite the large amount of works on this important topic of power system, the issue of robustness of the excitation controllers to the model uncertainties, external disturbances and measurement noises has not been fully studied and resolved. There is still a pressing need to develop practically useful excitation controllers with good performance and robustness to resolve this important issue.

2.7.2 Proposed solutions to the open problem

To provide a solution to the open problem as presented in the previous subsection, this thesis will develop a feedback linearizing H_∞ controller for the excitation control of SMIB system. For this purpose, the SMIB system will be linearized using feedback linearization to make the linearized system independent of operating points. The H_∞ mixed-sensitivity loop shaping control will then be applied to the feedback linearized system to provide the robustness against parametric uncertainties, external disturbances, and measurement noises. The partial feedback linearization will be used to avoid using the rotor angle, which is hard to measure, and to enable using the speed deviation as the output feedback. Because the speed deviation is the derivative of the rotor angle, it introduces more damping into the system to enhance transient stability. Different from the rotor angle, the speed deviation can be easily obtained from the speed measurement which is standard on the SGs in power systems and readily available in practice. The above described approach will also be applied to the multimachine power system to develop feedback linearizing H_∞ controller for the excitation control of multimachine system to enhance transient stability and robustness of the system.

2.8. Chapter Summary

This chapter has introduced the models of single machine and multimachine power systems for transient stability analysis and enhancement. It has also introduced the basic concept of excitation control for transient stability enhancement of power system, the performance measures and difficulties in excitation control. After an extensive literature review of the

existing results on the excitation controller design, this chapter has identified the open problem in the literature and proposed the solutions to resolve the open problem in the remainder of the thesis.

Chapter 3

Fundamentals of Feedback Linearization and H_∞ Mixed-Sensitivity Controller Design

3.1 Introduction

This chapter summarizes the controller design methods used in the thesis. It beings with the feedback linearization of both single-input and single-output (SISO) and multi-input multi-output (MIMO) nonlinear systems, and then introduces the basic ideas of robust controller design using H_∞ mixed-sensitivity minimization.

The organization of this chapter is as follows. Section 3.2 provides a brief overview of the feedback linearization technique for a SISO system and a MIMO system. Section 3.3 provides a brief overview of H_∞ mixed-sensitivity loop-shaping controller design. Section 3.4 summarizes the chapter.

3.2 Feedback Linearization

Traditionally, linear controllers are widely used in different applications including power systems. A linear controller is generally designed using the linear model of a plant, which is often obtained by linearizing the inherently nonlinear plant model around a specification operating point. As a result, the linear controller often depends on the operating points of the plant, and the performance may degrade significantly when the operation condition changes, and may even destabilize the closed-loop system. Feedback linearization is an effective method, developed in control theory, to overcome this problem for a class of feedback linearizable plants.

3.2.1 Feedback linearization of SISO system

The general form of a nonlinear system can be written as

$$\dot{x} = f(x) + g(x)u \tag{3.1}$$

$$y = h(x) \tag{3.2}$$

where x is the state vector with dimension n, $f(x)$ is an n-dimension vector field representing the nonlinear relationships of the states, $g(x)$ is another n-dimensional vector field containing the parametric as well as state information of the system associated with the control input, u represents the control input of the system with the dimension $m \leq n$ and $m = 1$ for an SISO system, y is a scalar variable representing the output of the nonlinear system, and $h(x)$ is a scalar function describing the nonlinear relationship of the system output and the sates. All the variable in the above are time function.

Assume the system (3.1)-(3.2) satisfies the conditions gives in [64]. Then using the feedback linearization technique [64], the system model (3.1) can be written as the following feedback linearized system

$$\dot{z} = Az + Bv \tag{3.3}$$

where

$$z = \begin{bmatrix} z_1 \\ z_2 \\ \vdots \\ z_r \end{bmatrix} = \begin{bmatrix} \varphi \\ \varphi_2 \\ \vdots \\ \varphi_r \end{bmatrix} = \begin{bmatrix} h(x) \\ L_f h(x) \\ \vdots \\ L_f^{r-1} h(x) \end{bmatrix}, A = \begin{bmatrix} 0 & 1 & 0 & \cdots & 0 \\ 0 & 0 & \ddots & \ddots & \vdots \\ \vdots & \vdots & \ddots & \ddots & 0 \\ \vdots & \vdots & \vdots & \ddots & 1 \\ 0 & \cdots & \cdots & \cdots & 0 \end{bmatrix}_{r \times r}, B = [0 \quad 0 \quad \cdots \quad 1]^T,$$

and v is the linear control input which can be generated by any linear control law. This liner control v is related to the original system input u by

$$v = L_f^r h(x) + L_g L_f^{r-1} h(x) u, \tag{3.4}$$

where $L_f h(x)$ is the Lie derivative of $h(x)$ along the vector field $f(x)$, $L_g h(x)$ is the Lie derivative of $h(x)$ along the vector field $g(x)$, and r is the relative degree of the system.

If the lie derivative of the function $L_f^{r-1}h(x)$ along the vector field $g(x)$ is not equal to zero then it is said that the system relative degree r.

The linear control input v can be designed based on the linear model (3.3). In this thesis, the H_∞ mixed-sensitivity loop-shaping method is used to design this linear control, which will be presented in section 3.4.

The controller design for the feedback linearized system (3.3) is straightforward when the relative degree of the nonlinear system equals the order of the system, i.e., $r = n$. In this case, the feedback linearized system (3.3) has the order n and is called the exactly linearized. Knowing v, the original control input u of the original system can be obtained from (3.4) as

$$u = \frac{v - a(x)}{b(x)}, \tag{3.5}$$

where $a(x) = L_f^n h(x)$ and $b(x =) L_g L_f^{n-1} h(x)$ as $r = n$.

When the relative degree r of the system is less than the order of the system n, the feedback linearized system (3.3) has the order $r < n$, and is called a partially linearized system. In this case, there are $n - r$ states of the original system (3.3)-(3.2) which are not transformed by the feedback linearization into the state of (3.3). These hidden states are uncontrollable by the linear control v. To stabilize the original system (3.1)-(3.2) using v, these hidden states must be internally stable. Denote β the hidden state vector, then the dynamics of β can be written as

$$\dot{\beta} = q(0, \beta), \tag{3.6}$$

with $q(0, \beta) = L_f \beta$. The subsystem (3.6) must be stable for the linear control v to stabilize the original system (3.1)-(3.2) [64]. If (3.6) is indeed stable, then the control input u to the original system (3.1) can be obtained from (3.4) as shown below

$$u = \frac{v - a(x)}{b(x)}, \tag{3.7}$$

where $a(x) = L_f^r h(x)$ and $b(x) = L_g L_f^{r-1} h(x)$ with $r < n$.

3.2.2 Feedback linearization of MIMO system

An MIMO system is usually the combination of multiple SISO systems to form a large-scale complex system. For example, when multiple SMIB (SISO) systems are connected together, a multimachine power (MIMO) system will be formed. In this case, each SISO system can be considered as a subsystem of the MIMO system. Therefore, the feedback linearization for SISO systems as discussed in the previous section can be easily extended to the MIMO system.

The multimachine power system discussed in section 2.3 is a special form of MIMO nonlinear system. It is nonlinear in the state vectors x but linear in the control inputs u. Such system is called the affine nonlinear system. An affine nonlinear system with N subsystems can be written as

$$\dot{x} = f(x) + \sum_{I=1}^{i=N} g_i(x) u_i \tag{3.8}$$

$$y_i = h_i(x) \tag{3.9}$$

where $i = 1, 2, 3, \cdots, N$, x is the state vector with dimension $n \times N$, where n is the order of each subsystem, $f(x)$ is a vector field with dimension $n \times N$ associated with the state vector x, g_i is the n-dimensional vector field for the ith subsystem associated with the control input, u_i is the control input of the ith subsystem with a dimension m which is usually less than the order of each subsystem, y_i is the output of the ith subsystem, and $h_i(x)$ is a scalar function of the state variables x that generates the output of the ith subsystem. For simplicity, this thesis considers only the MIMO system with one control input and one output in each subsystem. Therefore, the discussion below is confined to such MIMO system.

The feedback linearization decouples the MIMO system into N subsystems with only local variables [65]. Thus, the feedback linearization control can be implemented in a decentralized manner. The dynamical nonlinear model for each subsystem can be written as [65]

$$\dot{x}_i = f_i(x_i) + g_i(x_i)u_i \tag{3.10}$$

$$y_i = h_i(x_i) \tag{3.11}$$

Using feedback linearization technique, the model (3.10) for each subsystem can be written as the following feedback linearized system

$$\dot{z}_i = A_i z_i + B_i v_i \tag{3.12}$$

where

$$z_i = \begin{bmatrix} z_1 \\ z_2 \\ \vdots \\ z_{r_i} \end{bmatrix} = \begin{bmatrix} \varphi \\ \varphi_2 \\ \vdots \\ \varphi_{r_i} \end{bmatrix} = \begin{bmatrix} h_i(x) \\ L_{f_i}h_i(x) \\ \vdots \\ L_{f_i}^{r_i-1}h_i(x) \end{bmatrix}, A_i = \begin{bmatrix} 0 & 1 & 0 & \cdots & 0 \\ 0 & 0 & \ddots & \ddots & \vdots \\ \vdots & \vdots & \ddots & \ddots & 0 \\ \vdots & \vdots & \vdots & \ddots & 1 \\ 0 & \cdots & \cdots & \cdots & 0 \end{bmatrix}_{r\times r}, B_i = [0 \quad 0 \quad \cdots \quad 1]^T,$$

and v_i is the linear control input which can be written as

$$v_i = L_{f_i}^{r_i}h_i(x_i) + L_{gi}L_{f_i}^{r_i-1}h_i(x_i)u_i \tag{3.13}$$

The linear control input for each subsystem can be designed based on the linear model (3.12). In this thesis, this linear control input is designed using H_∞ mixed-sensitivity loop-shaping, to be described in section 3.4, for each subsystem.

When the relative degree of each subsystem is equal to its order, i.e., $r_i = n_i$, the feedback linearized subsystem is called the exactly linearized, and the control input u_i of the ith original subsystem can be obtained from (3.13) as follows

$$u_i = \frac{v_i - a_i(x_i)}{b_i(x_i)} \tag{3.14}$$

where $a_i(x_i) = L_{f_i}^{n_i}h_i(x_i)$ and $b_i(x_i) = L_{gi}L_{f_i}^{n_i-1}h_i(x_i)$ as $r_i = n_i$.

When the relative degree of the ith subsystem is less than its order, i.e., $r_i < n_i$, the feedback linearized subsystem is called partially linearized. Similar to SISO system, the dynamics of $n_i - r_i$ hidden states can be written as [64]

$$\dot{\beta}_i = q_i(0, \beta_i) \tag{3.15}$$

where $q_i(0, \beta_i) = L_f \beta_i$. If the internal dynamics as represented by (3.15) is stable for each subsystem, the original control input u_i of the ith original subsystem can be obtained from (3.13) as follows

$$u_i = \frac{v_i - a_i(x_i)}{b_i(x_i)} \tag{3.16}$$

where $a_i(x_i) = L_{f_i}^{r_i} h_i(x_i)$ and $b_i(x_i) = L_{gi} L_{f_i}^{r_i - 1} h_i(x_i)$ with $r_i < n_i$.

3.3 H_∞ Mixed-Sensitivity Loop Shaping Controller Design

H_∞ mixed-sensitivity loop shaping [66] is a powerful method to design the controllers with good control performance and robustness to the model uncertainties of the plant. It is based on the general closed-loop control system shown in the block diagram of Fig. 3.1.

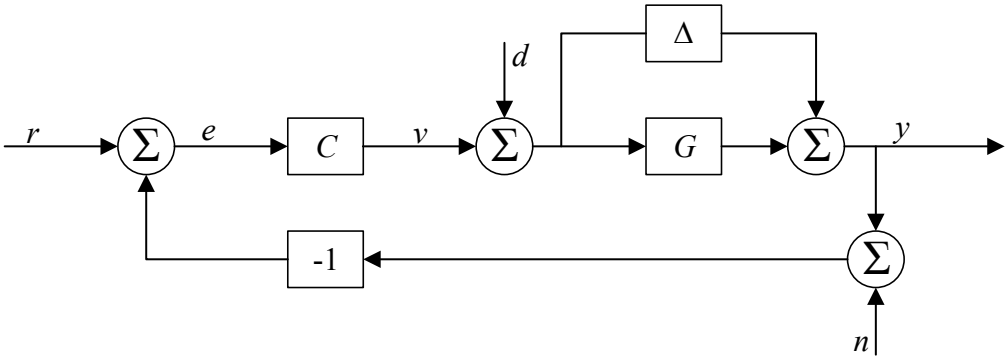

Fig. 3.1. A general feedback control system

In the block diagram, G is the nominal plant (model), Δ is the uncertainty of the nominal plant, C is the controller, y is the plant output to be controlled, r is the command reference, e is the control error, v is the controller output, d is the external disturbance, and n is the output measurement noise.

From the closed-loop system diagram, the following transfer functions can be obtained

$$T(s) = \frac{Y(s)}{R(S)} = \frac{C(s)G(s)}{1+C(s)G(s)} \tag{3.17}$$

$$S(s) = \frac{E(s)}{R(S)} = \frac{1}{1+C(s)G(s)} \tag{3.18}$$

where $Y(s)$, $E(s)$ and $R(s)$ are respectively the Laplace transforms of y, e and r, and $G(s)$ and $C(s)$ are the transfer functions of G and C, respectively. The transfer function $S(s)$ is called the sensitivity function and the transfer function $T(s)$ is called the complementary sensitivity function of the closed-loop system.

The robust H_∞ mixed-sensitivity loop shaping controller is designed by considering the external disturbances and model uncertainties through shaping the sensitivity and complementary sensitivity functions (3.17)-(3.18) of the nominal plant G to guarantee the robustness and control performance of the perturbed closed-loop system in Fig. 3.1 [66].

The stability of the closed-loop system can be guaranteed by the well-known small gain theorem. According to this theorem, the closed-loop system is stable if only and if

$$|\Delta(j\omega)||T(j\omega)| < 1 \tag{3.19}$$

for all ω. In practice, the uncertainties $\Delta(j\omega)$ are usually unknown and it is quite infeasible to design the controller that satisfies the condition (3.19). However, this problem can be avoided by replacing $\Delta(j\omega)$ with the largest anticipated perturbations in the form of the multiplicative perturbations. If the largest anticipated perturbation is represented by $W_\Delta(j\omega)$, then (3.19) can be written as

$$|W_\Delta(j\omega)\,||T(j\omega)| < 1 \tag{3.20}$$

for all ω.

The unstructured uncertainty $\Delta(j\omega)$ generally has high magnitude at low frequencies and low magnitude at high frequencies. Therefore, the largest anticipated perturbation $W_\Delta(j\omega)$ can be represented by a high-pass filter. In the design of the controller $C(s)$ with a complementary sensitivity function $T(s)$, the magnitude of $T(s)$ must satisfy

$$|T(j\omega)| < \frac{1}{|W_\Delta(j\omega)|} \tag{3.21}$$

for all ω. The satisfaction of the condition (3.21) for all $\omega \in [-\infty, \infty]$ can be avoided by converting (3.20) into the condition

$$\|W_\Delta(j\omega)T(j\omega)\|_\infty < 1 \tag{3.22}$$

where $\|\cdot\|_\infty$ represents the H_∞ norm of a transfer function. For a linear system with the transfer function $G(s)$, the H_∞ norm can be represented as $\|G(j\omega)\|_\infty = sup_\omega|G(j\omega)|$ which is also equivalent to $\|G(j\omega)\|_\infty = max_\omega|G(j\omega)|$ if it exists. Therefore, (3.20) holds if and only if (3.22) holds.

The stability conditions (3.21) and (3.22) can also be written as

$$|\Delta(j\omega)| < \frac{1}{|T(j\omega)|} \tag{3.23}$$

$$|\Delta(j\omega)| < \frac{1}{\|T(j\omega)\|_\infty} \tag{3.24}$$

for all ω. It can be seen from (3.24) that a smaller $\|T(j\omega)\|_\infty$ will allow a larger $|\Delta(j\omega)|$, which is the size of the model perturbation. Therefore, the $\frac{1}{\|T(j\omega)\|_\infty}$ is called the stability margin and is used to measure the robustness against plant model perturbations.

The stability margin can be maximized by minimizing $\|T(j\omega)\|_\infty$. However, since $T(j\omega) + S(j\omega) \equiv 1$ for all ω, it is quite infeasible to minimize $\|T(j\omega)\|_\infty$ in controller design as this will result in a larger $\|S(j\omega)\|_\infty$ and consequently, a poor control performance. Because sensitivity function $S(j\omega)$ is the error transfer function of $E(s) = S(j\omega)R(s)$, $\|S(j\omega)\|_\infty$

needs to be sufficiently small in order to reduce the control error $E(s)$. This conflicts with the requirement of small $\|T(j\omega)\|_\infty$ for large stability margin.

This difficulty can be avoided with the H_∞ mixed-sensitivity loop shaping scheme which uses a frequency dependent performance weighting function $W_p(j\omega)$ on $S(j\omega)$ and enforces

$$\left|W_p(j\omega)\right||S(j\omega)| < 1 \tag{3.25}$$

$$|S(j\omega)| < \frac{1}{|(W_p j\omega)|} \tag{3.26}$$

for all ω in the controller design. Since the command reference $R(s)$ is generally a low-frequency signal, $W_p(j\omega)$ can be chosen as a low-pass filter which forces the $S(j\omega)$ resulting from the designed controller $C(s)$ to have high gain at frequency and low gain at low frequency. To avoid the difficulty of validating (3.26) for all $\omega \in [-\infty, \infty]$, it is represented equivalently by

$$\left\|W_p(j\omega)S(j\omega)\right\|_\infty < 1 \tag{3.27}$$

Since the sensitivity function $S(j\omega)$ satisfying (3.27) is a high-pass filter and the complementary sensitivity function $T(j\omega)$ satisfying (3.22) is a low-pass filter, the conflict in controller design can be avoided by properly choosing the weighting functions $W_p(j\omega)$ and $W_\Delta(j\omega)$.

$W_p(s)$ is often called the performance weighting function and $W_\Delta(s)$ the uncertainty weighting function. Their inverse $1/W_p(j\omega)$ and $1/W_\Delta(j\omega)$ set the upper bounds of $S(j\omega)$ and $T(j\omega)$ for all ω, and hence shape the frequency responses of $S(j\omega)$ and $T(j\omega)$, respectively.

The closed-loop stability and good control performance of the system can be attained under the plant model perturbation, external disturbances and output measurement noises if the

conditions (3.22) and (3.27) hold simultaneously. These two conditions can be combined into a single design criterion to form the so-called H_∞ mixed-sensitivity

$$\left\| \begin{matrix} W_p(j\omega)S(j\omega) \\ W_\Delta(j\omega)T(j\omega) \end{matrix} \right\|_\infty = \left\| |W_p(j\omega)\,|S(j\omega)| + |W_\Delta(j\omega)\,|T(j\omega)| \right\|_\infty \tag{3.28}$$

The controller obtained by minimizing (3.28) is often called the H_∞ mixed-sensitivity loop shaping controller because the inverse of the weighting functions $1/W_p(j\omega)$ and $1/W_\Delta(j\omega)$ shape respectively the frequency responses of $S(j\omega)$ and $T(j\omega)$.

Given a linear plant with the transfer function $G(s)$ and the weighting functions $W_\Delta(s)$ and $W_p(s)$, the controller $C(s)$ that minimizes (3.28) can be readily computed using MATLAB command *mixsyn* [66]. The obtained controller $C(s) = mixsyn(G, W_p, [], W_\Delta)$ makes $|T(j\omega)| < \frac{1}{|W_\Delta(j\omega)|}$ and $|S(j\omega)| < \frac{1}{|W_\Delta(j\omega)\,|}$ for all ω and thereby, shaping the frequency responses of $T(j\omega)$ and $S(j\omega)$ specified by $W_\Delta(s)$ and $W_p(s)$.

3.5 Chapter Summary

This chapter has provided a brief introduction to the two controller design methods used later in the thesis. The first method introduced is the feedback linearization technique for both SISO and MIMO systems. It has been shown that the feedback linearization control is quite straightforward when the nonlinear system can be exactly linearized. When the system can only be partially linearized, there will be hidden states and it is essential to analyse the stability of these hidden states in order to use the feedback linearization control. The second method introduced is the technique of H_∞ mixed-sensitivity loop shaping controller. It uses two weighting functions with different frequency responses to describe the control performance and model uncertainties so as to avoid the conflicts in simultaneous minimization of the sensitivity and complementary sensitivity functions. It incorporates the weighted sensitivity

and complementary sensitivity function in a single H_∞ mixed-sensitivity function to design the controller which shapes the frequency responses of the sensitivity and complementary sensitivity functions described by the inverse of the weighting functions. These two powerful control design methods will be used in the next chapters to design high performance controllers for the SMIB and multimachine power systems.

Chapter 4

Feedback Linearizing H_∞ Mixed-sensitivity Controller Design for SMIB System

To provide a solution to the open problem stated in section 2.7, this chapter develops a robust excitation controller for the SMIB system. The development is based on the SMIB system model presented in Chapter 2, the feedback linearization method presented in section 3.2, and the robust H_∞ mixed-sensitivity loop shaping method described in section 3.3. The feedback linearization for the SISO system is used first to obtain the feedback linearized system. The robust H_∞ mixed-sensitivity loop shaping is then used for the feedback linearized model of the SMIB system to obtain a robust linear controller. This robust H_∞ mixed-sensitivity loop shaping controller is incorporated with the feedback linearizing control input in to enhance the robustness against external disturbances, parametric uncertainties and measurement noises. The performance of the designed controller is evaluated on a SMIB system under different operating conditions and compared with the feedback linearization plus LQR controller and the power system stabilizer (PSS) reported in the existing literature.

4.1 Feedback Linearization plus Linear Control of SMIB System

Many strategies have been proposed in the literature for the control of SMIB system. Of these strategies, the feedback linearization plus linear control recently proposed in [35, 67] is very promising. It is based on the dynamical model of the SMIB system discussed in Section 2.2 and recalled below.

$$\dot{\delta} = \omega - \omega_0 \tag{4.1}$$

$$\dot{\omega} = -\frac{D}{2H}(\omega - \omega_0) - \frac{\omega_0}{2H}P_m - \frac{\omega_0}{2H}\frac{V_s E'_q}{x'_{d\Sigma}}\sin\delta \quad (4.2)$$

$$\dot{E}'_q = \frac{1}{T'_d}E'_q + \frac{1}{T_{do}}\frac{(x_d - x'_d)V_s}{x'_{d\Sigma}}\cos\delta + \frac{1}{T_{do}}E_f \quad (4.3)$$

The SMIB system model (4.1)-(4.3) can be written in the following nonlinear state-space equation

$$\dot{x} = f(x) + g(x)u \quad (4.4)$$

$$y = h(x) \quad (4.5)$$

where

$$x = [\delta \quad \omega \quad E'_q]^T,\ f(x) = \begin{bmatrix} \omega - \omega_0 \\ -\frac{D}{2H}(\omega - \omega_0) - \frac{\omega_0}{2H}P_m - \frac{\omega_0}{2H}\frac{V_s E'_q}{x'_{d\Sigma}}\sin\delta \\ \frac{1}{T'_d}E'_q + \frac{1}{T_{do}}\frac{(x_d - x'_d)V_s}{x'_{d\Sigma}}\cos\delta \end{bmatrix},\ g(x) = \begin{bmatrix} 0 & 0 & \frac{1}{T_{do}} \end{bmatrix}^T,$$

$u = E_f$, and $y = h(x) = \omega - \omega_0$

In (4.4) and (4.5), x is the state vector, u is the input variable, y is the output variable, and the system order $n = 3$.

As discussed in section 3.2, if the relative degree of the system corresponding to the output function $h(x)$ is r and $r < n$, then the system can only be partially linearized. The coordinate transformation for such linearization can be represented by the $r - 1$ Lie derivatives of y in the normal form [35, 67] as $z = \left[h(x) \quad L_f h(x) \quad \cdots \quad L_f^{r-1}h(x)\right]^T$ where $L_f h(x) = \frac{\partial h(x)}{\partial x}f(x)$.

If the speed deviation $\omega - \omega_0$ of the synchronous generator is consider as the output of the system, then

$$L_f^{1-1}h(x) = h(x) = \omega - \omega_0 = \Delta\omega \quad (4.6)$$

And

$$L_g L_f^{1-1} h(x) = L_g h(x) = \frac{\partial h(x)}{\partial x} g(x) = 0 \tag{4.7}$$

But

$$L_f^{2-1} h(x) = L_f h(x) = \frac{D}{2H}\Delta\omega + \frac{P_m}{2H}\omega_0 - \frac{\omega_0}{2H}\frac{V_s E_q'}{x_{d\varepsilon}'}\sin\delta \tag{4.8}$$

And

$$L_g L_f^{2-1} h(x) = \frac{\partial\left(L_f h(x)\right)}{\partial x} g(x) = -\frac{\omega_0}{2H}\frac{V_s}{x_{d\varepsilon}'}\sin\delta\frac{1}{T_{do}} \neq 0 \tag{4.9}$$

Since $L_g L_f^{2-1} h(x) \neq 0$ as shown above, it follows from subsection 3.2.1 the relative degree $r = 2$ for the output function. Thus, the relative degree $r = 2 < n = 3$, and the system (4.4) can be partially linearized system with the output $y = \omega - \omega_0$ and synthetic control input v. The input-output mapping from v to y is a double integrator [35, 67]. With the synthetic input v, the system (4.1)-(4.3) can be written as [35, 67]

$$\dot{z}_1 = z_2 = L_f h(x) = \Delta\dot{\omega} = \dot{\omega} \tag{4.10}$$

$$\dot{z}_2 = v \tag{4.11}$$

where

$$v = L_f^2 h(x) + L_g L_f^{2-1} h(x) u, \tag{4.12}$$

$$L_f^2 h(x) = -\frac{1}{2Hx_{d\Sigma}'}\Delta\omega\,\omega_0 V_s E_q' \cos\delta - \frac{D}{2H}\dot{\omega} - \frac{1}{2Hx_{d\Sigma}'}\omega_0 V_s E_q \sin\delta\,,$$

$$L_g L_f^{2-1} h(x) = \frac{1}{2Hx_{d\Sigma}'}\omega_0 V_s \sin\delta\frac{1}{T_{do}}\,,$$

and $\Delta\omega = \omega - \omega_0$ and $\omega_0 = \text{constant}$ have been used to obtain (4.10).

Using the expressions of $L_f^2 h(x)$ and $L_g L_f^{2-1} h(x)$, (4.12) can be written as

$$v = -\frac{1}{2Hx_{d\Sigma}'}\Delta\omega\,\omega_0 V_s E_q' \cos\delta - \frac{D}{2H}\dot{\omega} - \frac{1}{2Hx_{d\Sigma}'}\omega_0 V_s E_q \sin\delta - \frac{1}{2Hx_{d\Sigma}'}\omega_0 V_s \sin\delta\frac{1}{T_{do}}u \tag{4.13}$$

Since $\dot{z}_1 = z_2 = \Delta\dot{\omega} = \dot{\omega}$, (4.11) can be written as

$$\Delta\ddot{\omega} = \dot{z}_2 = v = -\frac{1}{2Hx'_{d\Sigma}}\Delta\omega\,\omega_0 V_s E'_q \cos\delta - \frac{D}{2H}\dot{\omega} - \frac{1}{2Hx'_{d\Sigma}}\omega_0 V_s E_q \sin\delta\,\frac{1}{2Hx'_{d\Sigma}}\omega_0 V_s \sin\delta\,\frac{1}{T_{do}}u \tag{4.14}$$

From (4.14), the control law u for the SMIB system (4.4)-(4.5) can be derived as follows

$$u = \frac{1}{\frac{1}{2Hx'_{d\Sigma}}\omega_0 V_s \sin\delta\frac{1}{T_{do}}}\left(v - \frac{1}{2Hx'_{d\Sigma}}\Delta\omega\,\omega_0 V_s E'_q \cos\delta - \frac{D}{2H}\dot{\omega} - \frac{1}{2Hx'_{d\Sigma}}\omega_0 V_s E_q \sin\delta\right) \tag{4.15}$$

All the variables on the right hand sides of (4.15) are either physically measurable or can be expressed in terms of measured variables [35, 67]. The linear control input v needs to be obtained by using a linear control law for the linearized system represented by (4.10)-(4.11).

Using Laplace transform, the linearized SMIB system (4.10)-(4.11) can be written as

$$\Delta\omega(s) = Z_1(s) = \frac{1}{s^2}V(s) \tag{4.16}$$

where $\Delta\omega(s)$, $Z_1(s)$ and $V(s)$ are the Laplace transforms of $\Delta\omega$, z_1 and v, respectively. This is a single input and single output system (plant) with the transfer function

$G(s) = \frac{1}{s^2}$.

Hence it can be controlled by a linear controller that generates $V(s)$. The controller $V(s)$ is to stabilize $\Delta\omega(s)$ and force $\Delta\omega(s) = 0$, i.e. $\omega = \omega_0$, in steady-state. This is a standard output regulation problem which can be easily solved by the negative feedback of $\Delta\omega(s)$ through a controller with the transfer function $C(s)$, namely

$$V(s) = -C(s)\Delta\omega(s) = C(s)[\omega_0 - \omega(s)] \tag{4.17}$$

where ω_0 and $\omega(s)$ are the Laplace transfer functions of ω_0 and ω, and $\Delta\omega(s) = \omega - \omega_0$ and $\omega_0 = \text{constant}$ have been to obtain (4.17).

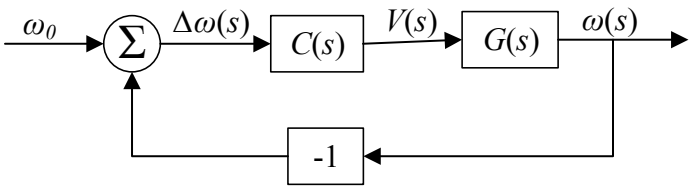

Fig. 4.1. Linear closed-loop control of the feedback linearized SMIB system

The linearized plant (4.16) and the linear controller (4.17) together form a closed-loop system shown in Fig. 4.1. As see from Fig. 4.1, the feedback regulation of $\Delta\omega$ is equivalent to the feedback control of ω with respect a command reference ω_0, where $\omega(s)$ is the output variable to be controlled and the negative feedback variable and $\Delta\omega$(s) is the control error. As discussed in Chapter 3, the sensitivity function $S(s)$ and complementary sensitivity function $T(s)$ for such a closed-loop system are given by

$$S(s) = \frac{1}{1+G(s)C(s)} \tag{4.18}$$

$$T(s) = \frac{G(s)C(s)}{1+G(s)C(s)} \tag{4.19}$$

The controlled output $\omega(s)$ and the control error $\Delta\omega(s)$ are related to the command reference ω_0 by

$$\omega(s) = T(s)\omega_0 \tag{4.20}$$

and

$$\Delta\omega(s) = S(s)\omega_0 \tag{4.21}$$

The feedback linearizing control input (4.15) and the linear control input (4.17) together form a double loop feedback system with the inner feedback linearizing control loop and the outer linear feedback control loop. With a properly designed $C(s)$, the linear feedback control loop renders full control of $\Delta\omega$ towards 0 inn steady state to achieve the desired control objective.

This also guarantees the stability of the internal state δ in (4.1), which becomes unobservable (hidden) from the system output after feedback linearization.

Since $\dot{\delta} = \Delta\omega = \omega - \omega_0$, $\Delta\omega = 0$ in steady state means that δ will be a bounded constant, therefore stable. Thus, the internal state δ of the SMIB system does not affect the overall stability as long as the closed-loop system in Fig. 4.1 is stabilized by the linear controller $C(s)$.

4.2 Analysis of Feedback Linearization of SMIB System with Parametric Uncertainty and Measurement Noise

The above feedback linearization plus linear control scheme and the internal stability analysis are derived from the SMIB system model (4.1)-(4.3). They are based on the assumption that the model is error free and the mechanical input power P_m is a constant, hence the feedback linearization control law (4.15) cancels precisely the system nonlinear dynamics to give the perfectly linearized system (4.10)-(4.11). In practice, this is often invalid. As discussed in Chapter 2, the parameters of (4.1)-(4.3) may change along with operation conditions, also the P_m may drift since it is controlled by separate controller with much slower response. As analysed in this section, these changes will introduce unstructured model perturbation and external disturbance into the linearize system (4.10)-(4.11).

Let ΔD, ΔH, $\Delta H x'_{d\Sigma}$, ΔT_{do} and ΔP_m be the deviations of D, H, $H x'_{d\Sigma}$, T_{do} and P_m from their nominal values, respectively. Then the parameters in (4.13) become

$\frac{D+\Delta D}{2(H+\Delta H)} = m_1 + \Delta m_1$,

$\frac{P_m+\Delta P_m}{2(H+\Delta H)} = m_2 + \Delta m_2$,

$\frac{1}{2(Hx'_{d\Sigma}+\Delta H x'_{d\Sigma})} = m_3 + \Delta m_3$, and

$\frac{1}{(T_{do}+\Delta T_{do})} = m_4 + \Delta m_4$

where

$m_1 = \frac{D}{2H} > 0$, $m_2 = \frac{P_m}{2H} > 0$, $m_3 = \frac{1}{2Hx'_{d\Sigma}} > 0$, and $m_4 = \frac{1}{T_{do}} > 0$ are the nominal parameters of the SMIB system, and

$\Delta m_1 = \frac{\Delta D - \Delta H D/H}{2(H+\Delta H)}$, $\Delta m_2 = \frac{\Delta P_m - \Delta H P_m/H}{2(H+\Delta H)}$, $\Delta m_3 = \frac{\Delta H x'_{d\Sigma}/H x'_{d\Sigma}}{2(Hx'_{d\Sigma}+\Delta H x'_{d\Sigma})}$ and $\Delta m_4 = \frac{\Delta T_{do}/T_{do}}{(T_{do}+\Delta T_{do})}$

are respectively the uncertainties of m_1, m_2, m_3 and m_4, which reduce to zero when $\Delta m_1 = \Delta m_2 = \Delta m_3 = \Delta m_4 = 0$.

With the above defined parameters and parametric uncertainties, the linearized equation (4.18) becomes

$$\Delta\ddot{\omega} = -(m_3 + \Delta m_3)\Delta\omega\,\omega_0 V_s E'_q \cos\delta - (m_1 + \Delta m_1)\dot{\omega}$$
$$-(m_3 + \Delta m_3)\,\omega_0 V_s E_q \sin\delta - (m_5 + \Delta m_5)\,\omega_0 V_s \sin\delta\, u \qquad (4.22)$$

Using (4.9), (4.18) can be simplified as

$$\Delta\ddot{\omega} = v - \Delta m_3 \Delta\omega\,\omega_0 V_s E'_q \cos\delta - \Delta m_1 \dot{\omega} - \Delta m_3\,\omega_0 V_s E_q \sin\delta - \Delta m_5\,\omega_0 V_s \sin\delta \qquad (4.23)$$

and the feedback linearization control input (4.13) for the nominal system can be written as

$$u = \frac{1}{m_3\,\omega_0 V_s \sin\delta m_4}(v - m_3\Delta\omega\,\omega_0 V_s E'_q \cos\delta - m_1\dot{\omega} - m_3\,\omega_0 V_s E_q \sin\delta) \qquad (4.24)$$

where $m_3 m_4 = m_5$.

Substituting the (4.24) into (4.23) gives

$$\Delta\ddot{\omega} = v - \Delta m_3\Delta\omega\,\omega_0 V_s E'_q \cos\delta - \Delta m_1\dot{\omega} - \Delta m_3\,\omega_0 V_s E_q \sin\delta$$
$$-\frac{\Delta m_5\,\omega_0 V_s \sin\delta}{m_5 \omega_0 V_s \sin\delta}(v - m_3\Delta\omega\,\omega_0 V_s E'_q \cos\delta - m_1\dot{\omega} - m_3\,\omega_0 V_s E_q \sin\delta) \qquad (4.25)$$

Define

$R_1 = \omega_0 V_s E'_q \cos\delta$

and

$R_2 = \omega_0 V_s E_q \sin\delta$.

Then (4.24) can be simplified as

$$\Delta\ddot{\omega} = v - \Delta m_3 \Delta\omega R_1 - \Delta m_1 \dot{\omega} - \Delta m_3 R_2 - \frac{\Delta m_5}{m_5}(v - m_3\Delta\omega R_1 - m_1\dot{\omega} - m_3 R_2) \quad (4.26)$$

which can further be simplified as

$$\Delta\ddot{\omega} = vK_1 - \Delta\omega R_1 K_2 - \Delta\dot{\omega}K_3 - R_2 K_4 \quad (4.27)$$

where

$K_1 = 1 - \frac{\Delta m_5}{m_5}$, $K_2 = \Delta m_3 + \frac{\Delta m_5 m_3}{m_5} = K_4$, and $K_3 = \Delta m_1 + \frac{\Delta m_5 m_1}{m_5}$.

Taking the Laplace transform of (4.27) gives

$$s^2\Delta\omega(s) = V(s)K_1 - \Delta\omega(s)R_1K_2 - s\Delta\omega(s)K_3 - R_2K_2 \quad (4.28)$$

which can further be rewritten as

$$\Delta\omega(s) = \frac{1}{s^2 + sK_3 + R_1K_2}(V(s)K_1 - R_2K_2) \quad (4.29)$$

In (4.16) the plant $G(s) = \frac{1}{s^2}$ which is the nominal plant model. In the presence of uncertainty, the these plant is not $G(s) = \frac{1}{s^2}$ but that (4.29). The describe derivation of the these plant from the nominal plant $\frac{1}{s^2}$, we define $\Delta(s) = \frac{(K_1-1)s^2 - sK_3 - R_1K_2}{s^2 + sK_3 + R_1K_2}$ and $K = \frac{K_2}{K_1}$, (4.29) can be simplified to

$$\Delta\omega(s) = \frac{1}{s^2}(1 + \Delta(s))(V(s) - R_2K) \quad (4.30)$$

Comparing (4.30) with (4.16), it can be seen that the parametric changes in the original nonlinear system (4.1)-(4-3) have introduced the unstructured perturbation $\Delta(s)$ and the additional external disturbance $-R_2K$ into the feedback linearized system (4.16). The transfer function $G(s)$ of (4.16) has become $G(s)(1 + \Delta(s))$ and its control input becomes $V(s) - R_2K$. Substituting these into Fig. 4.1 and using $\Delta\omega(s) = \omega(s) - \omega_0$ gives the closed-loop system resulting from parametric changes shown in Fig. 4.2, where a measurement noise $N(s)$ has also been included. In this case, the internal dynamics of the SMIB system is the same as the

nominal system since the dynamics of the hidden state δ given in (4.1) does not include any parameters. Therefore, if the linear controller $C(s)$ can stabilize the perturbed closed-loop system in Fig. 4.2, $\omega = \omega_0$ can be achieved in steady state and the δ will remain stable as discussed in previous section. However, the performance of the closed loop system can be significantly degraded if the controller $C(s)$ is not designed to account for the model perturbation and external disturbance. This is demonstrated in the next section.

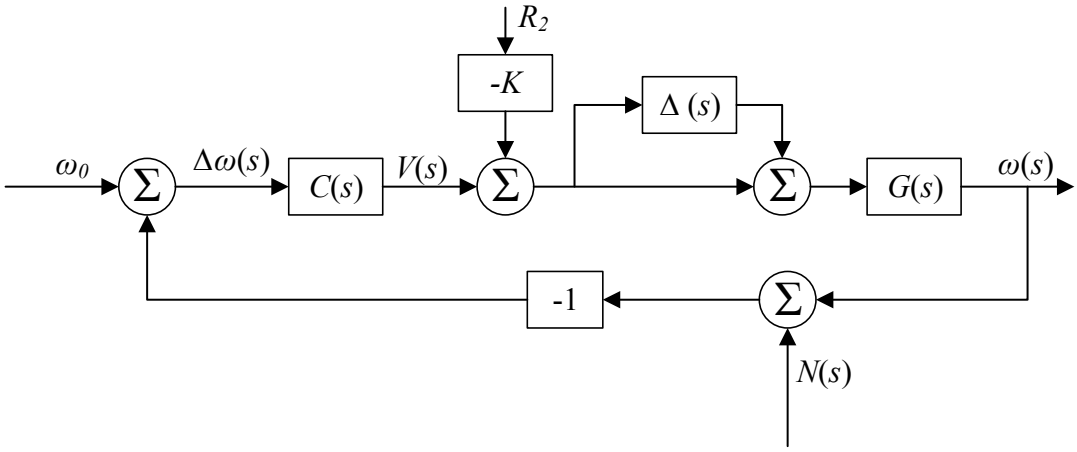

Fig. 4.2. Linear control of the feedback linearized SMIB system with model uncertainties and measurement noises

4.3 Evaluation of Existing Controller under Model Uncertainty and Measurement Noise

Recently, [35] and [67] have used an LQR in conjunction with the feedback linearization law (4.11) to control the SMIB system (4.1)-(4.3). This section examines the performance of this controller under the parametric uncertainties and measurement noises in the system (4.1)-(4.3).

The LQR is of the form

$$v = -Kz = -k_1 z_1 - k_2 z_2 \tag{4.31}$$

where $z_1 = \Delta\omega = \omega(s) - \omega_0$, $z_2 = \dot{z}_1 = \dot{\omega}$, $k_1 = 1$ and $k_2 = 1.732$ which are the best feedback gains gives in [35, 67]. The LQR (4.31) and the feedback linearization law (4.15) are

applied to an SMIB system in Simulink/SimPowerSystems of MATLAB. The SMIB system structure is shown in Fig. 4.3 and the system parameters are given in Appendix-I.

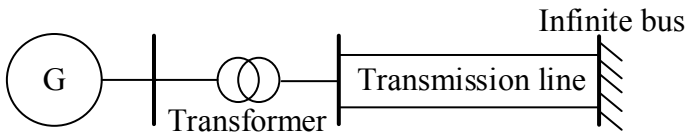

Fig. 4.3. A SMIB test system with parameter details given in Appendix-I

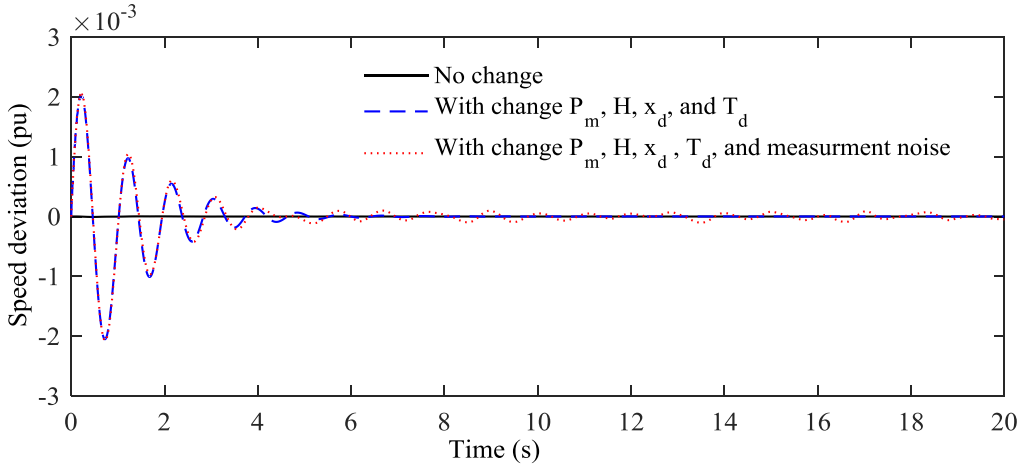

Fig. 4.4. Speed deviation $\Delta\omega$ of the SMIB system with an LQR-based feedback linearizing controller

The speed deviation $\Delta\omega$ of the SMIB system under the control of the LQR-based feedback linearizing controller is shown in Fig. 4.4. When there are no external disturbances or variations in parameters, the synchronous generator operates at the synchronous speed which is evident from the zero speed deviation as presented in Fig. 4.4. However, the speed deviation occurs when some parameters within the SMIB system are varied though the stability is still maintained. The speed deviation becomes continuously oscillating due to the effects of parameters variations and measurement noises. The simulation results are depicted in Fig. 4.4.

As seen from the simulation results, the LQR controller's performance degrades significantly. This is due to the model perturbation and external disturbance introduce by the parameter change as shown in Fig. 4.2. As discussed in Chapter 2, the parameter changes occur during major power grid events, such as short-circuit faults, changes in load demands which is reflected through the changes in mechanical power input P_m. Therefore, the effects of parametric uncertainties, external disturbances, and measurement noises need to be addressed in the design of linear controller. This is considered in the next section.

4.4 H_∞ Mixed-Sensitivity Loop Shaping Controller for SMIB System

As shown in Fig. 4.2, the linearized SMIB system contains an unstructured model perturbation $\Delta(s)$ and an external disturbance $-KR_2$. Let in Fig. 4.2 $d = -KR_2$, $\omega_0 = r$, $\omega = y$ and $\Delta\omega = e$, then the closed-loop system in Fig. 4.2 becomes that of Fig. 3.1. As discussed in Section 3.4, for the uncertain system in Fig. 3.1, an H_∞ mixed-sensitivity loop shaping controller can be designed to achieve good control performance and high robustness to the model perturbation. Such controller can be easily computed using the function "*mixsyn*" in the Robust Control Toolbox of MATLAB. To use the function "*mixsyn*", one needs to select the weighting functions $W_p(s)$ and $W_\Delta(s)$ first.

A classical approach to select the weight functions is to satisfy $\frac{1}{W_p}$ as the high-pass and $\frac{1}{W_\Delta}$ as the low-pass. Based on this approach, the following W_p is chosen for the nominal plant $G(s) = \frac{1}{s^2}$.

$$W_p(s) = \frac{0.52632\ (s+1.9)}{(s+0.0001)} \tag{4.32}$$

The sigma plot (frequency response) of the weighting function $1/W_p(s)$ shown in Fig. 4.5. The selection of this weight function $W_p(s)$ increases low frequency loop gain which in turns ensures better disturbance rejection capability, as $S(s)$ needs to be small at low frequencies.

Here, the gain crossover frequency for the sensitivity function $S(s)$ is made to below the crossover frequency of the desired loop-shape to prevent unwanted reduction in phase margin.

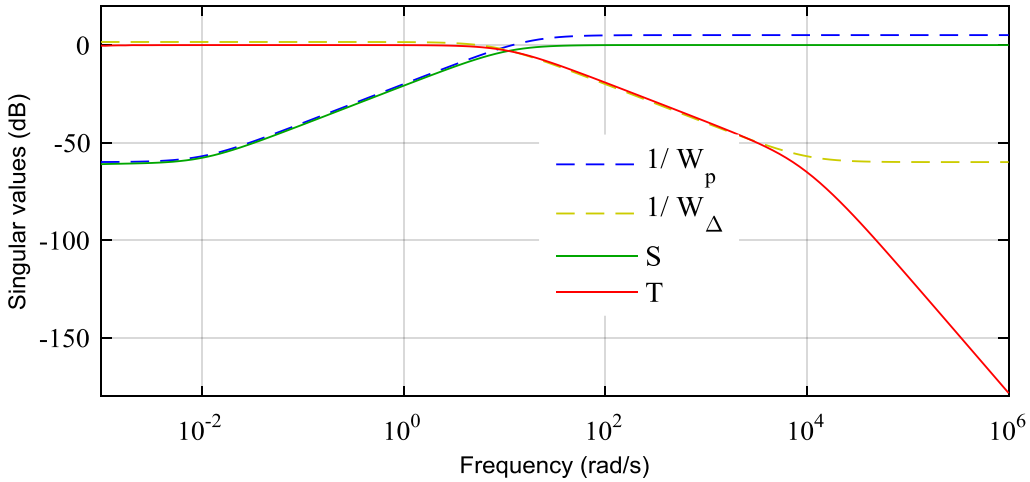

Fig 4.5. Sigma plots of $1/W_p(s)$, $1/W_{\Delta(s)}$, S(s) and $T(s)$ for the designed H_∞ mixed-sensitivity loop shaping controller

As $|W_\Delta(s)\,||T(s)| < 1$ and $\|W_\Delta(s)T(s)\|_\infty < 1$ for all ω, it can be said that the gain magnitude of the unstructured uncertainty $W_\Delta(s)$ is bounded by $1/T(s)$. Therefore, $W_\Delta(s)$ represents the largest size of probable plant perturbation. This uncertainty bound is selected as

$$W_\Delta(s) = \frac{10000\,(s+8.333)}{(s+10^5)} \tag{4.33}$$

The parameters of $W_\Delta(s)$ in (4.33) is chosen in such a way that $T(s)$ is small at high frequency but has sufficient bandwidth to secure fast response. The gain cross over frequency of $W_\Delta(s)$ appends phase lead and thus, maximizes the system's phase margin.

Using the weighting functions in equations (4.32) and (4.33), an H_∞ mixed-sensitivity loop shaping controller is computed by the "*mixsyn*" function in MATLAB. The resultant controller is as follows

$$C(s) = \frac{4.9728\times10^{6}\,(s+\times10^{5})\,(s+0.0001549)(s+0.4.508\times10^{-5})}{(s+9.979\times10^{4})\,(s+6413)\,(s+127.6)\,(s+9.829\times10^{-5})} \quad (4.34)$$

The sigma (frequency response) plots of the $1/W_p(s)$ and $1/W_\Delta(s)$ used to compute the controller (4.34) and the sigma plots of the $S(s)$ and $T(s)$ functions resulting from the controller are shown in Fig. 4.5. As seen in the plots, $S(j\omega)$ and $T(j\omega)$ functions are well and tightly shaped by the weighting functions $W_p(j\omega)$ and $W_\Delta(j\omega)$, respectively.

This linear output feedback controller (4.34) is used in conjunction with the feedback linearizing control law (4.15) to robustly stabilize the SMIB system under different operating conditions. The performance of the designed controller is shown in the next section and compared with the conventional PSS and LQR-based feedback linearizing controller in [35].

4.5. Controller Performance Evaluation

The designed controller is implemented on the SMIB system as shown in Fig. 4.3. The synchronous generator (G) is connected to an infinite bus through a transformer and two parallel transmission line. The details parameters of this SMIB system is provided in Appendix-I.

The excitation control signal of the exciter connected to the SMIB system is modified to implement the designed controller. The implementation block diagram of the design robust feedback linearizing H_∞ mixed-sensitivity loop shaping controller is shown in Fig. 4.6. As shown in Fig. 4.6, the modeling uncertainties are incorporated into the synchronous generator models, and the external disturbances and measurement noises are also incorporated into the implementation process.

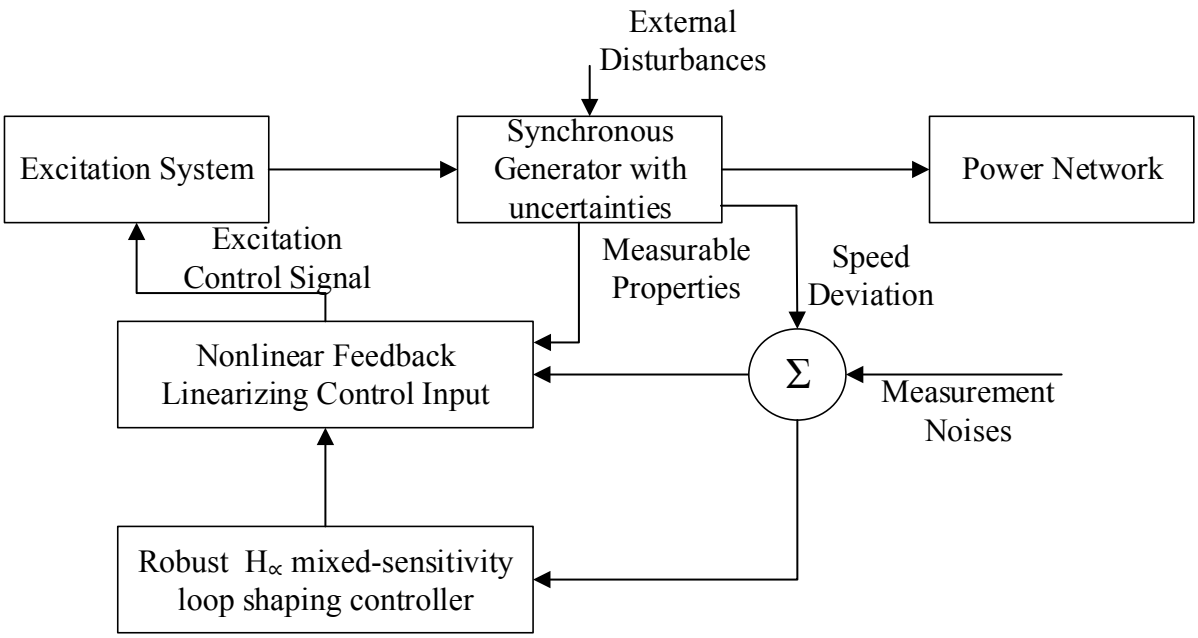

Fig. 4.6. Implementation block diagram of the robust feedback linearizing H_∞ mixed-sensitivity loop shaping controller

Based on the design procedure discussed above and the implementation block diagram, the performance of the designed controller is evaluated by considering different operating conditions. The following case studies are considered to demonstrate the designed feedback linearizing H_∞ mixed-sensitivity loop shaping controller (H_∞-PFBL).

i. Controller performance evaluation in the case of a three-phase short-circuit fault at the terminal of the synchronous generator,
ii. Controller performance evaluation in the case of a three-phase short-circuit fault at the middle of one of the two parallel transmission lines,
iii. Controller performance evaluation in the case of a step change in the mechanical power input to the synchronous generator, and
iv. Controller performance evaluation with changes in system parameters along with the inclusion of external disturbances and measurement noises.

The first three cases are analyzed based on the nominal model of the SMIB system. For these first two cases, the changes in the SMIB system (application of faults) occur at $t = 4.1$ s and sustain for 0.1 s, i.e., till $t = 4.2$ s. For this third case, the change in the mechanical power input occurs at $t = 4.1$ s and the system continues to operate with this change in the mechanical power input. For the last case, the changes are considered from the beginning of the operating, i.e., from $t = 0$ s. In all cases, the performance of the designed controller (H_∞-PFBL) is compared with an existing PSS [1] and a feedback linearizing controller with an LQR approach (LQR-PFBL) [35]. A quantitative analysis has also been include to evaluate the effectiveness of the designed controller in comparison with the PSS and LQR-PFBL. The following subsections provide the details of these case studies.

4.5.1. Case 1: Controller performance evaluation in the case of a three-phase short-circuit fault at the terminal of the synchronous generator

The three-phase short-circuit faults at the terminal of the synchronous generator is considered as the most severe faults in power systems. In this case study, a three-phase short-circuit fault is applied at the terminal of the synchronous generator at $t = 4.1$ s and the fault is cleared $t = 4.2$ s. In power system, the fault with a duration more than 3 cycles (0.06 s for 50 Hz) is considered as the severe fault. Since the applied fault is with a duration of 0.1 s (>(0.06 s), it can be considered as the sever fault. During the faulted period, the terminal voltage of the synchronous generator will be zero which can be seen from Fig. 4.7. Fig. 4.7 clearly shows that that the terminal voltage is zero during the faulted period with any controller. From the definition of stability, it is obvious that the stability problem here is basically the angle stability problem due to the domination of the synchronous generator. Therefore, the impact of this fault will not be severe from the voltage response of the synchronous generator. However, the post-fault

oscillations in the terminal voltage are more with the PSS (red line) while it is still visible with the LQR-PFBL (blue line). But there are no oscillations in the voltage response when the designed H_∞-PFBL (black line) is used.

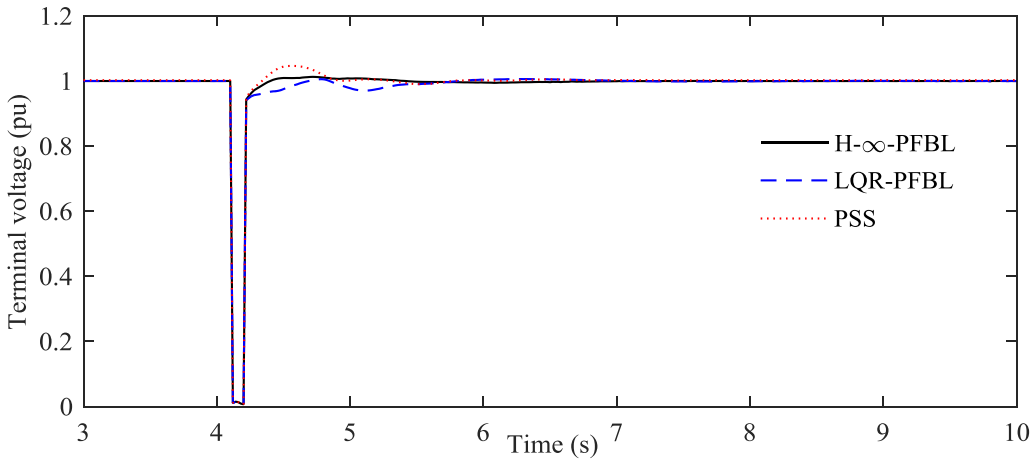

Fig. 4.7. Terminal voltage of the synchronous generator in the case of a three-phase short-circuit fault at the terminal of the synchronous generator

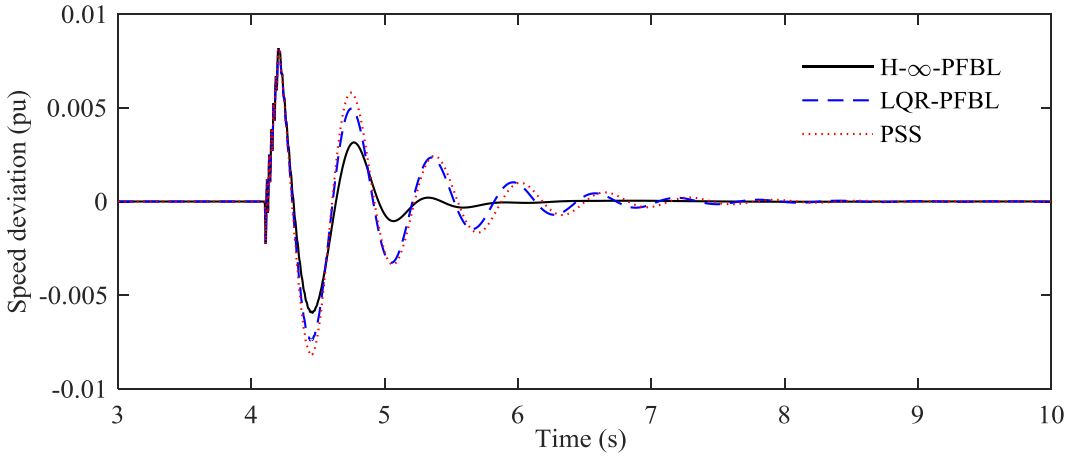

Fig. 4.8. Speed deviation of the synchronous generator in the case of a three-phase short-circuit fault at the terminal of the synchronous generator

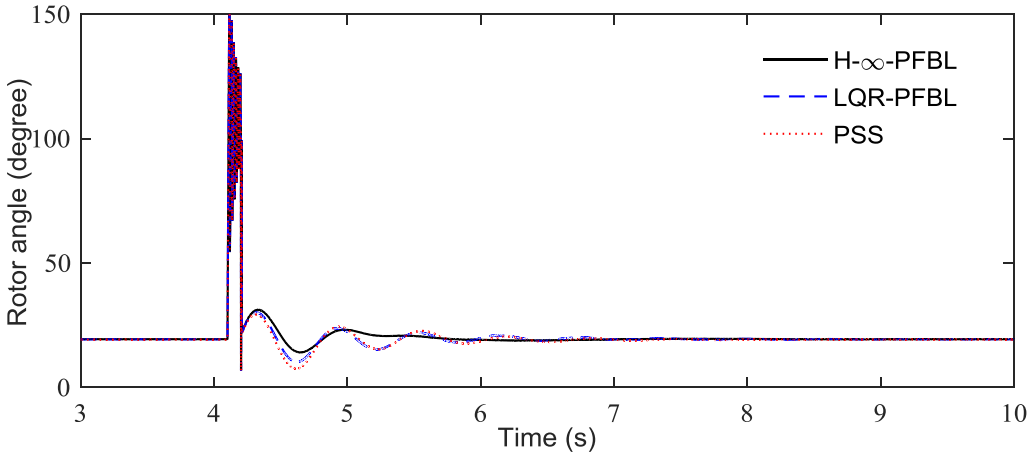

Fig. 4.9. Rotor angle of the synchronous generator in the case of a three-phase short-circuit fault at the terminal of the synchronous generator

Since the control objective is to operate the synchronous generator with synchronous speed, the designed H_∞-PFBL needs to ensure that the synchronous generator is operating at the synchronous speed as soon as the fault is cleared. The operation of the synchronous generator at the synchronous speed is ensured through the zero speed deviation. During the faulted period (from $t = 4.1$ s to $t = 4.2$ s), the speed deviation will be disturbed with any controller. Fig. 4.8 shows the speed deviation of the synchronous generator from where it can be seen that the speed deviation is more oscillating with larger overshoots (red line) when the PSS is used. The amplitudes of the oscillations are quite less when LQR-PFBL (blue line) is used though the settling time is quite similar to that of the PSS. But the oscillations are less with faster settling time when the designed H_∞-PFBL (black line) is in operation.

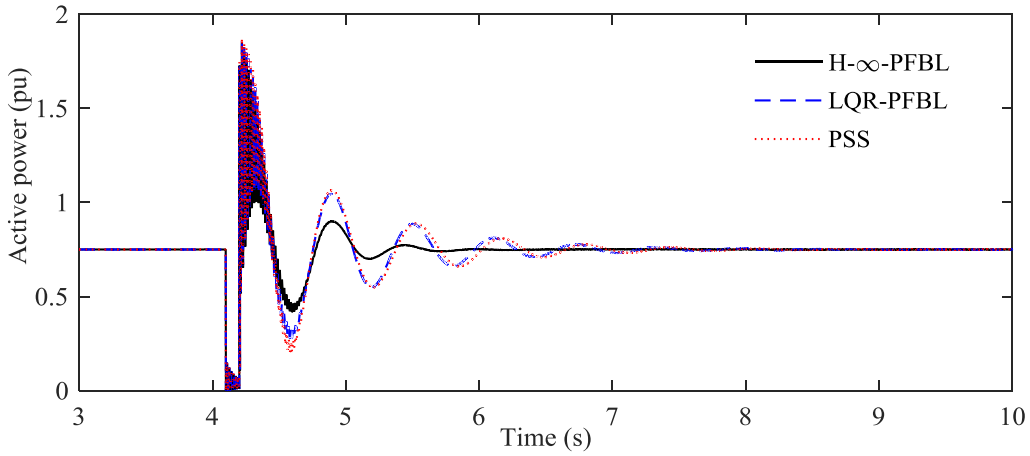

Fig. 4.10. Active power of the synchronous generator in the case of a three-phase short-circuit fault at the terminal of the synchronous generator

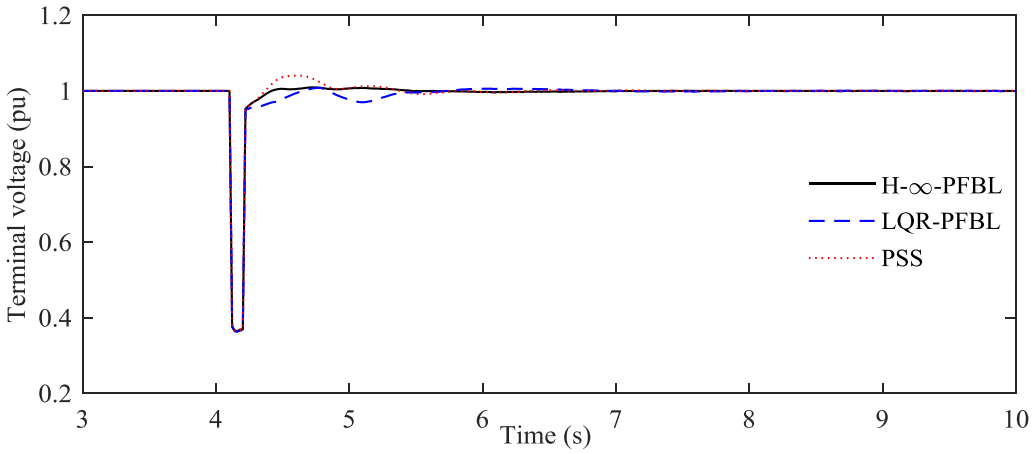

Fig. 4.11. Terminal voltage of the synchronous generator in the case of a three-phase short-circuit fault at the middle of one of the two parallel transmission lines

In such a condition, the rotor angle response is shown in Fig. 4.9 from where it can be seen that this rotor angle response is noisier than the speed deviation response as the speed deviation is the derivative of this rotor angle. The rotor angle response is taking longer time when the PSS (red line) and LQR-PFBL (blue line) are used while the oscillations are well-damped with the designed H_∞-PFBL (black line). Since the active power is related to the rotor angle of the synchronous generator, the active power response will also exhibit similar characteristics to that of the rotor angle responses which can be seen from Fig. 4.10. The designed H_∞-PFBL (black line) stabilizes both rotor angle and active power responses by adding extra damping within the SMIB system.

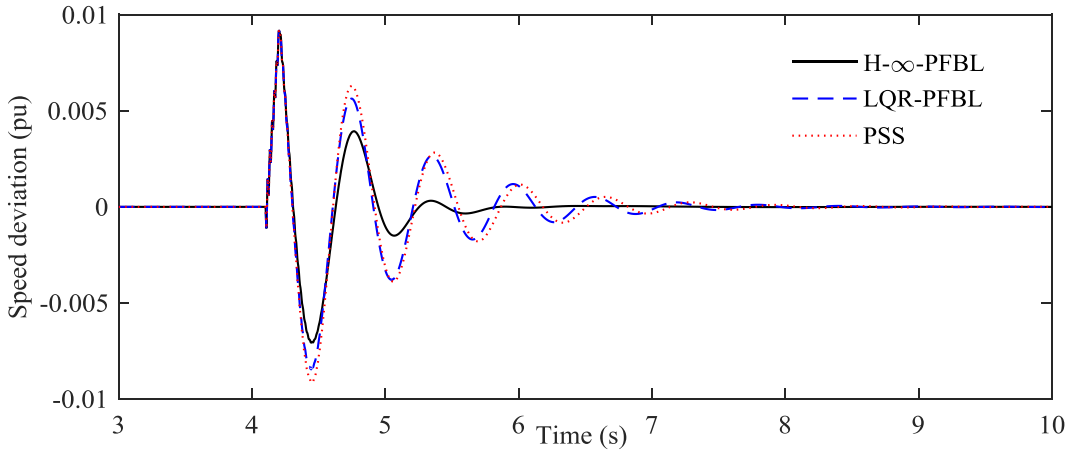

Fig. 4.12. Speed deviation of the synchronous generator in the case of a three-phase short-circuit fault at the middle of one of the two parallel transmission lines

4.5.2. Case 2: Controller performance evaluation in the case of a three-phase short-circuit fault at the middle of one of the two parallel transmission lines

In this case study, a three-phase short-circuit fault is applied at the middle of one of the two parallel transmission lines for a period of 0.1 s (from $t = 4.1$ s to $t = 4.2$ s). In this condition, the terminal voltage of the synchronous generator will not be zero as shown in the following Fig. 4.11. From Fig. 4.11, it can be seen that the terminal voltage exhibits less or no oscillations

due to this fault though the settling time for the PSS (red line) and the LQR-PFBL (blue line) is more than the designed H_∞-PFBL (black line). The speed deviation response corresponding to this situation is shown in Fig. 4.12 from where it can be seen that the SMIB system exhibits similar oscillating characteristics along with the similar settling time when the PSS (red line) and the LQR-PFBL (blue line) are used though the amplitudes of oscillations are lower with the LQR-PFBL (blue line). However, the designed H_∞-PFBL ensures the zero speed deviation in a much faster way as compared to the PSS and LQR-PFBL.

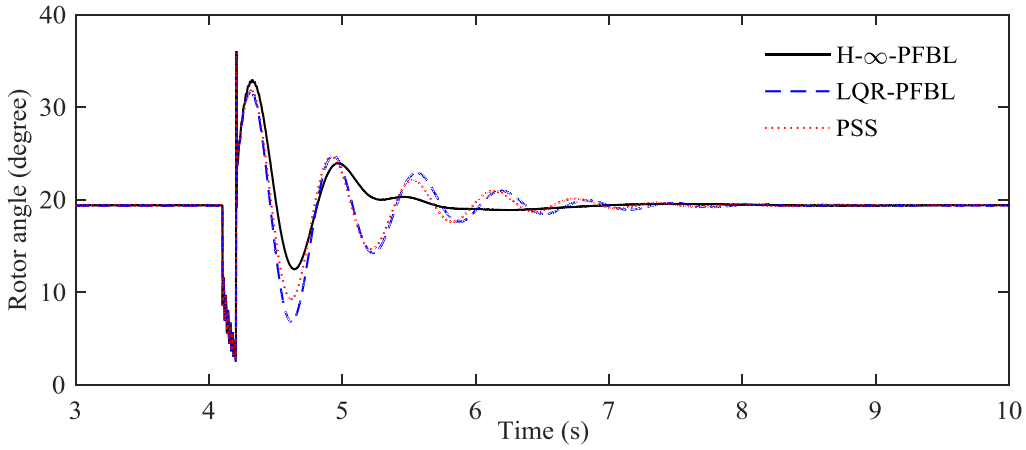

Fig. 4.13. Rotor angle of the synchronous generator in the case of a three-phase short-circuit fault at the middle of one of the two parallel transmission lines

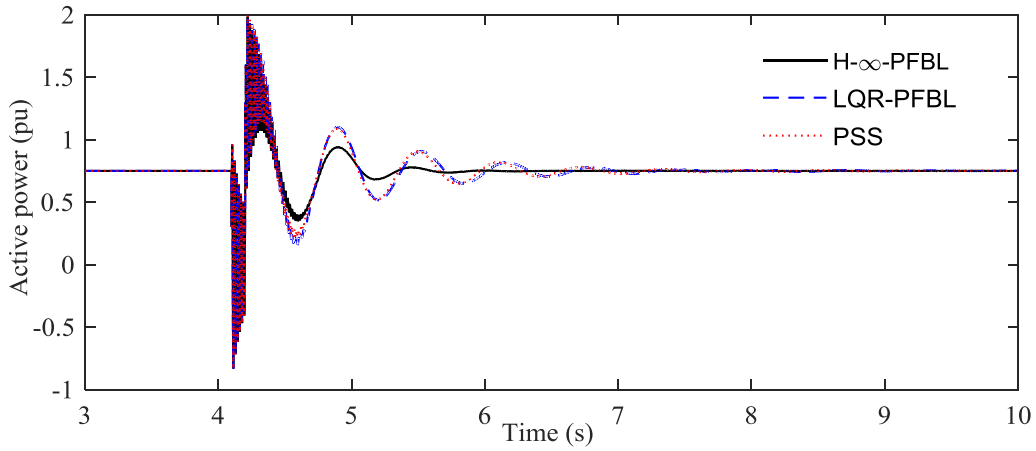

Fig. 4.14. Active power of the synchronous generator in the case of a three-phase short-circuit fault at the middle of one of the two parallel transmission lines

The rotor angle and active power responses are shown in Fig. 4.13 and Fig. 4.14, respectively. From Fig. 4.13, it can be seen that the rotor angle is more oscillating with the PSS and LQR-PFBL as these controllers provide less synchronizing torque as compared to the designed H_∞-PFBL while the similar effects are visible from the active power response.

4.5.3. Case 3: Controller performance evaluation in the case of a step change in the mechanical power input to the synchronous generator

In all previous cases, the generator is delivering 0.75 pu active power which also corresponds to a similar mechanical power input to the synchronous generator. In this case study, it is considered that the SMIB system is operating with $P_m = 0.75$ pu till $t = 4.1$ s. At $t = 4.1$ s, the mechanical power input changes from $P_m = 0.75$ pu to $P_m = 0.8$ pu and the SMIB system continues to operate with this change in the mechanical power input.

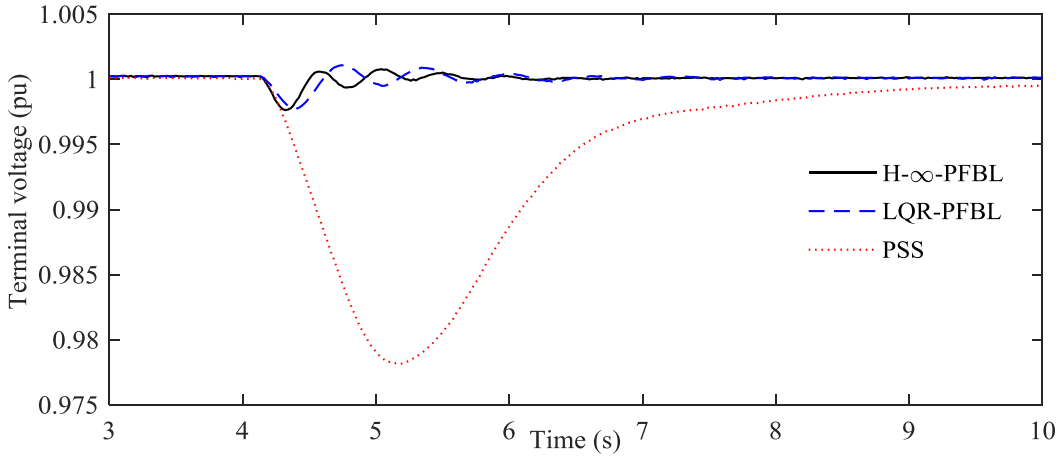

Fig. 4.15. Terminal voltage of the synchronous generator in the case of a step change in the mechanical power input to the synchronous generator

In such an operating condition, the synchronous generator will still have the same terminal voltage through it will be disturbed at $t = 4.1$ s as shown in Fig. 4.15. Since the PSS is designed

to operate at a fixed operating point, the terminal voltage will be severely disturbed as seen from Fig. 4.15 (red line). But the LQR-PFBL still provides reasonably acceptable performance in terms of maintaining the voltage as this controller is designed based on the independency of the operating points though there exist some oscillation which is obvious from Fig. 4.15 (blue line). But the terminal voltage response (black line in Fig. 4.15) is more stable with faster settling time when the designed H_∞-PFBL is in operation.

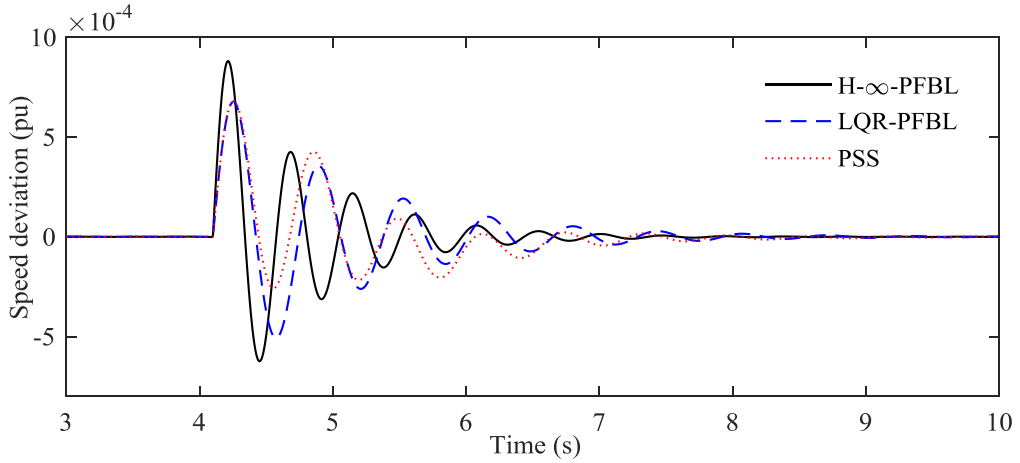

Fig. 4.16. Speed deviation of the synchronous generator in the case of a step change in the mechanical power input to the synchronous generator

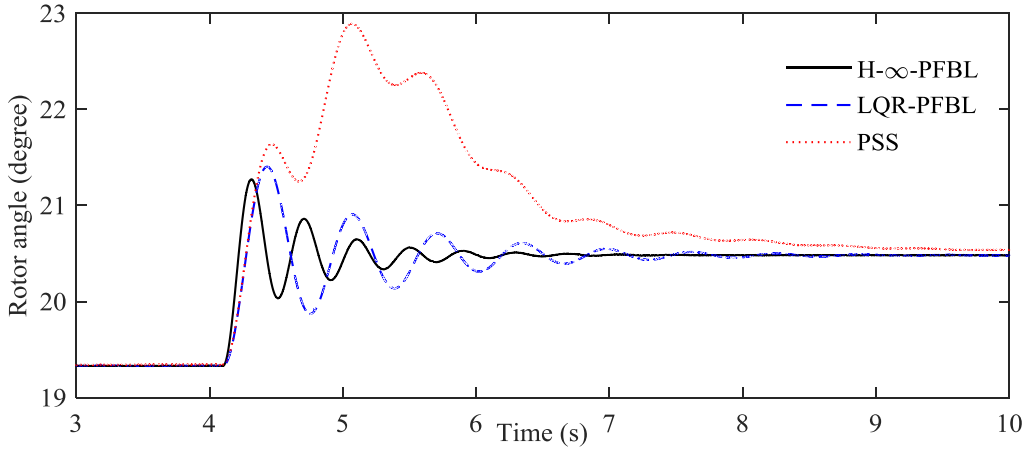

Fig. 4.17. Rotor angle of the synchronous generator in the case of a step change in the mechanical power input to the synchronous generator

Similarly, the speed deviation still needs to be maintained as zero due to the change in the mechanical power input since the synchronous generator always operates at the synchronous speed. Fig. 4.16 shows the speed deviation response of the synchronous generator from where it can be seen that the synchronous generator in the SMIB system has more oscillating behaviors when the PSS (red line) and LQR-PFBL (solid line) is used as compared to the H_∞-PFBL (black line). This clearly indicate the capability of adding extra damping torque of the designed H_∞-PFBL into the SMIB system while comparing with the PSS and LQR-PFBL.

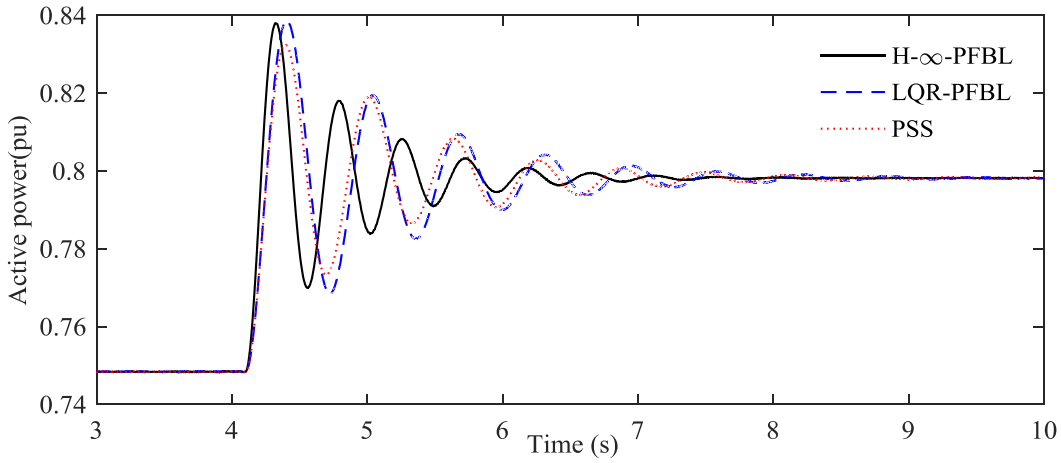

Fig. 4.18. Active power of the synchronous generator in the case of a step change in the mechanical power input to the synchronous generator

In this operating condition, the rotor angle and corresponding active power will settle down to their new steady-state values. The speed of settling down the rotor angle and active power responses depends on how fast the excitation control acts on this change in the mechanical power input. The designed controller settles down these responses in a much quicker way as compared to the PSS and LQR-PFBL which can be seen from Fig. 4.17 and Fig. 418.

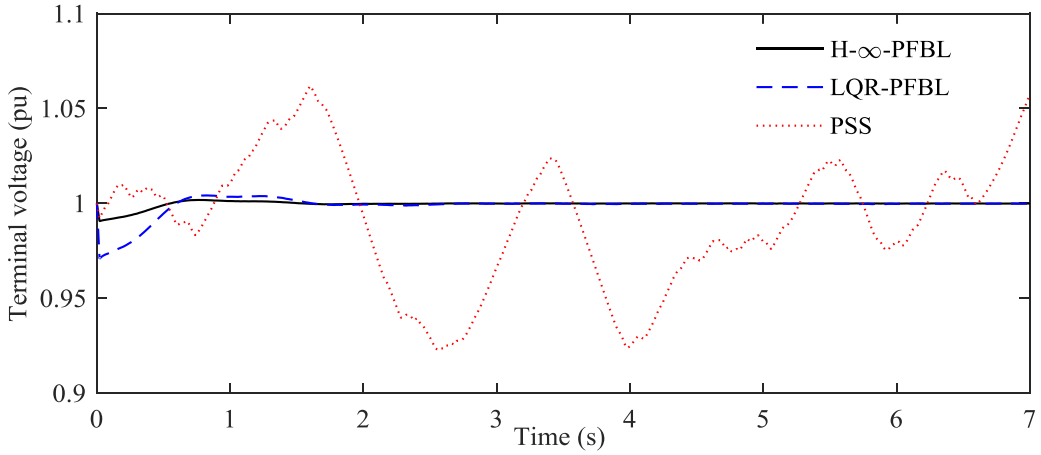

Fig. 4.19. Terminal voltage of the synchronous with changes in system parameters along with the inclusion of external disturbances and measurement noises

4.5.4. Case 4: Controller performance evaluation with changes in system parameters along with the inclusion of external disturbances and measurement noises

In this case study, the parameters as indicated during the design steps are varied from their nominal values from the beginning of the simulation. The variations are considered as $\Delta m_1 = 4.3\%$, $\Delta m_2 = 2.7\%$, $\Delta m_3 = 0.16\%$, $\Delta m_4 = 3.1\%$, $\Delta m_5 = 1.1\%$, and $\Delta m_6 = 3.1\%$. These variations clearly indicate that the parameters are slightly varied from their nominal values. Moreover, some external disturbances are included within the system while the measurement noises are incorporated with the speed deviation which are considered as white Gaussian noises with variances of 0.01. Even with these slight variations in the parameters along with the

inclusion of external disturbances and measurement noises, it can be seen that the system responses are significantly affected.

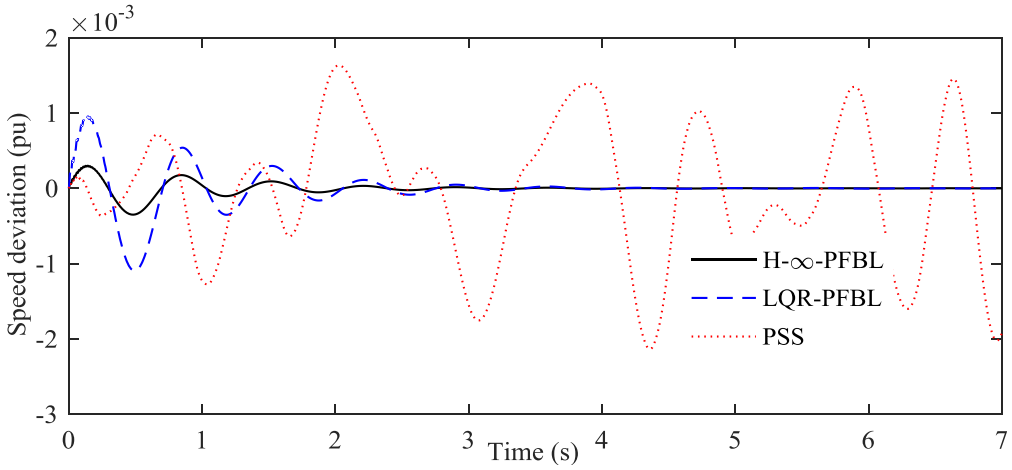

Fig. 4.20. Speed deviation of the synchronous with changes in system parameters along with the inclusion of external disturbances and measurement noises

The terminal voltage response will not be affected much with these changes while nonlinear controllers (both LQR-FBL and H_∞-PFBL) are used which can also be seen from Fig. 4.19. However, the terminal voltage response is quite unstable when the PSS is used. The speed deviation response is disturbed with any controller. However, it unstable or oscillating with the PSS (red line in Fig. 4.20). Moreover, the amplitudes of the oscillation for the speed deviation is more when the LQR-PFBL is used while it is considerably less when the designed H_∞-PFBL is used. The main reason behind this is that the designed controller has the robustness characteristics against parametric uncertainties, external disturbances, and measurement noises which have already been incorporated during the design process.

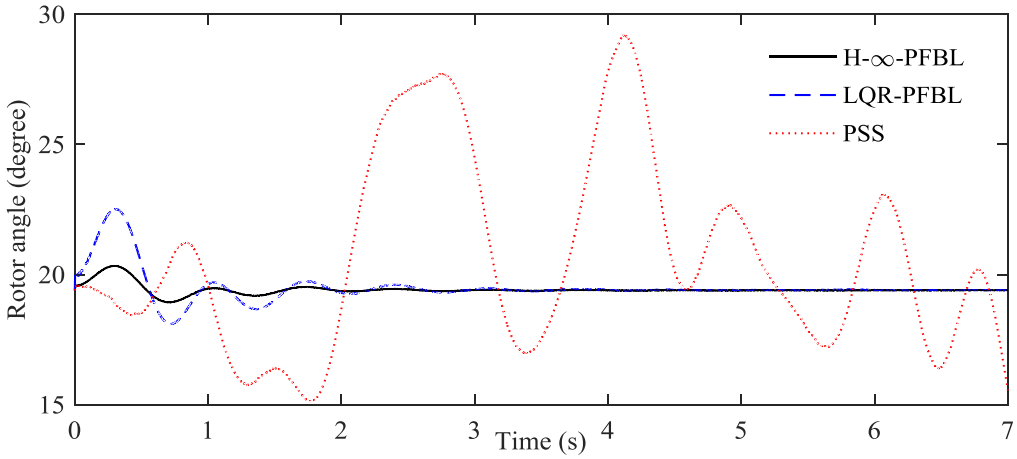

Fig. 4.21. Rotor angle of the synchronous with changes in system parameters along with the inclusion of external disturbances and measurement noises

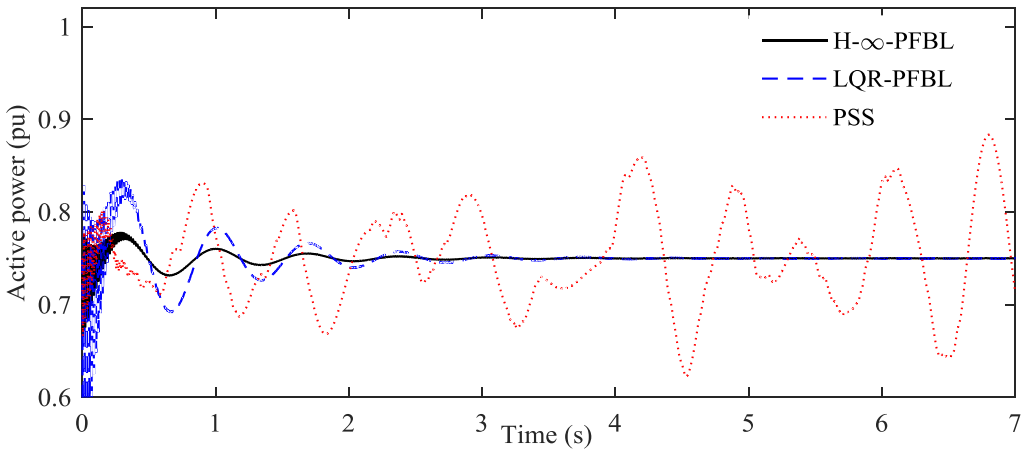

Fig. 4.22. Active power of the synchronous with changes in system parameters along with the inclusion of external disturbances and measurement noises

The rotor angle and the active power responses are shown in Fig. 4.21 and Fig. 4.22, respectively. Both of these responses are unstable when the PSS is used. However, the SMIB system is stable when LQR-PFBL and H_∞-PFBL are used though the later provides more stable responses for the rotor angle as well as the active power.

4.5.5. Quantitative comparison of the controller performance

The performance of the controller is also evaluated by considering the percentage overshoots, peak time, and settling time of all responses under four different case studies as discussed in the previous subsections.

Table 4.1. Percentage overshoot for different responses under different case studies

Cases	Terminal Voltage			Speed Deviation			Rotor Angle			Active Power		
	PSS	LQR-PFBL	H_∞-PFBL	PSS	LQR-PFBL	H_∞-PFBL	PSS	LQR-PFBL	H_∞-PFBL	PSS	LQR-PFBL	H_∞-PFBL
Case 1	4	0.6	0.9	0.6	0.5	0.3	47	5.4	5.5	31.3	29.5	15.1
Case 2	4	0.8	0.8	0.62	0.56	0.4	12.75	12.75	13.8	35	35	18
Case 3	2	0.1	0.1	0.04	0.03	0.04	11.83	10.64	9.97	9	13	12
Case 4	6.2	0.4	0.2	0.12	0.04	0.02	53.47	18.5	7.05	10.67	11.33	2.67

Table 4.2. Peak time for different responses under different case studies

Cases	Terminal Voltage			Speed Deviation			Rotor Angle			Active Power		
	PSS	LQR-PFBL	H_∞-PFBL	PSS	LQR-PFBL	H_∞-PFBL	PSS	LQR-PFBL	H_∞-PFBL	PSS	LQR-PFBL	H_∞-PFBL
Case 1	4.54	4.78	4.46	4.2	4.2	4.2	4.3	4.3	4.3	4.88	4.88	4.88
Case 2	4.58	4.78	4.68	4.2	4.2	4.2	4.9	4.9	4.9	4.8	4.8	4.8
Case 3	5.18	4.74	4.58	4.27	4.27	4.2	4.46	4.3	4.42	4.4	4.4	4.32
Case 4	0.16	0.78	0.78	1.05	0.58	0.58	4.12	0.3	0.3	0.13	3.2	0.3

The percentage overshoots and peak time for the terminal voltage, speed deviation, rotor angle, and active power are shown in Table 4.1 and Table 4.2, respectively. From these tables, it can be summarized that for the first two cases all controllers exhibit similar characteristics. In some cases, the existing controllers perform better than the designed as the existing controllers are

mainly designed specifically for these nominal parameters. However, the designed controller performs better as compared to the PSS and LQR-PFBL for the last two cases when the changes in mechanical power input, parametric uncertainties, external disturbances, and measurement noises are considered.

Table 4.3. Settling time for different responses under different case studies

Cases	Terminal Voltage			Speed Deviation			Rotor Angle			Active Power		
	PSS	LQR-PFBL	H_∞-PFBL	PSS	LQR-PFBL	H_∞-PFBL	PSS	LQR-PFBL	H_∞-PFBL	PSS	LQR-PFBL	H_∞-PFBL
Case 1	0.64	1.18	0.22	2.8	2.5	1.8	2.54	4.54	0.99	3.32	3.32	1.4
Case 2	1.52	2.54	0.78	3.8	3.6	1.6	3.7	3.7	1.64	3.22	3.22	1.28
Case 3	4.8	2.96	1.9	2.8	2.7	1.8	5.3	3.9	2	4.5	4.5	3
Case 4	$\propto$	2.7	0.9	$\propto$	2.5	1	$\propto$	3.5	1.9	$\propto$	3.27	1.8

But the superiority of the designed controller can be clearly seen from the settling time as shown in Table 4.3. From Table 4.3, it can be seen that the settling time for the H_∞-PFBL is much faster than the PSS and LQR-PFBL in all cases. In some cases (especially in the last case), the PSS cannot guarantee the stability of the system. In all cases, the values of settling times are well-below 3 to 5 s which is the timeframe to maintain the transient stability of power systems. Thus, it can be said that the designed controller enhances the transient stability of power systems over a wide range of operating points.

For all cases, it can be seen that the designed H_∞-PFBL performs much better as compared to the PSS and LQR-PFBL in terms of the settling time, which indicates additional damping provided by the designed controller.

4.6 Chapter Summary

After a brief introduction of the result of [35, 67] on feedback linearization of the SMIB system, this chapter has provided a detailed mathematical analysis on the impacts of parametric changes in the SMIB model on the linearized system. The analysis has revealed that the parametric changes in the SMIB model result in unstructured model perturbation and external disturbance which may severely affect the control performance of the feedback linearization plus LQR control proposed in [35, 67]. Based on this analysis, this chapter has then designed an H_∞ mixed-sensitivity loop shaping controller to enhance the performance and robustness of the overall control system. The performance of the designed feedback linearization plus H_∞ mixed-sensitivity loop shaping control scheme is evaluated on an SMIB system by considering both nominal and perturbed models under different operating situations. Simulation results clearly indicate that the designed controller outperforms the PSS and LQR-based feedback linearizing controllers.

Chapter 5

Feedback Linearizing H_∞ Mixed-sensitivity Controller Design for Multimachine Power Systems

This chapter generalizes the results of Chapter 4 to the multimachine power system to provide a solution to the open problem stated in Section 2.7 for the multimachine system. Since the multimachine power system is an MIMO system, the technique of MIMO system feedback linearization described in Section 3.2 is used first to obtain the feedback linearized subsystems which are decoupled from each other. Similar technique to that of Section 4.3 is then used to analyse the impact of parametric changes in the original multimachine system on the feedback linearized subsystems. The analysis result shows the need for the robust controller for each linearized subsystem. Based on the analysis result, the H_∞ mixed-sensitivity loop-shaping controller is designed for the linear control of each linearized subsystem.

5.1 Feedback Linearization plus Linear Control of Multimachine Power System

Many strategies have been proposed in the literature for the control of multimachine power system. Of these strategies, the feedback linearization plus linear control recently proposed in [6, 63] for multimachine power system will be presented in this section.

Recall from Section 2.3 the dynamical model of the ith machine in a power system with N machines.

$$\dot{\delta}_i = \omega_i - \omega_{0i} \tag{5.1}$$

$$\dot{\omega}_i = \frac{D_i}{2H_i}(\omega_i - \omega_{0i}) + \frac{\omega_{0i}}{2H_i}P_{mi} - \frac{\omega_{0i}}{2H_i}\left(E_{qi}'^2 G_{ii} + E_{qi}' \sum_{\substack{j=1 \\ j\neq i}}^{n} E_{qj}' B_{ij} \sin\delta_{ij}\right) \tag{5.2}$$

$$\dot{E}'_{qi} = -\frac{1+(x_{di}-x'_{di})B_{ii}}{T_{doi}} E'_{qi} + \frac{x_{di}-x'_{di}}{T_{doi}} \sum_{\substack{j=1 \\ j\neq i}}^{n} E'_{qj} B_{ij} \cos\delta_{ij} + \frac{1}{T_{doi}} E_{fi} \tag{5.3}$$

It has the order $n_i = 3$ and relative degree $r_i = 2$.

Using (5.1)-(5.3) and considering all the N machines in the system, the following nonlinear state-space equation can be derived for the *ith* machine.

$$\dot{x} = f(x) + \sum_{i=1}^{N} g_i(x) u_i \tag{5.4}$$

$$y_i = h_i(x_i) \tag{5.5}$$

where $i = 1, 2, \cdots, N$,

$$x = \begin{bmatrix} \delta_1 \\ \omega_1 \\ E'_{q1} \\ \vdots \\ \delta_i \\ \omega_i \\ E'_{qi} \\ \vdots \\ \delta_N \\ \omega_N \\ E'_{qN} \end{bmatrix}, \quad f(x) = \begin{bmatrix} \omega_1 - \omega_{01} \\ \frac{D_1}{2H_1}(\omega_1 - \omega_{01}) + \frac{\omega_{01}}{2H_1}(P_{m1} - P_{e1}) \\ \frac{1}{T_{do1}}(E'_{q1} - (x_{d1} - x'_{d1})I_{d1}) \\ \vdots \\ \omega_1 - \omega_{01} \\ \frac{D_i}{2H_i}(\omega_i - \omega_{0i}) + \frac{\omega_{0i}}{2H_i}(P_{mi} - P_{ei}) \\ \frac{1}{T_{doi}}(E'_{qi} - (x_{di} - x'_{di})I_{di}) \\ \vdots \\ \omega_N - \omega_{0N} \\ \frac{D_N}{2H_N}(\omega_N - \omega_{0N}) + \frac{\omega_{0N}}{2H_N}(P_{mN} - P_{eN}) \\ \frac{1}{T_{doN}}(E'_{qN} - (x_{dN} - x'_{dN})I_{dN}) \end{bmatrix}, \quad g_i(x) = \begin{bmatrix} 0 & \cdots & 0 & \cdots & 0 \\ 0 & \cdots & 0 & \cdots & 0 \\ \frac{1}{T_{do1}} & \cdots & 0 & \cdots & 0 \\ \vdots & \cdots & \vdots & \cdots & \vdots \\ 0 & \cdots & 0 & \cdots & 0 \\ 0 & \cdots & 0 & \cdots & 0 \\ 0 & \cdots & \frac{1}{T_{doi}} & \cdots & 0 \\ \vdots & \cdots & \vdots & \cdots & \vdots \\ 0 & \cdots & 0 & \cdots & 0 \\ 0 & \cdots & 0 & \cdots & 0 \\ 0 & \cdots & 0 & \cdots & \frac{1}{T_{doN}} \end{bmatrix},$$

$u_i = E_{fi}$, and $y_i = \Delta\omega_i = \omega_i - \omega_{0i}$.

In (5.4)-(5.5), x is the state vector of all machines with the dimension $3N$, u_i and y_i are the input and output variables of the ith machine, respectively. Because the relative degree of (5.1)-(5.3) is $r_i = 2$, the relative degree r for all machines in the state equation (5.4)-(5.5) is $r = r_i \times N = 2N < 3N$.

According to the feedback linearization reviewed in Section 3.2, the system (5.4)-(5.5) can be partially linearized. The coordinate transformation for such linearization can be represented by the $r-1$ Lie derivatives of y in the normal form [6, 63]

$z_i = \begin{bmatrix} h_i(x) & L_f h_i(x) & \dots & L_f^{r-1} h_i(x) \end{bmatrix}^T$ where $L_f h_i(x) = \frac{\partial h_i(x)}{\partial x} f(x)$.

The condition and procedure for calculating the relative degree of the multimachine power system in the form of (5.4) and (5.5) are well described in [6, 63]. It has been shown that the the system (5.4)-(5.5)) can be partially linearized to a linear system with the output $y_i = \Delta\omega_i = \omega_i - \omega_{0i}$ and the synthetic control input v_i. The input-output mapping from v_i to y_i is a second (rth) order integrator [6, 63]. With the synthetic input v_i, the system (5.1)-(5.3) can be written as the following linearized form [6, 63]

$$(\dot{z}_1)_1 = L_f \Delta\omega_1 = \Delta\omega_1, \tag{5.6}$$

$$(\dot{z}_2)_1 = v_1, \tag{5.7}$$

where

$$v_1 = L_f^2 \Delta\omega_1 + L_g L_f^{2-1} \Delta\omega_1 u_1, \tag{5.8}$$

$$(\dot{z}_1)_2 = L_f \Delta\omega_2 = \Delta\omega_2, \tag{5.9}$$

$$(\dot{z}_2)_2 = v_2, \tag{5.10}$$

and

$v_2 = L_f^2 \Delta\omega_2 + L_g L_f^{2-1} \Delta\omega_2 u_2$.

The generalized linear system for the ith machine can be written as

$$(\dot{z}_1)_i = L_f \Delta\omega_i = \Delta\omega_i \tag{5.11}$$

$$(\dot{z}_2)_i = v_i \tag{5.12}$$

where

$$v_i = L_f^2 \Delta\omega_i + L_g L_f^{2-1} \Delta\omega_i u_i, \tag{5.13}$$

$$L_{f_i}^2 \Delta\omega_i = -\frac{D_i}{2H_i}\Delta\dot{\omega}_i - \frac{\omega_{0i}}{2H_i} Q_{ei}\Delta\omega_i - \frac{\omega_{0i}}{2H_i} P_{ei},$$

and

$$L_{g_i} L_{f_i}^{2-1} \Delta\omega_i = -\frac{\omega_{0i}}{2H_i}\frac{P_{ei}}{E'_{qi}}\frac{1}{T_{doi}}.$$

Using above $L_{f_i}^2 \Delta\omega_i$and $L_{g_i} L_{f_i}^{2-1} \Delta\omega_i$ in (5.13) gives

$$v_i = -\frac{D_i}{2H_i}\dot{\omega}_i - \frac{\omega_{0i}}{2H_i} Q_{ei}\Delta\omega_i - \frac{\omega_{0i}}{2H_i} P_{ei} - \frac{\omega_{0i}}{2H_i}\frac{P_{ei}}{E'_{qi}}\frac{1}{T_{doi}} u_i \tag{5.14}$$

Since$(\dot{z}_1)_i = (z_2)_i = \Delta\dot{\omega}_i = \dot{\omega}_i$, (5.12) can be written as

$$\ddot{\omega}_i = (\dot{z}_2)_i = v_i = -\frac{D_i}{2H_i}\dot{\omega}_i - \frac{\omega_{0i}}{2H_i} Q_{ei}\Delta\omega_i - \frac{\omega_{0i}}{2H_i} P_{ei} - \frac{\omega_{0i}}{2H_i}\frac{P_{ei}}{E'_{qi}}\frac{1}{T_{doi}} u_i \tag{5.15}$$

From (5.14), the control law u_i for the multimachine system can be derived as

$$u_i = \frac{1}{\frac{\omega_{0i} P_{ei}}{2H_i E'_{qi}} \frac{1}{T_{doi}}} (v_i - -\frac{D_i}{2H_i}\Delta\dot{\omega}_i - \frac{\omega_{0i}}{2H_i} Q_{ei}\Delta\omega_i - \frac{\omega_{0i}}{2H_i} P_{ei}) \tag{5.16}$$

where $i = 1, 2, \cdots, N$. All the variables on the right hand sides of (5.16) are either physically measurable or can be expressed in terms of measured variables [6, 63]. But the linear control input v_i needs to be generated by a linear controller for the linearized subsystems (5.11)-(5.12).

Using Laplace transform, the linearized subsystem (5.11)-(5.12) can be written as

$$\Delta\omega_i(s) = (Z_1)_i(s) = \frac{1}{s^2} V_i(s) \tag{5.17}$$

where $(Z_1)_i(s)$ is the Laplace transform of $(z_1)_i$. This is an SISO system with the transfer function

$$G(s) = \frac{1}{s^2}$$

and hence can be controlled by an independent linear controller. Similarly to the SMIB case discussed in Section 4.1, the control input $V_i(s)$ can be simply generated by a dynamic controller using output negative feedback

$$V_i(s) = -C_i(s)\Delta\omega_i(s) = C_i(s)[\omega_{0i} - \omega_i(s)] \quad (5.18)$$

where $C_i(s)$ is the transfer function of the controller, and ω_{0i} and $\omega_i(s)$ are respectively the Laplace transforms of ω_{0i} and ω_i.

The same as the SMIB case in Section 4.1, (5.17)-(5.18) form a linear closed-loop control system, the plant of the system is $G_i(s) = \frac{1}{s^2}$ which is the transfer function of the feedback linearized subsystem, the output is $\omega_i(s)$, the command reference is $\omega_{0i}(s)$, and the control error is $\Delta\omega_i(s) = \omega_{0i} - \omega_i(s)$. The sensitivity and complementary sensitivity functions of this closed-loop system are respectively

$$S_i(s) = \frac{1}{1+G_i(s)C_i(s)} \quad (5.19)$$

$$T_i(s) = \frac{G_i(s)C_i(s)}{1+G_i(s)C_i(s)} \quad (5.20)$$

The controlled output $\omega_i(s)$ and the control error $\Delta\omega_i(s)$ are related to the command reference ω_{0i} by

$$\omega_i(s) = T_i(s)\omega_{0i} \quad (5.21)$$

and

$$\Delta\omega_i(s) = S_i(s)\omega_{0i} \quad (5.22)$$

The feedback linearizing control input (5.16) and the linear control (5.16) together form a double loop feedback system with the inner feedback linearizing control loop and outer linear control loop. The same as SMIB case, with a properly designed $C_i(s)$, the feedback control loop renders full control of $\Delta\omega_i(s)$ towards 0 in steady-state, which guarantees the desired control objective and also the stability of the hidden internal state δ_i. The excitation controller for each synchronous generator can be designed using the above partial feedback linearization scheme and a linear controller design technique.

5.2 Analysis of Feedback Linearization of Multimachine Power System under Parametric Uncertainty and Measurement Noise

Similar to the SMIB case discussed in Section 4.2, the parameters in (5.1)-(5.3) are subject to change all the time. These changes introduce unstructured model perturbation and external disturbance into the feedback linearized model (5.17). This can be shown similarly to that of Section 4.2 for the SMIB system. A brief description is given below.

With parametric changes the parameters in (5.15) can be written as

$\frac{D_i+\Delta D_i}{2(H_i+\Delta H_i)} = m_{1i} + \Delta m_{1i}$,

$\frac{P_m+\Delta P_m}{2(H_i+\Delta H_i)} = m_{2i} + \Delta m_{2i}$,

$\frac{1}{2(H_i x'_{di\Sigma}+\Delta H_i x'_{di\Sigma})} = m_{3i} + \Delta m_{3i}$, and

$\frac{1}{(T_{doi}+\Delta T_{doi})} = m_{4i} + \Delta m_{4i}$

where

$m_{1i} = \frac{D_i}{2H_i} > 0$, $m_{2i} = \frac{P_m}{2H_i} > 0$, $m_{3i} = \frac{1}{2H_i x'_{di\Sigma}} > 0$, and $m_{4i} = \frac{1}{T_{doi}} > 0$

are the nominal parameters of the multimachine power system, and

$\Delta m_1 = \frac{\Delta D_i - \Delta H_i D_i/H_i}{2(H_i+\Delta H_i)}$, $\Delta m_2 = \frac{\Delta P_m - \Delta H_i P_m/H_i}{2(H_i+\Delta H_i)}$, $\Delta m_3 = \frac{\Delta H_i x'_{d\Sigma}/H x'_{d\Sigma}}{2(H_i x'_{di\Sigma}+\Delta H_i x'_{di\Sigma})}$ and $\Delta m_4 = \frac{\Delta T_{doi}/T_{doi}}{(T_{doi}+\Delta T_{doi})}$

are respectively the uncertainties of m_{1i}, m_{2i}, m_{3i} and m_{4i}, which reduce to zero when $\Delta m_{1i} = \Delta m_{2i} = \Delta m_{2i} = \Delta m_{2i} = 0$.

With the above defined parameters and parametric uncertainties, the linearized (5.15) becomes

$$\Delta\ddot{\omega}_i = -(m_{1i} + \Delta m_{1i})\dot{\omega}_i - (m_{3i} + \Delta m_{3i})\omega_{0i} Q_{ei} \Delta\omega_i$$
$$-(m_{3i} + \Delta m_{3i})\omega_{0i} P_{ei} - (m_{5i} + \Delta m_{5i})\omega_{0i} \frac{P_{ei}}{E'_{qi}} u_i \quad (5.23)$$

Using (5.14), (5.23) can be simplified to

$$\Delta\ddot{\omega}_i = v_i - \Delta m_{1i}\dot{\omega}_i - \Delta m_{3i}\omega_{0i}Q_{ei}\Delta\omega_i - \Delta m_{3i}\omega_{0i}P_{ei} - \Delta m_{5i}\omega_{0i}\frac{P_{ei}}{E'_{qi}}u_i \quad (5.24)$$

and the feedback linearized control input (5.15) for the nominal system can be written as

$$u_i = \frac{1}{m_{5i}\omega_{0i}\frac{P_{ei}}{E'_{qi}}u_i}(v_i - m_{1i}\Delta\dot{\omega}_i - m_{3i}\omega_{0i}Q_{ei}\Delta\omega_i - m_{3i}\omega_{0i}P_{ei}) \quad (5.25)$$

where $m_{3i}m_{4i} = m_{5i}$.

Substituting (5.25) into (5.24) gives

$$\Delta\ddot{\omega}_i = v_i - \Delta m_{1i}\dot{\omega}_i - \Delta m_{3i}\omega_{0i}Q_{ei}\Delta\omega_i - \Delta m_{3i}\omega_{0i}P_{ei}$$
$$-\frac{\Delta m_{5i}}{m_{5i}}(v_i - m_{1i}\dot{\omega}_i - m_{3i}\omega_{0i}Q_{ei}\Delta\omega_i - m_{3i}\omega_{0i}P_{ei}) \quad (5.26)$$

Defining $R_{1i} = \omega_{0i}Q_{ei}$ and $R_{2i} = \omega_{0i}P_{ei}$, (5.26) can be simplified to

$$\Delta\ddot{\omega}_i = v_i - \Delta m_{1i}\Delta\dot{\omega}_i - \Delta m_{3i}R_1\Delta\omega_i - \Delta m_{3i}R_2$$
$$-\frac{\Delta m_{5i}}{m_{5i}}(v_i - m_{1i}\Delta\dot{\omega}_i - m_{3i}R_1\Delta\omega_i - m_{3i}R_2) \quad (5.27)$$

Equation (5.27) can be further simplified as

$$\Delta\ddot{\omega}_i = K_{1i}v_i - K_{2i}R_{1i}\Delta\omega_i - K_{3i}\Delta\dot{\omega}_i - K_{4i}R_{2i} \quad (5.28)$$

where

$K_{1i} = 1 - \frac{\Delta m_{5i}}{m_{5i}}$, $K_{2i} = \Delta m_{3i} + \frac{\Delta m_{5i}m_{3i}}{m_{5i}} = K_4$, and $K_{3i} = \Delta m_{1i} + \frac{\Delta m_5 i m_{1i}}{m_{5i}}$.

Taking the Laplace transform of (5.28) yields

$$s^2\Delta\omega_i(s) = V_i(s)K_{1i} - \Delta\omega_i(s)R_{1i}K_{2i} - s\Delta\omega_i(s)K_{3i} - R_{2i}K_{4i} \quad (5.29)$$

which can be further rewritten as

$$\Delta\omega_i(s) = \frac{1}{s^2 + sK_{3i} + R_{1i}K_{2i}}(V_i(s)K_{1i} - R_{2i}K_{4i}) \quad (5.30)$$

Defining $\Delta_i = \frac{(K_{1i}-1)s^2 - sK_{3i} - R_{1i}K_{4i}}{s^2 + sK_{3i} + R_{1i}K_{4i}}$ and $K_i = \frac{K_{4i}}{K_{1i}}$, (5.30) can be written as

$$\Delta\omega_i(s) = \frac{1}{s^2}(1 + \Delta_i)(V_i(s) - R_{2i}K_i) \tag{5.31}$$

which is exactly the same as its SMIB counterpart (4.25). The perturbed system (5.31) and the linear controller (5.18) form a closed-loop system shown in Fig. 5.1.

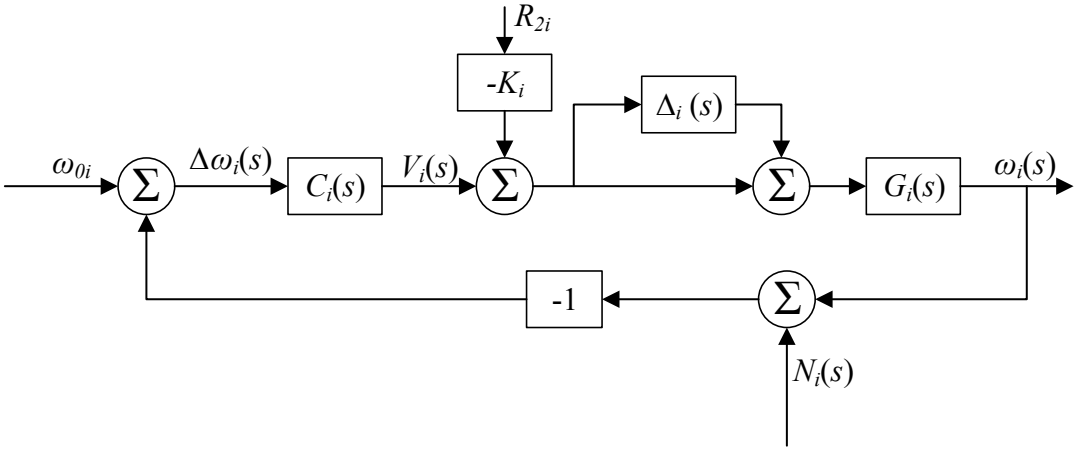

Fig. 5.1. Linear of the feedback linearized multimachine power system with model uncertainties and measurement noises

5.3 H_∞ Mixed-Sensitivity Loop Shaping Controller for Multimachine System

As shown in Section 5.1 and 5.2, the interconnected multimachine system (5.1)-(5.3) can be feedback linearized and the linearized systems are independent of each other without coupling and have the same $G_i(s) = \frac{1}{s^2}$. In the presence of parameter changes in (5.1)-(5.3), each linearize control system becomes that of Fig. 5.1, with model perturbation $\Delta_i(s)$ and external disturbance $R_{2i}K_i$. These individual linear control systems are exactly the same as the linear control system of the SMIB case shown in Fig. 4.2. Therefore, the same H_∞ mixed-sensitivity loop shaping controller designed in Section 4.4 can be applied to each machine in the multimachine power system as the linear controller $C_i(s)$.

Based on this approach, the same $W_{pi}(s)$ and $W_{\Delta i}(s)$ as given below are used to design each $C_i(s)$

$$W_{pi}(s) = \frac{0.52632\ (s+1.9)}{(s+0.0001)} \tag{5.32}$$

$$W_{\Delta i}(s) = \frac{10000\ (s+8.333)}{(s+10^5)} \tag{5.33}$$

The resultant robust controller for the multimachine power system using the above weights $W_{pi}(s)$ and $W_{\Delta i}(s)$ is

$$C_i(s) = \frac{4.9728\times10^6\ (s+\times10^5)\ (s+0.0001549)(s+0.4.508\times10^{-5})}{(s+9.979\times10^4)\ (s+6413)\ (s+127.6)\ (s+9.829\times10^{-5})} \tag{5.34}$$

This linear output feedback controller is used in conjunction with the feedback linearizing control law (5.16) to robustly stabilize each machine, which in turn stabilizes the entire system under different operating conditions. The performance of the designed controller is evaluated in the following section and compared with the conventional PSS and LQR-based feedback linearizing controller in [6].

5.4 Controller Performance Evaluation

Since the partial feedback linearization decouples the nonlinear multimachine power system into separate subsystem, the multimachine control problem is decomposed into several single machine problems. From the control design process for the multimachine power system, it can be seen that the controller can be designed for individual machine and implemented in a similar way to that of the SMIB system. Therefore, the implementation block of the each controller is exactly the same as that in Fig. 4.6.

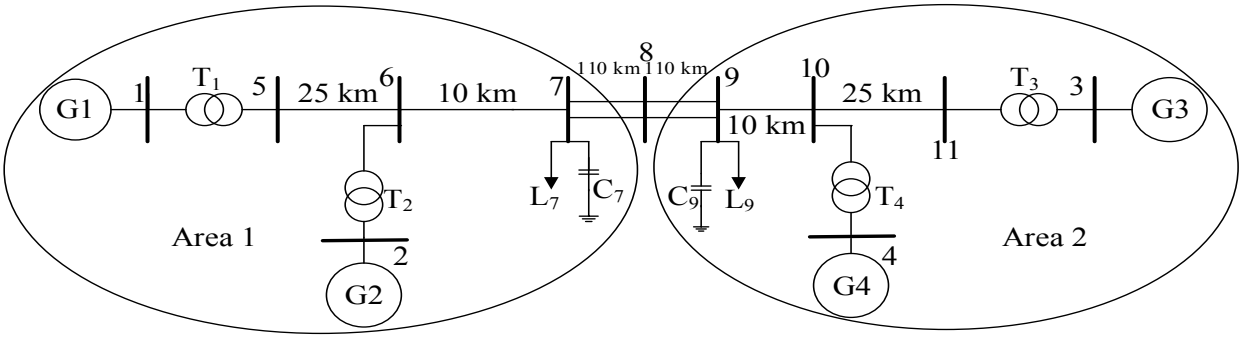

Fig. 5.2. A two-area four machine test power system

The performance of the feedback linearization plus H_∞ mixed-sensitivity loop shaping excitation controller for the multimachine power system (H_∞-PFBL) is evaluated on a two-area four machine power system shown in Fig. 5.2. There are two areas in the system. Each are has two connected SG to share power. The details of this system can be found in [1] and the parameters used in the simulation are provided in Appendix-II.

While implementing advanced controllers in multimachine power systems, the controllers are not implemented with all machines as this is not a cost-effective approach. For this reason, the generators which affect the stability of the system are selected through the modal analysis. This is beyond the scope of this thesis and hence omitted. In [1, 6], it has been identified that the synchronous generator G1 along with other synchronous generator G3 are more sensitive to the overall stability of the system. Therefore, the designed H_∞-PFBL is implemented with on these two generators instead of all four generators. The synchronous generator G2 is considered as the reference generator. In this simulation, the limits of all excitation systems are considered as ± 6 pu.

The performance of the designed controller is evaluated by considering different operating conditions. The following case studies are considered in this chapter to demonstrate the designed feedback linearizing H_∞ mixed-sensitivity loop shaping controller (H_∞-PFBL):

i. Controller performance evaluation in the case of a three-phase short-circuit fault at the terminal of G1,
ii. Controller performance evaluation in the case of a three-phase short-circuit fault at the middle of one of the two parallel transmission lines between bus-7 and bus-8,
iii. Controller performance evaluation in the case of a step change in the mechanical power input to G3, and
iv. Controller performance evaluation with changes in the parameters and the presence of external disturbances and measurement noises in G3.

The first three cases are analyzed based on the nominal model of the two-area four machine system while the last case considers the parametric uncertainties, external disturbances, and measurement noises. For these first two cases, faults occur at $t = 10$ s and sustain for 0.15 s, i.e., till $t = 10.15$ s. For this third case, the change in the mechanical power input occurs at $t = 10$ s to G3 and the system continues to operate with this change in the mechanical power input. For the last case, the changes are considered from the beginning of the operating, i.e., from $t = 0$ s. In all cases, the performance of the designed controller (H_∞-PFBL) is compared with an existing PSS [1] and a feedback linearizing controller with an LQR approach (LQR-PFBL) [6]. The following subsections provide more details about these case studies. It is worth to note that the significances of the responses are exactly similar to those for the SMIB system though this section includes the responses for both G1 and G3. Therefore, all case studies are briefly explained in this chapter. Moreover, some quantitative results are included at the end of this section to analyze the superiority of the designed controller.

5.4.1 Case 1: Controller performance evaluation in the case of a three-phase short-circuit fault at the terminal of G1

In this case study, a three-phase short-circuit fault is applied at the terminal of G1 at $t = 10$ s and the fault is cleared $t = 10.15$ s. During the faulted period, the terminal voltage of the G1 will be zero which can be seen from Fig. 5.3 though the terminal voltage of G3 will also be disturbed as shown in Fig. 5.4. Fig. 5.3 clearly shows that that the terminal voltage is zero during the faulted period with any controller. The impact of this fault will not be severe from the voltage response of G1 and G3 as the stability problem is an angle stability. However, the post-fault oscillations in the terminal voltages are more with the PSS (red line) while it is still visible with the LQR-PFBL (blue line). But there are less oscillations in the voltage response when the designed H_∞-PFBL (black line) is used.

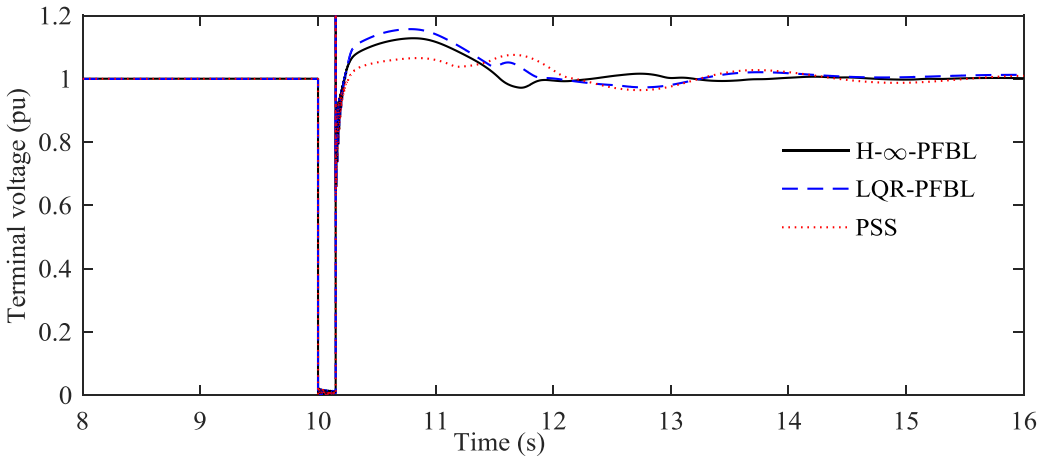

Fig. 5.3. Terminal voltage of G1 under a three-phase short-circuit fault at the terminal of G1

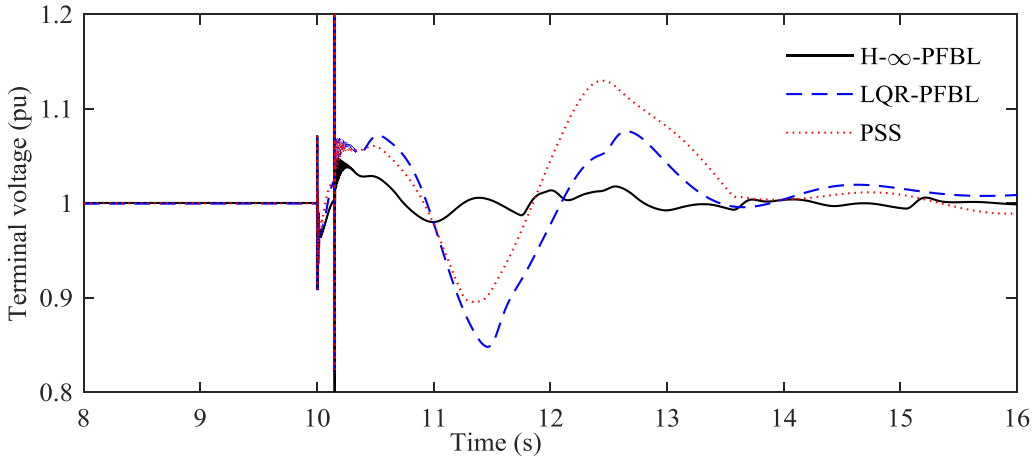

Fig. 5.4. Terminal voltage of G3 under a three-phase short-circuit fault at the terminal of G1

During the faulted period (from $t = 10$ s to $t = 10.15$ s), the speed deviations of both G1 and G3 will be disturbed with any controller. Fig. 5.5 and Fig. 5.6 show the speed deviation of G1 and G3, respectively from where it can be seen that the speed deviations are more oscillating with larger overshoots (red line) when the PSSs are used. The amplitudes of the oscillations are quite less when LQR-PFBL (blue line) is used. But the oscillations are less with faster settling time when the designed H_∞-PFBL (black line) is in operation.

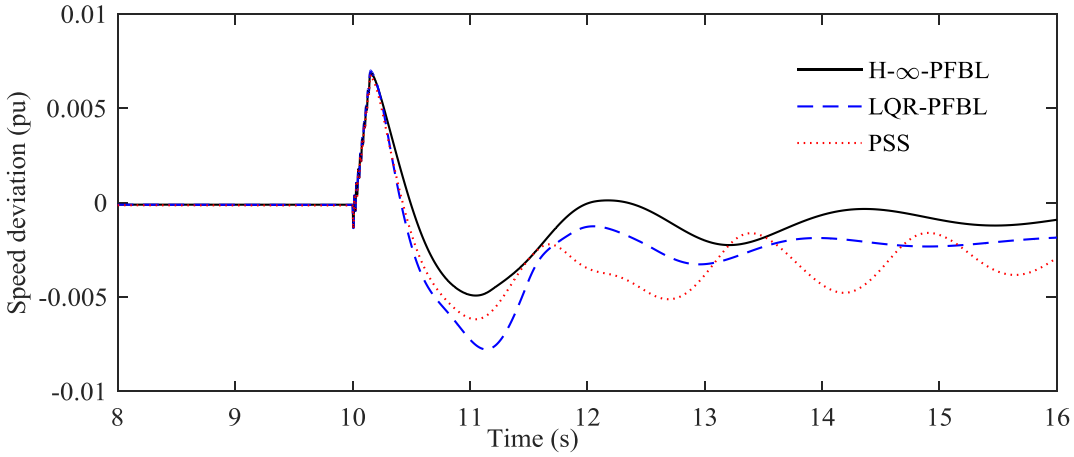

Fig. 5.5. Speed deviation of G1 under a three-phase short-circuit fault at the terminal of G1

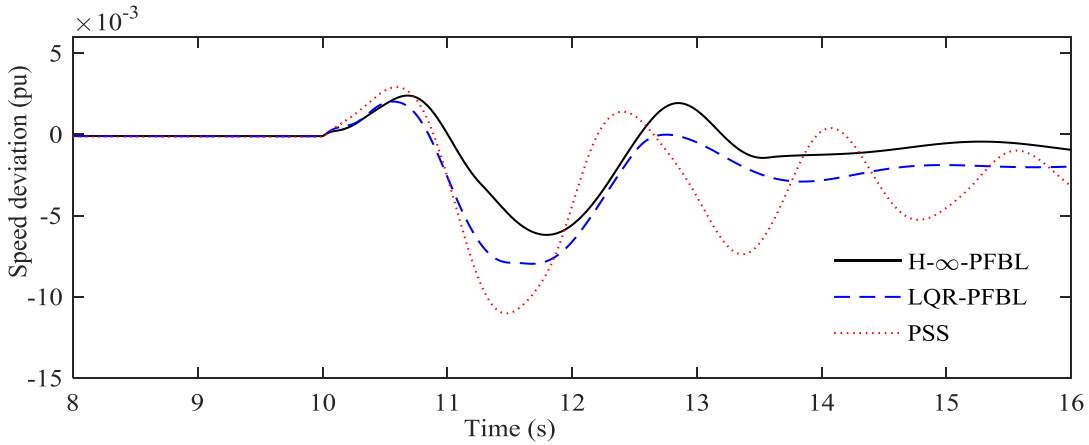

Fig. 5.6. Speed deviation of G3 under a three-phase short-circuit fault at the terminal of G1

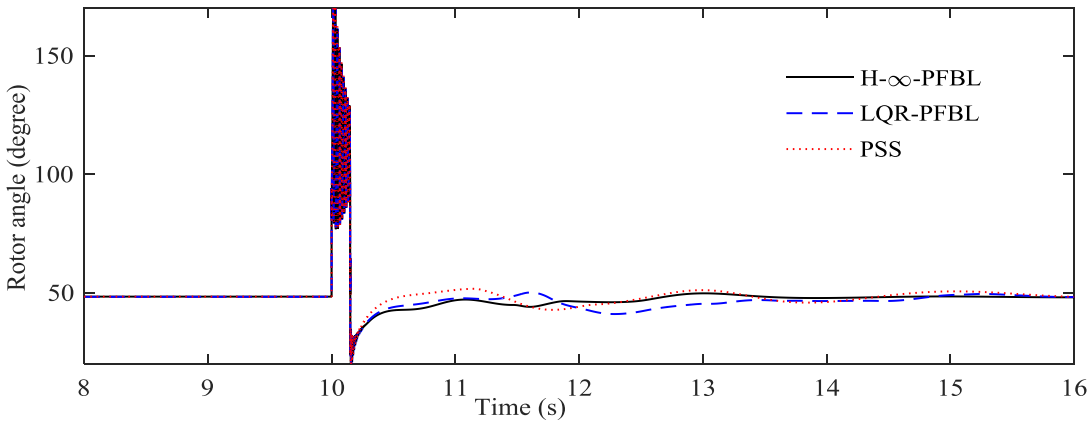

Fig. 5.7. Rotor angle of G1 under a three-phase short-circuit fault at the terminal of G1

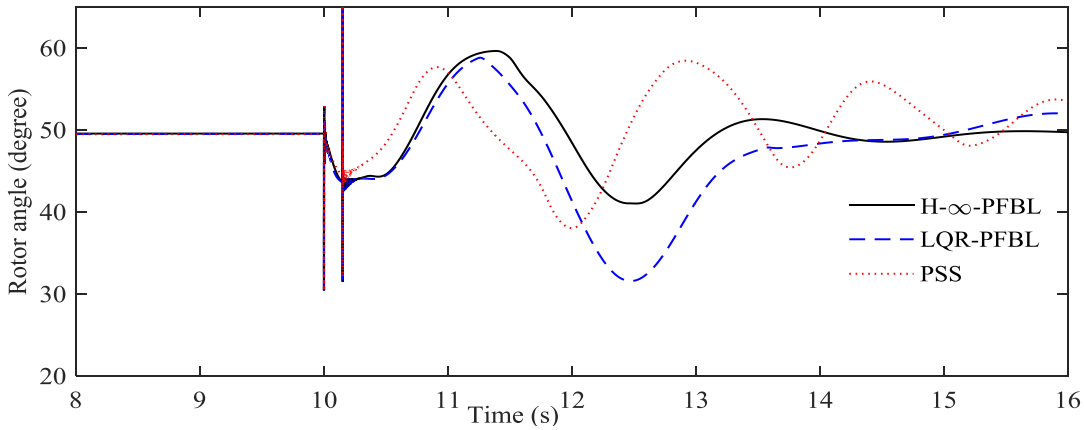

Fig. 5.8. Rotor angle of G3 under a three-phase short-circuit fault at the terminal of G1

In such a condition, the rotor angle responses of G1 and G3 are shown in Fig. 5.7 and Fig. 5.8, respectively from where it can be seen that these rotor angle responses are noisier than the speed deviation responses. The rotor angle responses are taking longer time when the PSSs (red line) and LQR-PFBL (blue line) are used while the oscillations are well-damped with the designed H_∞-PFBL (black line). Since the active power is related to the rotor angle of the synchronous generator, the active power response will also exhibit similar characteristics to that of the rotor angle responses which can be seen from Fig. 5.9 and Fig 5.10. The designed H_∞-PFBL (black line) stabilizes both rotor angle and active power responses by adding extra damping through the excitation systems of G1 and G3.

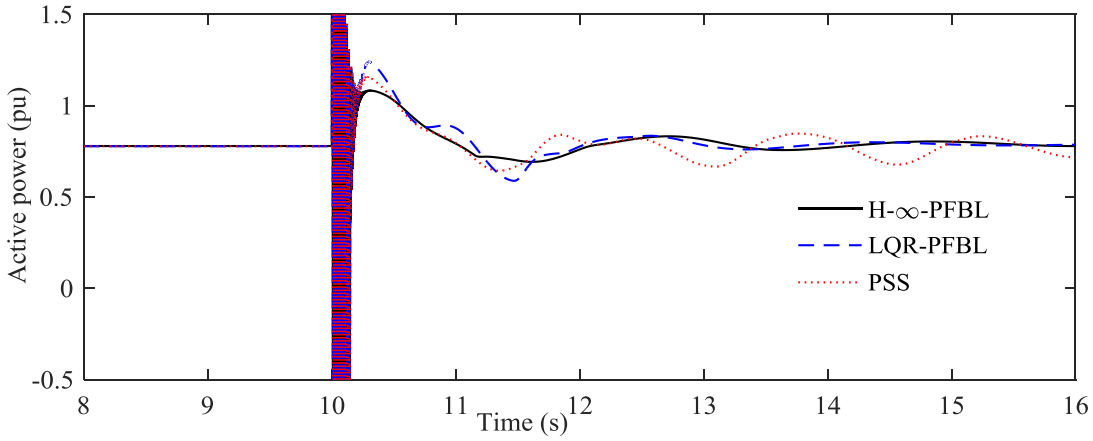

Fig. 5.9. Active power of G1 under a three-phase short-circuit fault at the terminal of G1

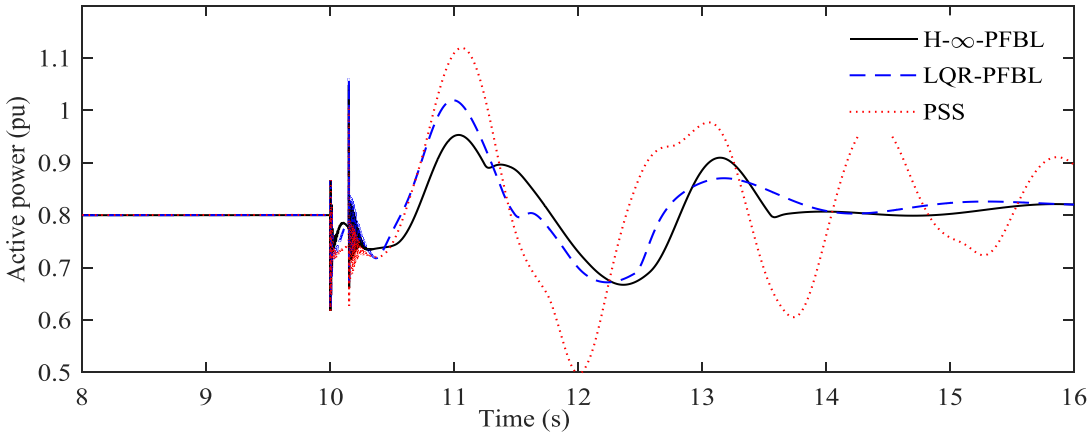

Fig. 5.10. Active power of G3 under a three-phase short-circuit fault at the terminal of G1

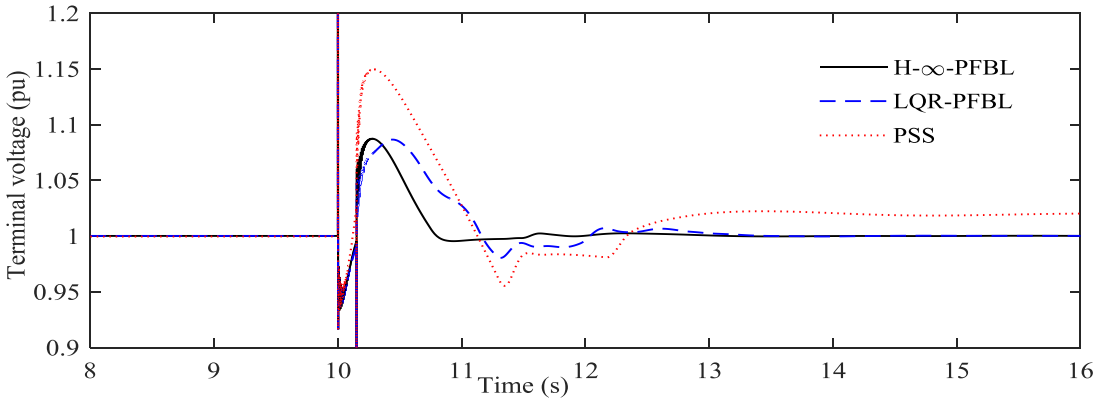

Fig. 5.11. Terminal voltage of G1 under a three-phase short-circuit fault at the middle of one of the two parallel transmission lines bus-7 and bus-8

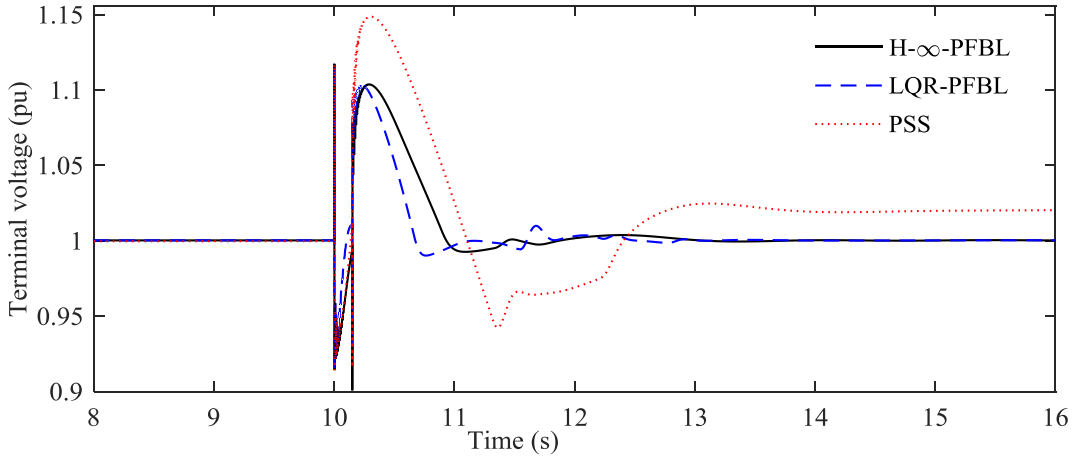

Fig. 5.12. Terminal voltage of G3 under a three-phase short-circuit fault at the middle of one of the two parallel transmission lines bus-7 and bus-8

5.4.2 Case 2: Controller performance evaluation in the case of a three-phase short-circuit fault at the middle of one of the two parallel transmission lines bus-7 and bus-8

In this case study, a three-phase short-circuit fault is applied at the middle of one of the two parallel transmission lines between bus-7 and bus-8 for a period of 0.15 s (from $t = 10$ s to $t = 10.15$ s). In this condition, the terminal voltages of both G1 and G3 will not be zero as shown in Fig. 5.11 and Fig. 5.12, respectively. From these figures, it can be seen that the terminal

voltages exhibit less or no oscillations due to this fault though the settling time for the PSS (red line) and the LQR-PFBL (blue line) is more than the designed H_∞-PFBL (black line). The speed deviation responses corresponding to this situation are shown in Fig. 5.13 and Fig. 5.14 from where it can be seen that G1 and G3 exhibit more oscillating characteristics with more settling times when the PSS (red line) and the LQR-PFBL (blue line) are used though the amplitudes of oscillations are lower with the LQR-PFBL (blue line). However, the designed H_∞-PFBL ensures the zero speed deviation in a much faster way as compared to the PSS and LQR-PFBL.

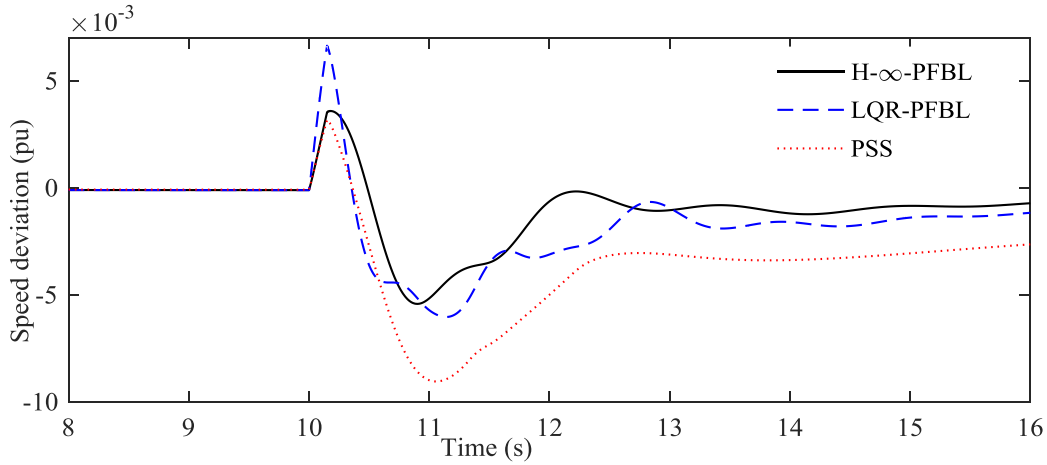

Fig. 5.13. Speed deviation of G1 under a three-phase short-circuit fault at the middle of one of the two parallel transmission lines bus-7 and bus-8

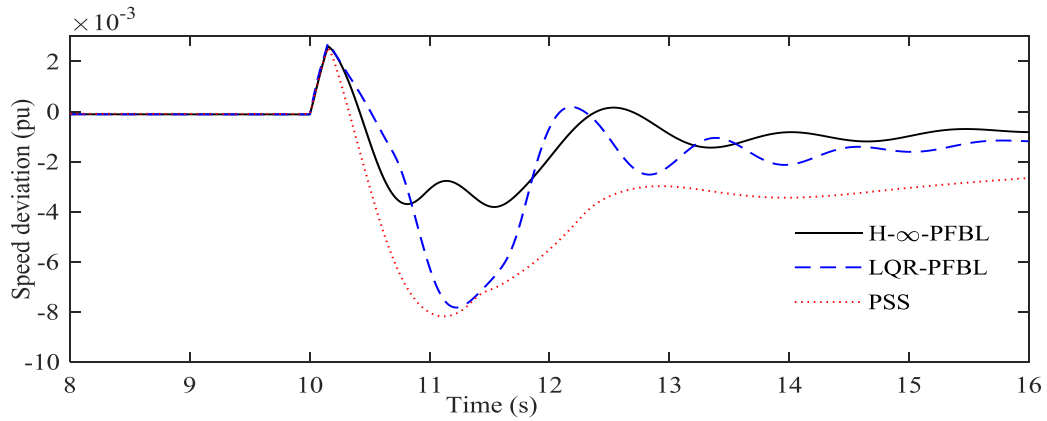

Fig. 5.14. Speed deviation of G3 under a three-phase short-circuit fault at the middle of one of the two parallel transmission lines bus-7 and bus-

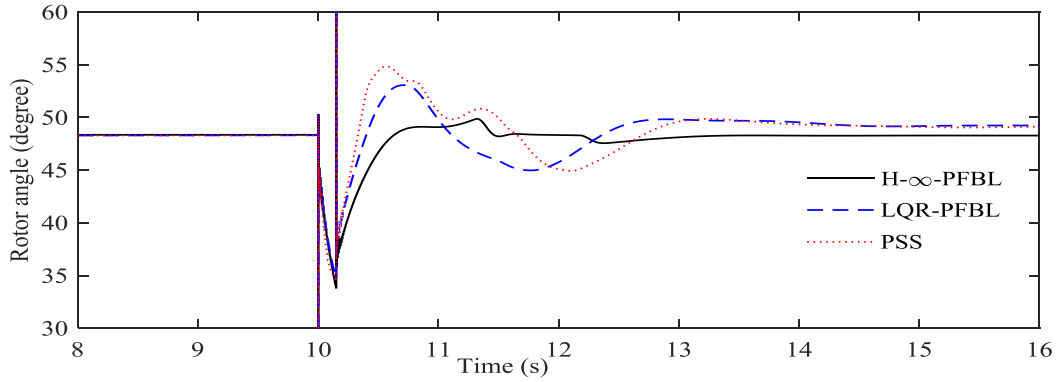

Fig. 5.15. Rotor angle of G1 under a three-phase short-circuit fault at the middle of one of the two parallel transmission lines bus-7 and bus-8

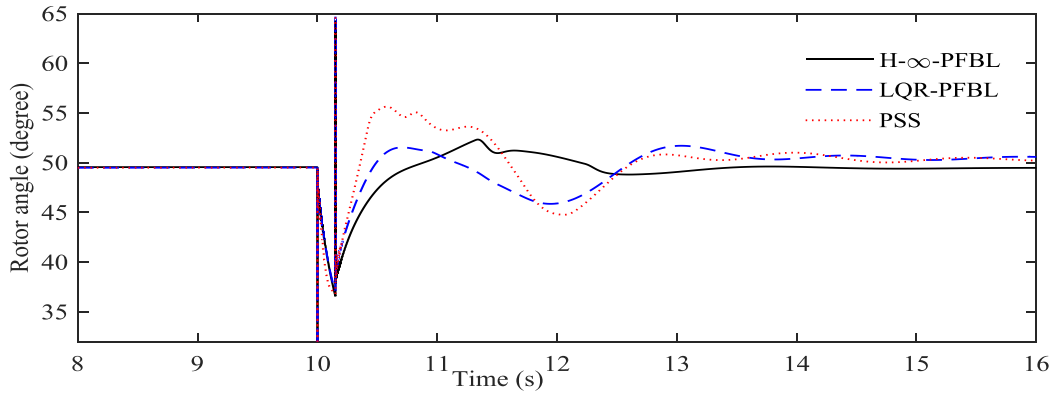

Fig. 5.16. Rotor angle of G3 under a three-phase short-circuit fault at the middle of one of the two parallel transmission lines bus-7 and bus-8

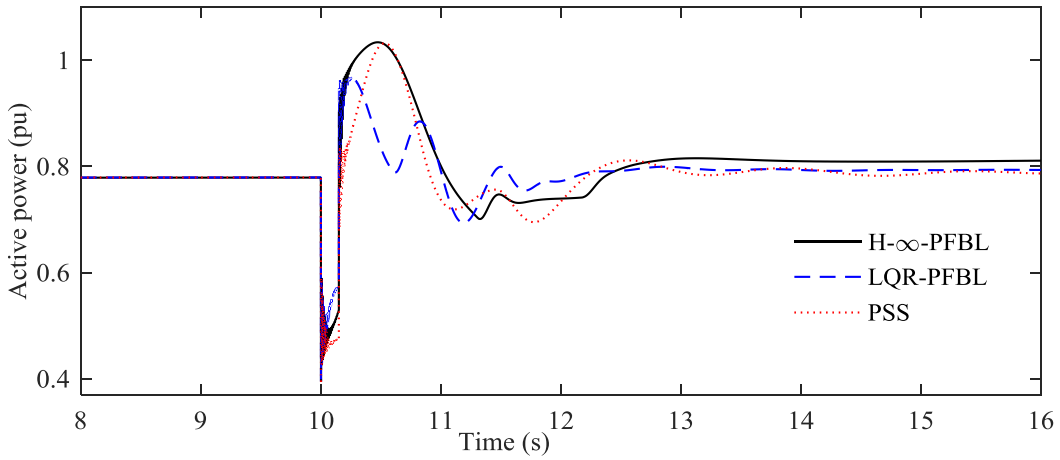

Fig. 5.17. Active power of G1 under a three-phase short-circuit fault at the middle of one of the two parallel transmission lines bus-7 and bus-8

The rotor angle and active power responses are shown from Fig. 5.15 to Fig. 5.18 for both G1 and G3. From these figures, it can be seen that the rotor angle responses are more oscillating with the PSS and LQR-PFBL as these controllers provide less synchronizing torque as compared to the designed H_∞-PFBL while the similar effects are visible from the active power responses.

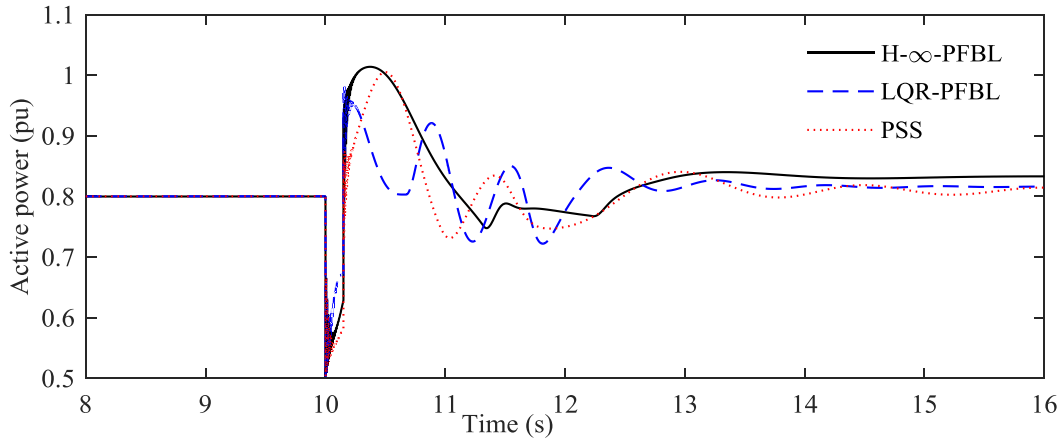

Fig. 5.18. Active power of G3 under a three-phase short-circuit fault at the middle of one of the two parallel transmission lines bus-7 and bus-8

5.4.3 Case 3: Controller performance evaluation in the case of a step change in the mechanical power input to G3

In all previous cases, the generator G3 is delivering 0.8 pu active power which also corresponds to a similar mechanical power input to the synchronous generator. In this case study, it is considered that G3 is operating with $P_m = 0.8$ pu till $t = 10$ s. At $t = 10$ s, the mechanical power input changes from $P_m = 0.8$ pu to $P_m = 0.9$ pu and the whole system continues to operate with this change in the mechanical power input.

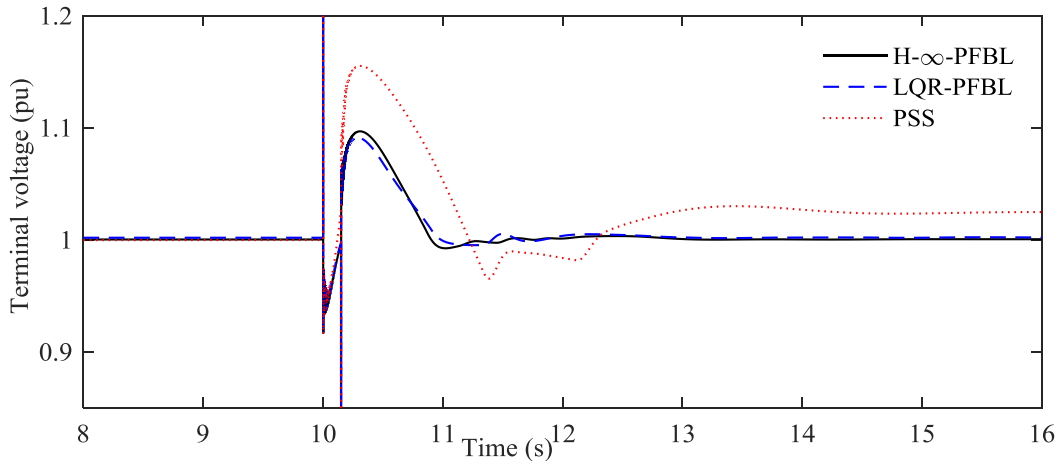

Fig. 5.19. Terminal voltage of G1 under a step change in the mechanical power input to G3

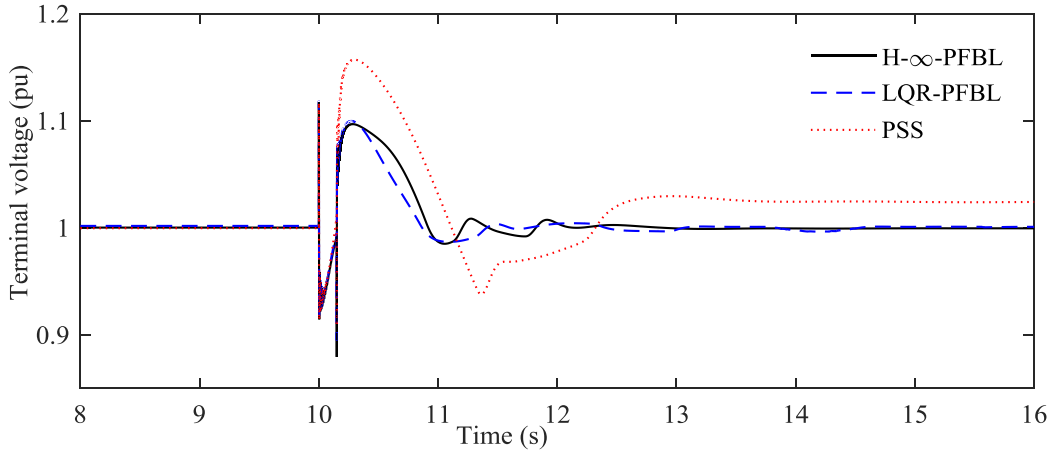

Fig. 5.20. Terminal voltage of G3 under a step change in the mechanical power input to G3

In such an operating condition, G1 and G1 will still have the same terminal voltage through these will be disturbed at $t = 10$ s as shown in Fig. 5.19 and Fig. 5.20. Since the PSS is designed to operate a fixed operating point, the terminal voltage will be severely disturbed which can also be seen from these figures (red line). But the LQR-PFBL still provides reasonably acceptable performance in terms of maintaining the voltage as this controller is designed based on the independency of the operating points though there exist some

oscillations. But the terminal voltage responses are more stable with faster settling time when the designed H_∞-PFBL is in operation.

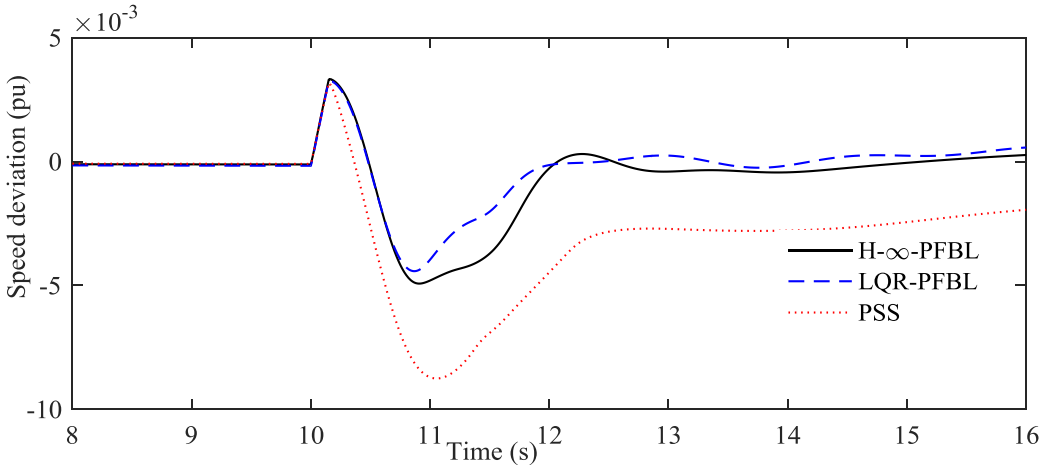

Fig. 5.21. Speed deviation of G1 under a step change in the mechanical power input to G3

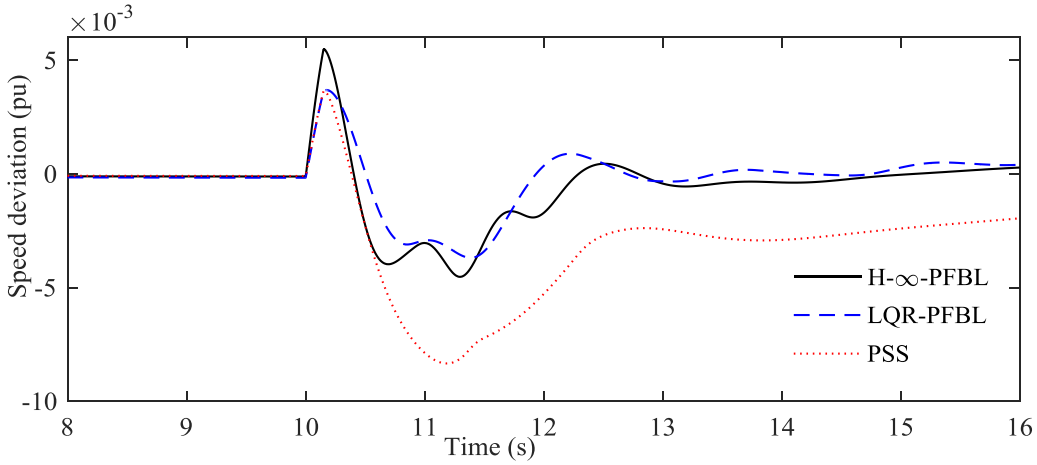

Fig. 5.22. Speed deviation of G3 under a step change in the mechanical power input to G3

Similarly, the speed deviation still needs to be maintained as zero due to the change in the mechanical power input as the synchronous generator always operates at the synchronous speed. Fig. 5.21 and Fig. 5.22 show the speed deviation responses of the synchronous generator from where it can be seen that there are more oscillations when the PSS (red line) and LQR-PFBL (solid line) are used as compared to the H_∞-PFBL (black line). This clearly indicate the

capability of adding extra damping torque of the designed H_∞-PFBL into the SMIB system while comparing with the PSS and LQR-PFBL.

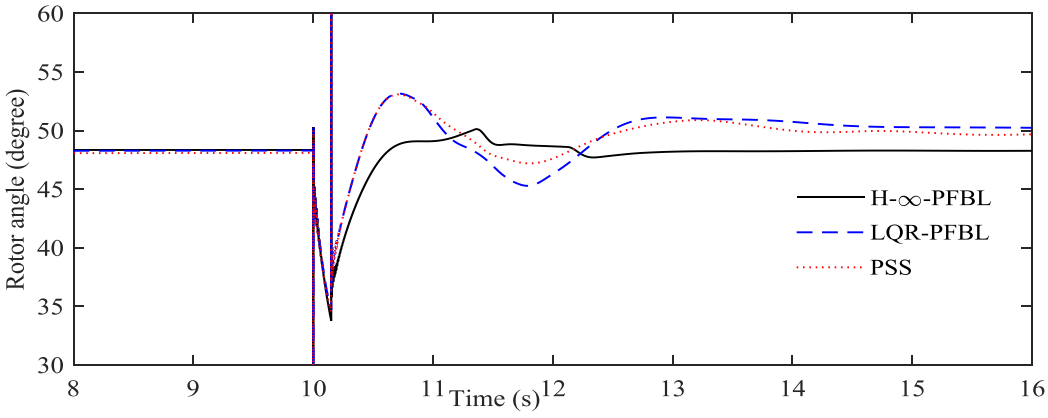

Fig. 5.23. Rotor angle of G1 under a step change in the mechanical power input to G3

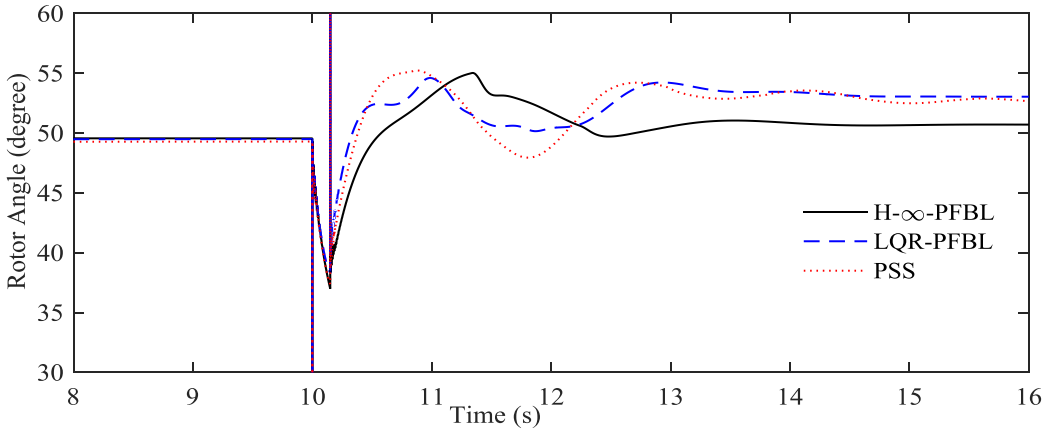

Fig. 5.24. Rotor angle of G3 under a step change in the mechanical power input to G3

In this operating condition, the rotor angle and corresponding active power will settle down to their new steady-state values only for G3 while these remain same for G1. The speed of settling down the rotor angle and active power responses for G3 depend on how fast the excitation control act on this change in the mechanical power input to G3. The designed controller settles down these responses in a much quicker way as compared to the PSS and LQR-PFBL which can be seen from Fig. 5.23 to Fig. 5.26

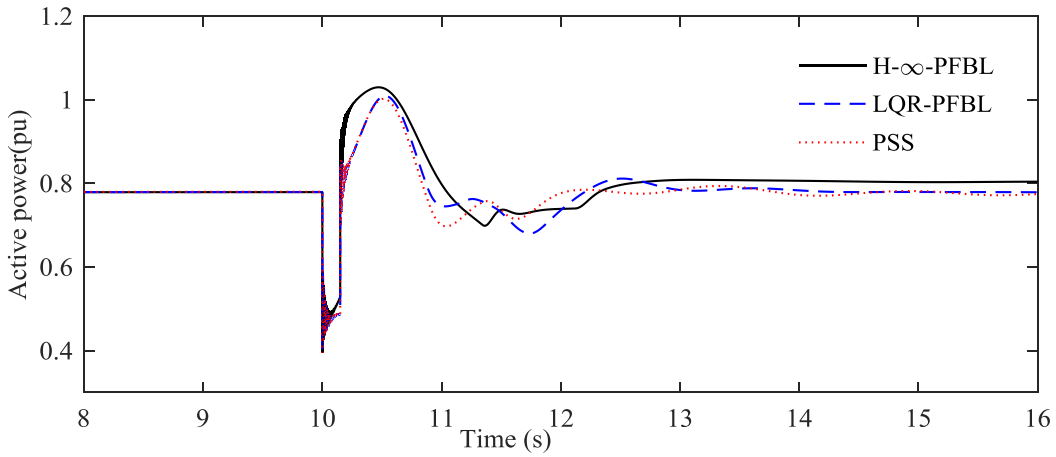

Fig. 5.25. Active power of G1 under a step change in the mechanical power input to G3

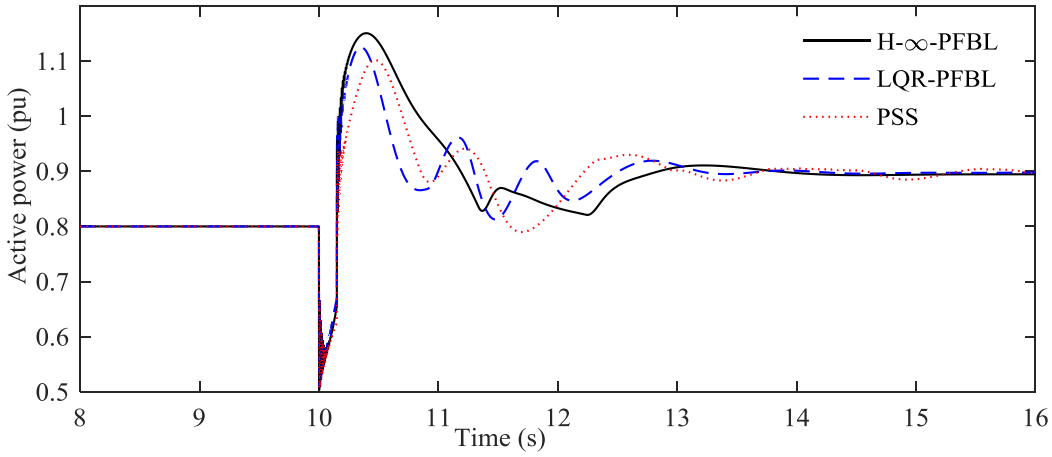

Fig. 5.26. Active power of G3 under a step change in the mechanical power input to G3

5.4.4 Case 4: Controller performance evaluation with the changes in system parameters and the presence of external disturbances and measurement noises in G3

From Fig. 5.27, Bode diagram the complementary sensitivity function $T(j\omega)$ for LQR controller and H_∞ loop shaping controller.

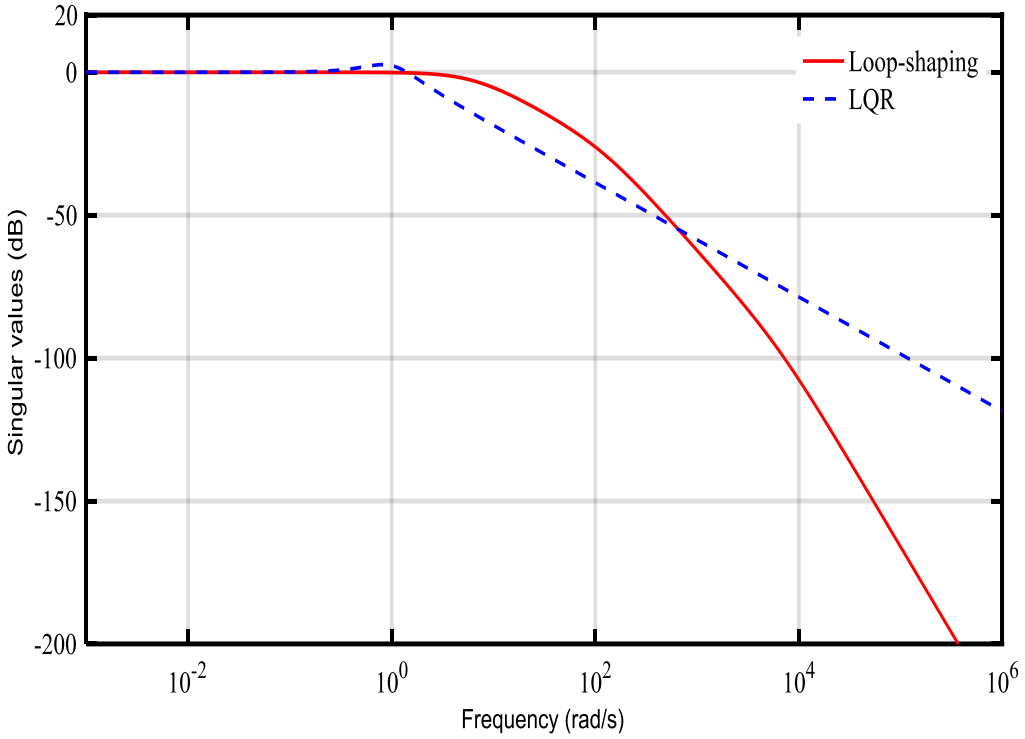

Fig. 5.27. Bode diagram of the complementary sensitivity function T for LQR controller and loop-shaping based H_∞ controller.

For LQR controller $\|T(j\omega)\|_\infty = 1.3649$ and for the designed controller is $\|T(j\omega)\|_\infty = 1.0246$. Robust stability margin of the synchronous generator is determined by $\|T(j\omega)\|_\infty^{-1}$, which equals the $|\Delta(s)|$ the close loop system can tolerate. As can be seen, for LQR controller the robust stability margin is $\|T(j\omega)\|_\infty^{-1} = 0.7327$, and that of the designed controller is$\|T(j\omega)\|_\infty^{-1} = 0.9743$. The stability margin of the designed controller is $\frac{0.9743}{0.7327}$ tines larger than that of LQR controller.

In this case study, the parameters as indicated during the design steps are varied from their nominal values from the beginning of the simulation and this has been done only for G3. The

variations are considered as $\Delta m_1 = 2.1\%$, $\Delta m_2 = 1.09\%$, $\Delta m_3 = 0.53\%$, $\Delta m_4 = 2.5\%$, $\Delta m_5 = 2.9\%$, and $\Delta m_6 = 2.5\%$. These variations clearly indicate that the parameters are slightly varied from their nominal values of G3. Moreover, some external disturbances are included within the system while the measurement noises are incorporated with the speed deviation which are considered as white Gaussian noises with variances of 0.01.

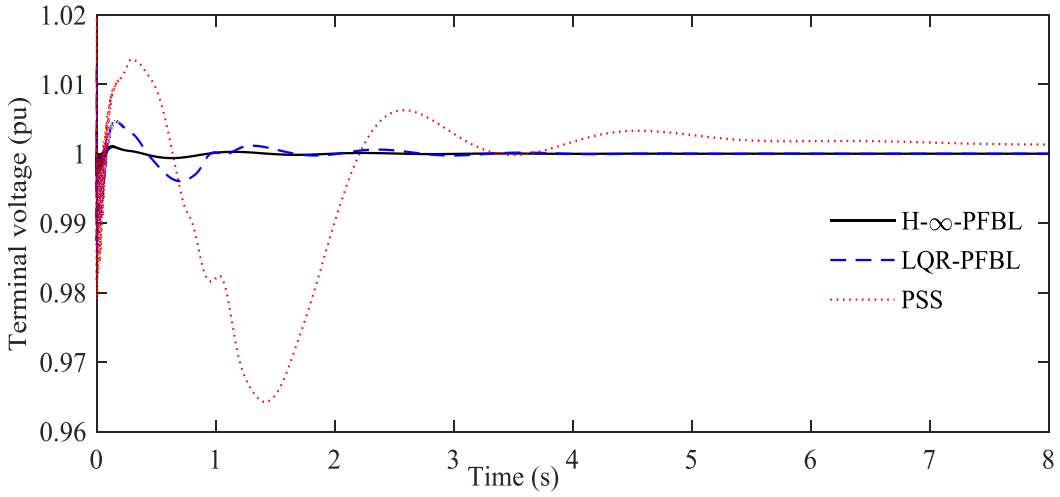

Fig. 5.28. Terminal voltage of G1 with changes in the parameters and the presence of external disturbances and measurement noises in G3

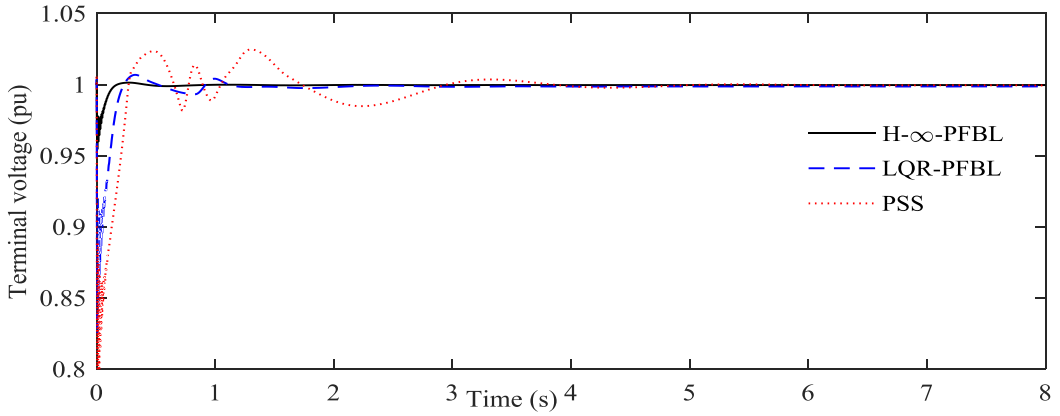

Fig. 5.29. Terminal voltage of G3 with changes in the parameters and the presence of external disturbances and measurement noises in G3

The terminal voltage response will not be affected much with these changes while nonlinear controllers (both LQR-FBL and H_∞-PFBL) are used which can also be seen from Fig. 5.28 and Fig. 5.29. The speed deviation responses are also disturbed with any controller. However, it more oscillating with the PSS (red line in Fig. 5.30 and Fig. 5.31). Moreover, the amplitudes of the oscillations for the speed deviation is more when the LQR-PFBL is used while it is considerably less with the designed H_∞-PFBL which are due to the extra robustness properties of the proposed scheme.

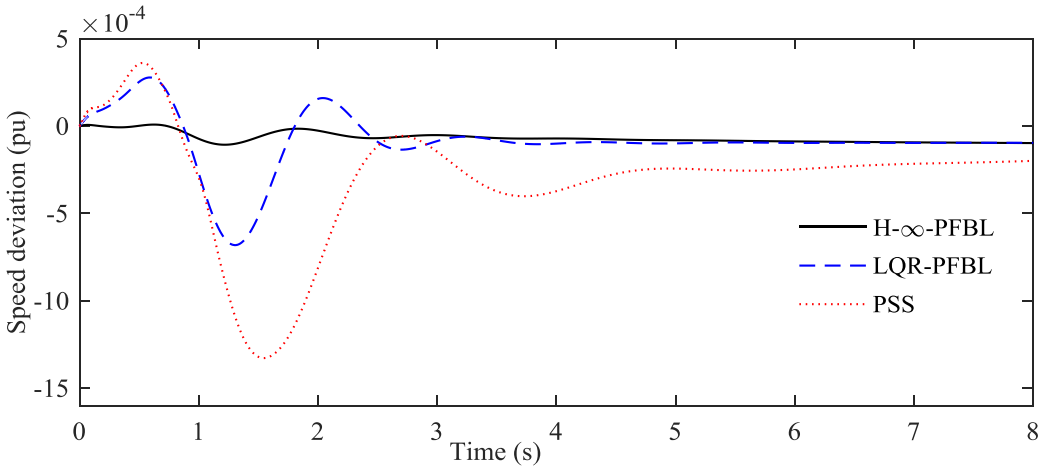

Fig. 5.30. Speed deviation of G1 with changes in the parameters and the presence of external disturbances and measurement noises in G3

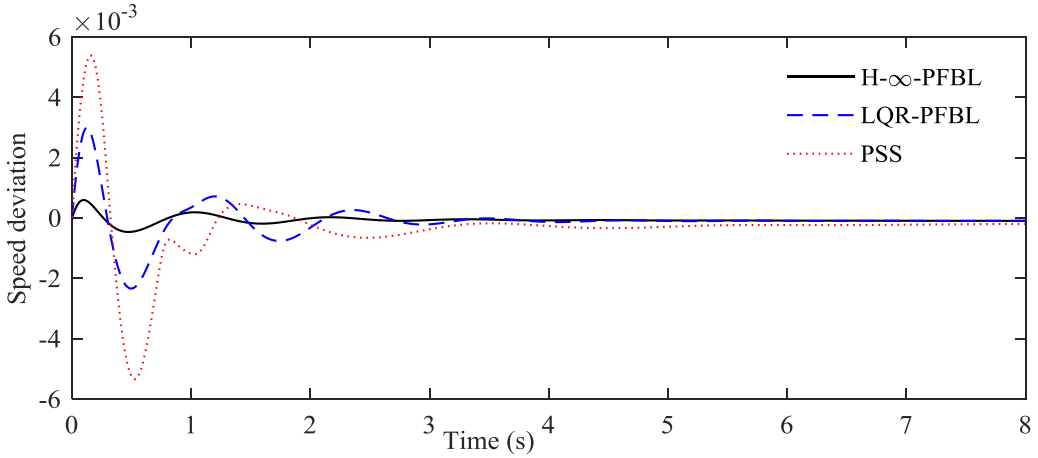

Fig. 5.31. Speed deviation of G3 with changes in the parameters and the presence of external disturbances and measurement noises in G3

The rotor angle and the active power responses of both G1 and G3 are shown from Fig. 5.32 to Fig. 5.35. All these responses are more oscillating when the PSS is used. However, the oscillations are less when LQR-PFBL and H_∞-PFBL are used though the later provides more stable responses for both rotor angle and active power responses.

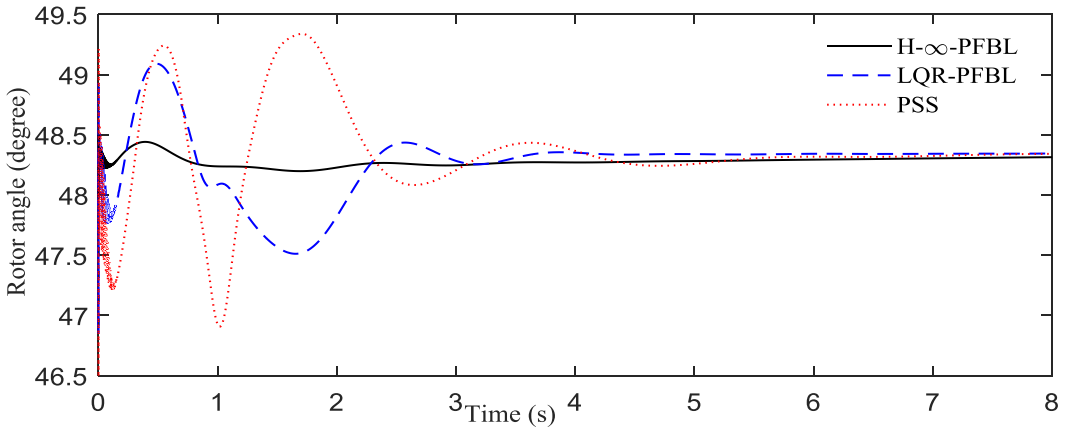

Fig. 5.32. Rotor angle of G1 with changes in the parameters and the presence of external disturbances and measurement noises in G3

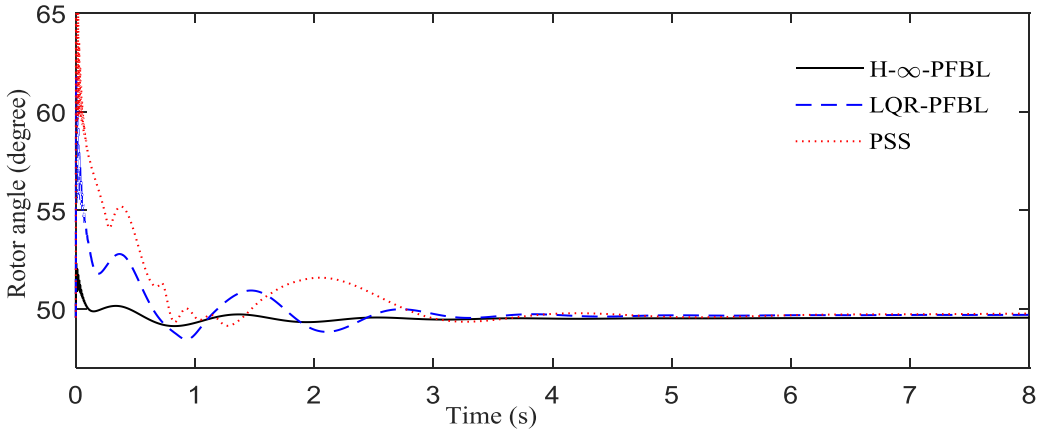

Fig. 5.33. Rotor angle of G3 with changes in the parameters and the presence of external disturbances and measurement noises in G3

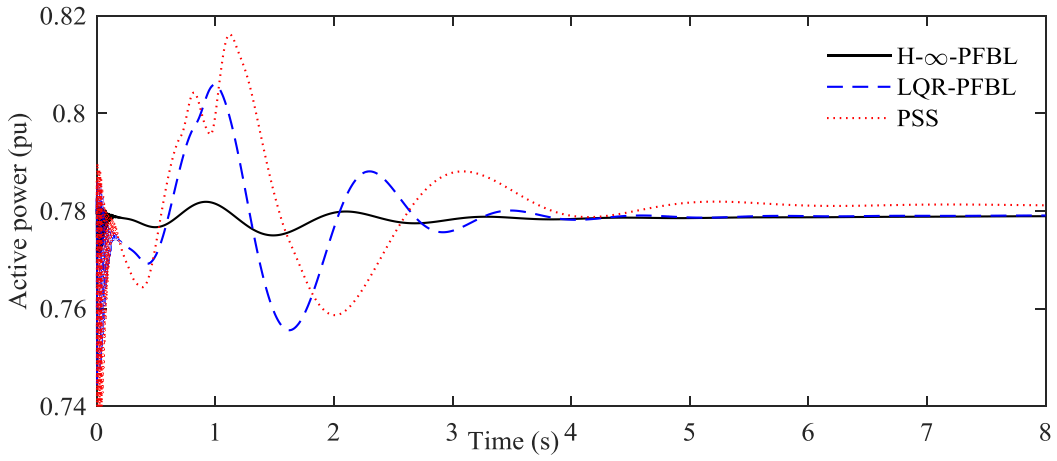

Fig. 5.34. Active power of G1 with changes in the parameters and the presence of external disturbances and measurement noises in G3

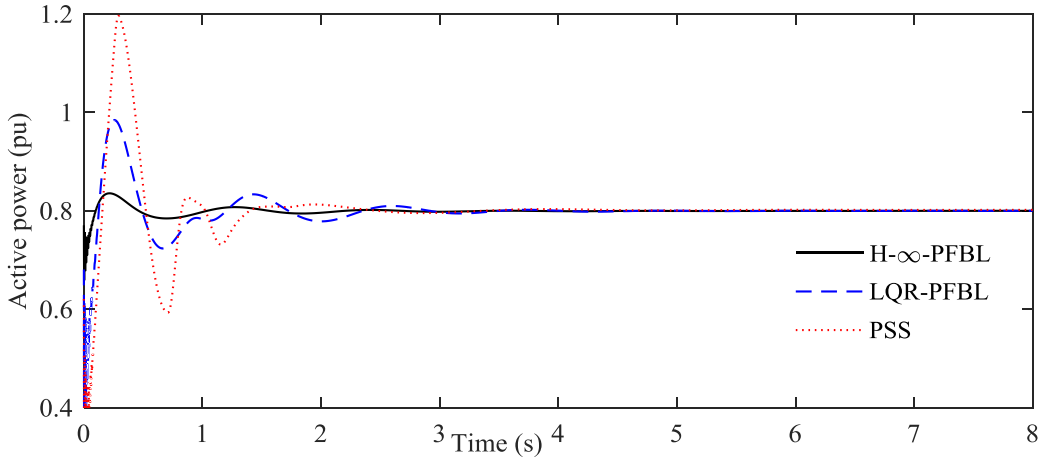

Fig. 5.35. Active power of G3 with changes in the parameters and the presence of external disturbances and measurement noises in G3

5.4.5 Quantitative comparison of the controller performance

The performance of the designed controllers for G1 and G3 are also evaluated by considering the percentage overshoots, peak time, and settling time of all responses under four different case studies as discussed in the previous subsections.

Table 5.1. Percentage overshoot for different responses of G1 under different case studies

Cases	Terminal Voltage			Speed Deviation			Rotor Angle			Active Power		
	PSS	LQR-PFBL	H_∞-PFBL	PSS	LQR-PFBL	H_∞-PFBL	PSS	LQR-PFBL	H_∞-PFBL	PSS	LQR-PFBL	H_∞-PFBL
Case 1	6	7.1	3.8	0.11	0.8	0.63	17.67	20.04	21.69	39.78	27.52	19.15
Case 2	15	10	10	0.92	0.79	0.35	13.4	5.16	6.77	26.7	19.76	26.75
Case 3	15.7	10	9.7	0.3	0.3	0.5	12.48	11.9	21.1	40.7	41.3	43.75
Case 4	1.4	0.5	0.1	0.5	0.2	0.05	14.78	9.96	4.48	50	22.5	3.75

Table 5.2. Percentage overshoot for different responses of G3 under different case studies

Cases	Terminal Voltage			Speed Deviation			Rotor Angle			Active Power		
	PSS	LQR-PFBL	H_∞-PFBL	PSS	LQR-PFBL	H_∞-PFBL	PSS	LQR-PFBL	H_∞-PFBL	PSS	LQR-PFBL	H_∞-PFBL
Case 1	6	15	12	0.62	0.79	0.5	4.16	2.2	1.42	47.4	59.2	38.7
Case 2	15	8.8	8.8	0.9	0.7	0.6	11.95	9.08	1.77	33.9	24.35	32.9
Case 3	15.5	9.1	7.3	0.32	0.32	0.32	8.34	8.34	1.26	31.3	31.3	32.39
Case 4	1.5	0.5	0.1	0.3	0.2	0.07	2.88	2.53	1.23	4.63	2.83	0.5

The percentage overshoots of G1 and G3 are shown in Table 5.1 and Table 5.2, respectively. From these tables, it can be seen that these overshoots in all responses (terminal voltages, speed deviations, rotor angle, and active power) are quite similar for the first two cases where the nominal values of the system parameters are used. In some cases, the existing controllers perform better than the designed controller for the first two cases. The main reason behind

these is that the existing controllers are mainly designed specifically for these nominal parameters. However, the performance of the designed controller are much better in terms of the overshoots in all responses for the last two cases when model uncertainties, external disturbances and measurement noises are considered.

Table 5.3. Peak time for different responses of G1 under different case studies

Cases	Voltage			Speed Deviation			Rotor Angle			Active Power		
	PSS	LQR-PFBL	H_∞-PFBL	PSS	LQR-PFBL	H_∞-PFBL	PSS	LQR-PFBL	H_∞-PFBL	PSS	LQR-PFBL	H_∞-PFBL
Case 1	10.46	10.51	10.27	11.5	11.5	11.8	10.9	11.26	11.36	11.0	10.98	11.0
Case 2	10.29	10.23	10.3	11.3	11.3	10.8	10.5	10.7	11.33	10.5	10.21	10.5
Case 3	10.29	10.31	10.28	10.1	10.15	10.15	10.8	10.99	11.33	10.5	10.42	10.4
Case 4	0.29	0.17	0.14	0.15	0.10	0.10	0.38	0.36	0.36	0.29	0.22	0.23

Table 5.4. Peak time for different responses of G3 under different case studies

Cases	Terminal Voltage			Speed Deviation			Rotor Angle			Active Power		
	PSS	LQR-PFBL	H_∞-PFBL	PSS	LQR-PFBL	H_∞-PFBL	PSS	LQR-PFBL	H_∞-PFBL	PSS	LQR-PFBL	H_∞-PFBL
Case 1	11.77	10.76	10.76	11.1	11.1	11.1	11.9	11.6	11.07	10.3	10.3	10.33
Case 2	10.3	10.44	10.28	11.1	11.1	10.9	10.5	10.7	11.32	10.5	10.26	10.46
Case 3	10.31	10.1	10.1	10.1	10.1	10.1	10.7	10.7	11.37	10.4	10.49	10.58
Case 4	0.28	0.15	0.09	0.51	0.63	0.58	0.52	0.44	0.42	0.81	0.8	0.78

The peak times also exhibit the similar characteristic to that of that percentage overshoots which are shown in Table 5.3 and Table 5.4 for G1 and G3, respectively. From these two tables, it can be seen that the designed controller performs better for the last two cases while comparing

with the PSS and LQR-PFBL. However, the settling time provides more inside for such oscillating responses.

Table 5.5. Settling time for different responses of G1 under different case studies

Cases	Voltage			Speed Deviation			Rotor Angle			Active Power		
	PSS	LQR-PFBL	H_∞-PFBL	PSS	LQR-PFBL	H_∞-PFBL	PSS	LQR-PFBL	H_∞-PFBL	PSS	LQR-PFBL	H_∞-PFBL
Case 1	5.63	5.1	3.13	7.8	3.3	3.3	8.7	6.31	4.51	10.2	5.8	4.52
Case 2	3.98	3.44	2.74	2.6	4.3	3.2	3.7	3.68	2.31	5.52	3.74	3.14
Case 3	3.02	2.86	2.2	4.73	5.02	3.37	3.7	3.03	2.92	3.58	3.58	2.93
Case 4	5.3	3.76	1.01	5.39	3.56	1.63	4.52	4.51	1.58	3.09	3.09	1.54

Table 5.6. Settling time for different responses of G3 under different case studies

Cases	Voltage			Speed Deviation			Rotor Angle			Active Power		
	PSS	LQR-PFBL	H_∞-PFBL	PSS	LQR-PFBL	H_∞-PFBL	PSS	LQR-PFBL	H_∞-PFBL	PSS	LQR-PFBL	H_∞-PFBL
Case 1	4.1	4.1	2.1	7.8	4.8	4.8	5.3	5.32	2.77	5.73	4.35	4.35
Case 2	3.52	3.32	0.67	2.3	3.3	2.4	2.9	2.7	2.22	5.15	2.65	2.65
Case 3	3.68	2.64	1.4	5.1	4.35	2.75	3.83	3.71	2.06	2.75	2.73	2.68
Case 4	5.54	3.75	0.89	5.32	3.22	0.27	5.55	4.2	1.3	5.16	4.2	2.85

The settling times for different responses of G1 and G3 are shown in Table 5.5 and table 5.6, respectively. From these tables, it can be seen that the settling times are less than 5 s for a large-scale multimachine power system when the designed controller is used. However, there are some cases when the settling times are more than 5 s with the existing PSS and LQR-PFBL. According to the timeframe for the transient stability as mentioned in [1], the settling time needs to be within 5 s. However, the existing controllers cannot guarantee the transient stability

of multimachine power systems in some cases. But the designed controller always ensures the transient stability.

5.5 Chapter Summary

This chapter has extended the results of Chapter 4 for SMIB system to the multimachine system. Using the MIMO system feedback linearization technique discussed in Section 3.2, this chapter has shown that the nonlinearity of an interconnected multimachine power system can be cancelled and the subsystems can be decoupled by the feedback linearization. As the feedback linearized subsystems are decoupled, the same analysis and controller design technique used in Chapter 4 for SMIB system can be applied to the multimachine system. Based on this, this chapter has used the same technique as that used in Section 4.3 to analyze the impact of parametric changes in the original mutlimachine system on the feedback linearized subsystems. It has shown that these parametric changes introduce the unstructured model perturbation and external disturbance into the linearized subsystems, which again calls for the same H_∞ mixed-sensitivity loop-shaping controller to improve the control perform and robustness of the closed-loop subsystems. An H_∞ mixed-sensitivity loop-shaping controller has therefore been designed and used in conjunction with the feedback linearization control for each subsystem (machine). The designed controller has been evaluated on a two-area power system and compared with the existing PSS and an LQR-based feedback linearizing controller results under different operating conditions. Simulation results clearly indicate that the designed controller performs the PSS and LQR-based feedback linearizing controller for multimachine power system.

Chapter 6

Conclusions and Future Research Directions

6.1 Conclusions

It was clear that the designed robust feedback linearizing H_∞ mixed-sensitivity loop shaping excitation controller outperforms the existing excitation controllers. The control problem has been formulated by considering model uncertainties, external disturbances, and measurement noises. A brief overview feedback linearization and H_∞ mixed-sensitivity loop shaping controller design has been presented as the excitation controllers for the SMIB system and multimachine power system has been designed based on these approaches.

From this study, the following generalized conclusions can be made

- The existing power system stabilizers do not have the capability to provide robustness against changes in operating conditions as well as against modeling uncertainties, external disturbances, and measurement noises.
- The existing feedback linearizing excitation controller based on the linear quadratic regulator (LQR) is independent of the operating points. However, its performance degrades when the parameters are even slightly varied from their nominal values.
- The partial feedback linearization technique allows to use the speed deviation of the synchronous generators, which is more realistic and helps to add more damping into the system as compared to the unmeasurable rotor angle feedback.
- The partial feedback linearization simplifies the multimachine excitation problem to single machine problems by decomposing the whole system into several subsystems with reduced-orders.

- The proposed approach does not require any information from the neighboring subsystems and thus can be implemented in a decentralized manner.
- The designed feedback linearizing H_∞ mixed-sensitivity loop shaping excitation controller uses only the output feedback of the system as the feedback and thus, avoids the measurements of different states in the state feedback controllers.
- The designed controller provides robustness against different operating conditions as well as against model uncertainties, external disturbances, and measurement noises.
- As the designed controller provides more damping to the system, the settling time is faster with less overshoots as compared to the existing controllers.

6.2. Directions for Future Research

The proposed scheme can be expanded by considering the following points:

- The synchronous generator models in power system can be considered as higher-order models to achieve more accurate control results.
- The dynamics of the turbine-governor system can be included so that the controller will have the capability to respond to the changes in loads.
- There is a lot of ongoing works on the renewable energy integration. The proposed control scheme can be used to design controller for wind and solar generation systems.
- The proposed control scheme can be applied to hybrid AC/DC microgrids to control the microgrids.

Appendix

Appendix-I: Data for the SMIB System

Table A-I. Data of the SMIB system (in pu)

Machine	AVR
200 MW x_d=1.863 x'_d=0.296 x_q=0.474 T'_d=6.9 s $\omega_s = 314.16$ H=2.5 D=4	$K_A = 200$ $T_A = 0.02$s $E_{fd}^{mim} = -5.43$ $E_{fd}^{max} = 6.03$

Appendix-II: Data for the Two-Area Four Machine Power System

Each area consists of two coupled units, each having a rating of 900 MVA and 20 kV. The generator parameters in pu on the rated MVA and kV base are as follows:

$x_d = 1.863, x'_d = 0.3, x''_d = 0.25, x_q = 1.72, x'_q = 0.55, x''_q = 0.25, x_l = 0.2, R_a = 0.0025,$ $T'_{d0} = 8\ s, T'_{q0} = 0.4\ s, T''_{d0} = 0.03\ s, T''_{q0} = 0.05\ s, A_{Sat} = 0.015, B_{Sat} = 9.6, H = 6.5$ (for G1 and G2), $H = 6.175$ (for G3 and G4)

Each step-up transformer has an impedance of $0 + j0.15$ per unit on 900 MVA and 20/230 kV base, and has an off-nominal ratio of 1.0.

The parameters of the transmission line in per unit on 100 MVA, 230 kV base are

$r = 0.0001\ pu/km$, $x_L = 0.001pi/km$, $b_c = 0.00175\ pu/km$

The system is operating with area 1 exporting 400 MW to area 2, and the generating units are loaded as follows:

G1: $P = 700$ MW, $Q = 185$ MVAr, $E_t = 1.03\angle 20.2°$

G2: $P = 700$ MW, $Q = 235$ MVAr, $E_t = 1.01\angle 10.5°$

G3: $P = 719$ MW, $Q = 176$ MVAr, $E_t = 1.03\angle -6.8°$

G4: $P = 700$ MW, $Q = 202$ MVAr, $E_t = 1.01\angle -17.0°$

The load and reactive power supplied (Q_c) by the shunt capacitors at buses 7 and 9 are as follows:

Bus 7: $P_L = 967$ MW, $Q_L = 100$ MVAr, $Q_C = 200$ MVAr

Bus 9: $P_L = 1767$ MW, $Q_L = 100$ MVAr, $Q_C = 350$ MVAr

AVR of each unit

$K_A = 200$, $T_A = 0.02$s, $E_{fd}^{mim} = 0$, $E_{fd}^{max} = 12.3$

References

[1] P. Kundur, Power System Stability and Control. *New York: McGraw-Hill,* 1994.

[2] M. A. Mahmud, M. J. Hossain, and H. R. Pota, "Effects of large dynamic loads on interconnected power system stability," *International Journal of Power and Energy Systems,* vol. 44, no. 1, pp. 357-363, January 2013.

[3] C. Dou, Q. Jia, S. Jin, and Z. Bo, "Delay-independent decentralized stabilizer design for large interconnected power systems based on WAMS," *International Journal of Electrical Power and Energy Systems,* vol. 29, no. 10, pp. 775–782, Dec. 2007.

[4] S. S. Lee and J. Park, "Design of reduced-order observer-based variable structure power system stabiliser for unmeasurable state variables," *IEE Proc.– Generation, Transmission and Distribution,* vol. 145, no. 5, pp. 525–530, Sept. 1998.

[5] K. Ogata, Modern Control Engineering. *New York: Prentice Hall,* 2010.

[6] M. A. Mahmud, H. R. Pota, M. Aldeen, and M. J. Hossain, "Partial feedback linearizing excitation controller for multimachine power systems to enhance transient stability," *IEEE Trans. on Power Systems,* vol. 29, no. 2, pp. 561 – 571, March 2014.

[7] F. P. Demello and C. Concordia, "Concepts of synchronous machine stability as affected by excitation control," *IEEE Trans. on Power Appartus and Systems,* vol. PAS-88, no. 4, pp. 316–329, April 1969.

[8] F. P. deMello, "Measurement of synchronous machine rotor angle from analysis of zero sequence harmonic components of machine terminal voltage," *IEEE Trans. on Power Delivery,* vol. 9, no. 4, pp. 1770–1777, Oct. 1994.

[9] F. P. deMello, L. N. Mannett, and J. Undrill, “Practical approaches to supplementary stabilizing from accelerating power,” *IEEE Trans. on Power Appartus and Systems,* vol. PAS-97, no. 5, pp. 1515–1522, Sept. / Oct. 1978.

[10] R. A. Ramos, A. C. P. Martins, and N. G. Bretas, “An improved methodology for the design of power system damping controllers,” *IEEE Trans. on Power Systems,* vol. 20, no. 4, pp. 1938–1945, 2005.

[11] G. Rogers, Power system oscillations. Boston, USA: Kluwer Academic Publishers, 2000.

[12] A. Dy´sko, W. E. Leithead, and J. O’Reilly, “Enhanced power system stability by coordinated PSS design,” *IEEE Trans. on Power Systems,* vol. 25, no. 1, pp. 413–422, 2010.

[13] M. Ramirez-Gonzalez and O. P. Malik, “Power system stabilizer design using an online adaptive neuro fuzzy controller with adaptive input link weights,” *IEEE Trans. on Energy Conversion,* vol. 23, no. 3, pp. 914–922, Sept. 2008.

[14] G. Gurrala and I. Sen, “Power system stabilizers design for interconnected power systems,” *IEEE Trans. on Power Systems,* vol. 25, no. 2, pp. 1042– 1051, 2010.

[15] N. N. Islam, M. A. Hannan, Hussain Shareef, and Azah Mohamed, "An application of backtracking search algorithm in designing power system stabilizers for large multi-machine system." *Neurocomputing* vol. 237, pp. 175-184, 2017.

[16] H. Yousef, Hisham M. Soliman, and Mohamed Albadi, "Nonlinear power system excitation control using adaptive wavelet networks." *Neurocomputing,* vol. 230, pp. 302-311, 2017.

[17] Y. Wan, “Nonlinear robust control for single-machine infinite-bus power systems with input saturation,” *Bulletin of the Polish Academy of Sciences Technical Sciences,* vol. 65, no. 1, pp. 3-9, 2017.

[18] A. R. Roosta, D. Georges and N. Hadj-Said, "Nonlinear control for power systems based on a backstepping method," *Proceedings of the 40th IEEE Conference on Decision and Control (Cat. No.01CH37228),* Orlando, FL, 2001, pp. 3037-3042 vol.4.

[19] T. K. Roy, M. A. Mahmud, Weixiang Shen, and A. M. T. Oo, “Nonlinear excitation control of synchronous generators based on adaptive backstepping method,” in *IEEE 10th Conference on Industrial Electronics and Applications,* pp.11-16, 15-17 June 2015.

[20] T. K. Roy, M. A. Mahmud, A. M. T. Oo, and H. R. Pota, “Nonlinear adaptive backstepping excitation controller design for higher-order models of synchronous generators,” *in 20th IFAC World Congress,* July 2017.

[21] T. K. Roy, M. A. Mahmud, W. X. Shen and A. M. T. Oo, “A nonlinear adaptive backstepping approach for coordinated excitation and steam-valving control of synchronous generators,” *10th Asian Control Conference (ASCC),* Kota Kinabalu, pp. 1-6, 2015.

[22] T. K. Roy, M. A. Mahmud, W. X. Shen and A. M. T. Oo, “Robust adaptive backstepping excitation controller design for simple power system models with external disturbances,” *IEEE Conference on Control Applications (CCA),* Sydney, NSW, 2015, pp. 715-720, 2015.

[23] A. G. Loukianov, J. M. Canedo, L. M. Fridman and A. Soto-Cota, "High-Order Block Sliding-Mode Controller for a Synchronous Generator With an Exciter System," in *IEEE Transactions on Industrial Electronics,* vol. 58, no. 1, pp. 337-347, Jan. 2011.

[24] R. S. Munoz-Aguilar, A. Doria-Cerezo, E. Fossas and R. Cardoner, "Sliding Mode Control of a Stand-Alone Wound Rotor Synchronous Generator," in *IEEE Transactions on Industrial Electronics,* vol. 58, no. 10, pp. 4888-4897, Oct. 2011.

[25] R. S. Muñoz-Aguilar, P. Rodríguez, A. Dòria-Cerezo, I. Candela and A. Luna, "Sensor-less Sliding Mode Control of a stand-alone wound rotor synchronous generator with unbalanced load," *IECON 2011 - 37th Annual Conference of the IEEE Industrial Electronics Society,* Melbourne, VIC, 2011, pp. 3982-3987.

[26] Galaz, Martha, Romeo Ortega, Alexandre S. Bazanella, and Aleksandar M. Stankovic., "An energy-shaping approach to the design of excitation control of synchronous generators," *Automatica 39,* no. 1 (2003): 111-119.

[27] Luo, Xiao Shu. "Passivity-based adaptive control of chaotic oscillations in power system." *Chaos, Solitons & Fractals 31*, no. 3 (2007): 665-671.

[28] Y. Zheng, J. Zhou, W. Zhu, C. Zhang, C. Li, and W. Fu, "Design of a multimode intelligent model predictive control strategy for hydroelectric generating unit," *Neurocomputing,* vol. 207, pp. 287–299, 2016.

[29] V. Rajkumar and R. R. Mohler, "Bilinear generalized predictive control using the thyristor-controlled series-capacitor," in *IEEE Transactions on Power Systems,* vol. 9, no. 4, pp. 1987-1993, Nov 1994.

[30] M. A. Mahmud, M. J. Hossain, and H. R. Pota, "Nonlinear excitation control of power systems with dynamic loads via feedback linearization," *In Proc. of 20th Australasian Universities Power Engineering Conference (AUPEC 2010) ,* 5-8 December, 2010, Canterbury, New Zealand.

[31] M. A. Mahmud, M. J. Hossain, and H. R. Pota, "Robust nonlinear state feedback for power systems under structured uncertainty," *In Proc. of 18th IFAC World Congress,* 28 August-2 September, 2011, Milano, Italy.

[32] W. Mielczarski and A. M. Zajaczkowski, "Nonlinear field voltage control of a synchronous generator using feedback linearization," *Automatica,* vol. 30, no. 10, pp. 1625–1630, Oct. 1994.

[33] Youyi Wang, David J. Hill, Robust nonlinear coordinated control of power systems, *Automatica,* Volume 32, Issue 4, 1996, Pages 611-618.

[34] G. Kenn´e, R. Goma, H. Nkwawo, F. L.-Lagarrigue, A. Arzand´e, and J. C. Vannier, "An improved direct feedback linearization technique for transient stability enhancement and voltage regulation of power generators," *International Journal of Electrical Power and Energy Systems,* vol. 32, no. 7, pp. 809–816, Sept. 2010.

[35] M. A. Mahmud, M. J. Hossain, and H. R. Pota, "Nonlinear excitation controller for power systems using zero dynamic design approach," *In Proc. of 43rd North American Power Symposium (NAPS2011),* 4-6 August, Boston, MA, USA.

[36] M. A. Mahmud, M. J. Hossain, H. R. Pota and M. S. Ali, "Zero dynamic excitation controller design for power system with dynamic load," *In Proc. of 21st Australasian Universities Power Engineering Conference (AUPEC2011)*, 24-26 September, 2011, Brisbane, Australia.

[37] Y. Wang, G. H. Zhang, and D. J. Hill, "Robust power system transient stability enhancement: A global control approach," in *6th IFAC Symposium on nonlinear control systems,* 2004, pp. 1325–1330.

[38] M. A. Mahmud, H. R. Pota, and M. J. Hossain, "Robust zero dynamic excitation controller for power systems under structured uncertainty," *In Proc. of the 2nd Australian Control Conference (AUCC),* 15-16 November, 2012, Sydney, Australia.

[39] M. A. Mahmud, "An alternative LQR-based excitation controller design for power systems to enhance small-signal stability," *International Journal of Electrical Power and Energy Systems,* vol. 63, pp. 1-7, December, 2014.

[40] A. J. A. Simoes Costa, F. D. Freitas, and A. S. e Silva, "Design of decentralized controllers for large power systems considering sparsity," *IEEE Trans. on Power Systems,* vol. 12, no. 1, pp. 144–152, Feb. 1997.

[41] R. A. Lawson, D. A. Swann, and G. F. Wright, "Minimization of power system stabilizer torsional interaction on large steam turbine-generators," *IEEE Trans. on Power Appartus and Systems,* vol. PAS-97, no. 1, pp. 183–190, Jan. / Feb. 1978.

[42] A. Kumar, "Power system stabilizers design for multimachine power systems using local measurements," *IEEE Transactions on Power Systems,* vol. 31, no. 3, pp. 2163–2171, 2016.

[43] C. A. King, J. W. Chapman, and M. D. Ilic, "Feedback linearizing excitation control on a full-scale power system model," *IEEE Tans. on Power Systems,* vol. 9, no. 2, pp. 1102–1109, 1994.

[44] K.-I. Jung, T.-W. Y. K.-Y. Kim, and G. Jang, "Decentralized control for multimachine power systems with nonlinear interconnections and disturbances," *International Journal of Control, Automation, and Systems,* vol. 3, no. 2, pp. 270–277, Jun. 2005.

[45] B. K. Kumar, S. N. Singh, and S. C. Srivastava, “A decentralized nonlinear feedback controller with prescribed degree of stability for damping power system oscillations,” *Electric Power Systems Research,* vol. 77, no. 3–4, pp. 204–211, Mar. 2007.

[46] A. E. Leon, J. A. Solsona, and M. I. Valla, “Comparison among nonlinear excitation control strategies used for damping power system oscillations,” *Energy Conversion and Management,* vol. 53, no. 1, pp. 55–67, Jan. 2012.

[47] S. Jain and F. Khorrami, "Application of a decentralized adaptive output feedback based on backstepping to power systems," *Proceedings of 1995 34th IEEE Conference on Decision and Control,* New Orleans, LA, 1995, pp. 1585-1590 vol.2.

[48] T. K. Roy, M. A. Mahmud, Weixiang Shen, and A. M. T. Oo, “Nonlinear adaptive excitation controller design for multimachine power systems with unknown stability sensitive parameters,” in *IEEE Transactions on Control Systems Technology*, vol.PP, no.99, pp.1-13, December 2016.

[49] T. K. Roy, M. A. Mahmud, Weixiang Shen, and A. M. T. Oo, “Nonlinear adaptive coordinated controller design for multimachine power systems to improve transient stability,” in *IET Generation Transmission & Distribution,* vol. 10, no. 13, pp.3353-3363, July 2016.

[50] T. K. Roy, M. A. Mahmud, Weixiang Shen and A. M. T. Oo, “Nonlinear adaptive excitation controller design for multimachine power systems,” *IEEE Power & Energy Society General Meeting,* pp. 1-5, 2015.

[51] T. K. Roy, M. A. Mahmud, Weixiang Shen, A. M. T. Oo, and M. E. Haque, “Robust nonlinear adaptive backstepping excitation controller design for rejecting external disturbances in multimachine power systems,” *International Journal of Electrical Power & Energy Systems,* vol. 84, pp. 76-86, January 2017.

[52] A. Colbia-Vega, J. de León-Morales, L. Fridman, O. Salas-Peña, M.T. Mata-Jiménez, Robust excitation control design using sliding-mode technique for multimachine power systems, *Electric Power Systems Research,* Volume 78, Issue 9, September 2008, pp. 1627-1634.

[53] X. G. Yan, C. Edwards, S. K. Spurgeon and J. A. M. Bleijs, "Decentralised sliding-mode control for multimachine power systems using only output information," in *IEE Proceedings - Control Theory and Applications,* vol. 151, no. 5, pp. 627-635, 23 Sept. 2004.

[54] X-G. Yan, and S. K. Spurgeon, and C. Edwards, "Application of decentralised sliding mode control to multimachine power systems," in *Variable Structure Control of Complex Systems: Analysis and Design, Springer International Publishing*, 2017, pp. 297-313.

[55] Yuanzhang Sun, Tielong Shen, Romeo Ortega and Qianjin Liu, "Decentralized controller design for multimachine power systems based on the Hamiltonian structure," *Proceedings of the 40th IEEE Conference on Decision and Control (Cat. No.01CH37228),* Orlando, FL, 2001, pp. 3045-3050 vol.4.

[56] Furtat, Igor B., and Alexander L. Fradkov. "Robust control of multi-machine power systems with compensation of disturbances." *International Journal of Electrical Power & Energy Systems* 73 (2015): 584-590.

[57] J. J. Ford, G. Ledwich and Z. Y. Dong, "Efficient and robust model predictive control for first swing transient stability of power systems using flexible AC transmission systems devices," in *IET Generation, Transmission & Distribution,* vol. 2, no. 5, pp. 731-742, September 2008.

[57] Thabit, Mohammed Mansoor Bin. "Nonlinear model predictive control of multi-machine power system." *PhD diss., King Fahd University of Petroleum and Minerals (Saudi Arabia),* 2013.

[59] D. Gan, Z. Qu, and H. Cai, "Multi machine power system excitation control design via theories of feedback linearization control and nonlinear robust control," *International Journal of Systems Science,* vol. 31, no. 4, pp. 519–527, 2000.

[60] Q. Lu, Y. Sun, and S. Mei, Nonlinear Control Systems and Power System Dynamics. *Boston: Kluwer Academic Publishers,* 2001.

[61] M. A. Mahmud, M. J. Hossain, and H. R. Pota, "Transient stability enhancement of multimachine power systems using nonlinear observer-based excitation controller," *International Journal of Electrical Power and Energy Systems,* vol. 58, pp. 57 – 63, June 2014.

[62] M. A. Mahmud, H. R. Pota, and M. J. Hossain, "Full-order nonlinear observer-based excitation controller design for interconnected power systems via exact linearization approach," *International Journal of Power and Energy Systems,* vol. 41, no. 1, pp. 54-62, October 2012.

[63] M. A. Mahmud, H. R. Pota, and M. J. Hossain, "Zero dynamic excitation controller for multimachine power systems to augment transient stability and voltage regulation," *In Proc. of IEEE PES General Meeting,* 22-26 July, 2012, San Diego, USA.

[64] A. Isidori, Nonlinear Control Systems. *Berlin: Springer-Verlag,* 2nd Edition, 1989.

[65] M. A. Mahmud, Robust Nonlinear Feedback Linearizing Control for Power Systems to Enhance Transient Stability, *PhD Thesis,* UNSW Australia, 2012.

[66] Åström, Karl Johan. "Control system design lecture notes for ME 155A." *Department of Mechanical and Environmental Engineering University of California Santa Barbara,* 333, 2002.

[67] M. A. Mahmud, M. J. Hossain, and H. R. Pota, "Selection of output function in nonlinear feedback linearizing excitation control for power systems," *In Proc. of the 1st Australian Control Conference (AUCC2011),* 10-11 November, 2011, Melbourne, Australia.